4-24-2020

Modeling Drought, Drought Teleconnection, and its Effect on Groundwater Level Dynamics in the Biscayne Aquifer

Anteneh Z. Abiy
Florida International University, aabiy001@fiu.edu

FLORIDA INTERNATIONAL UNIVERSITY

Miami, Florida

MODELING DROUGHT, DROUGHT TELECONNECTION, AND ITS EFFECT ON GROUNDWATER LEVEL DYNAMICS IN THE BISCAYNE AQUIFER

A dissertation submitted in partial fulfillment of

the requirements for the degree of

DOCTOR OF PHILOSOPHY

in

EARTH SYSTEM SCENCES

by

Anteneh Zewdie Abiy

2020

To: Dean Michael R. Heithaus
College of Arts, Sciences and Education

This dissertation, written by Anteneh Zewdie Abiy, and entitled Modeling Drought, Drought Teleconnection, and its Effect on Groundwater Level Dynamics in the Biscayne Aquifer, having been approved in respect to style and intellectual content, is referred to you for judgment.

We have read this dissertation and recommend that it be approved.

_____
Wossenu Abtew

_____
Dean Whitman

_____
René M. Price

_____
Assefa M. Melesse, Major Professor

Date of Defense: April 24, 2020

The dissertation of Anteneh Zewdie Abiy is approved.

_____
Dean Michael R. Heithaus
College of Arts, Sciences and Education

_____
Andrés G. Gil
Vice President for Research and Economic Development
and Dean of the University Graduate School

Florida International University, 2020

DEDICATION

To my wife Meseret A. Lisanu

ACKNOWLEDGMENTS

I would like to thank The Almighty GOD for blessing me with a loving family and faith that keep me run how much the road is rugged and how much the mountain is rolling. I would like to thank GOD for surrounding me with people who are filled with loving, care and diligent in their decisions. Me, as I stand, I am a weak person, but the love, kindness and thoughtfulness of you have gave me the endurance to walk successfully.

My deepest gratitude goes to my major professor Dr. Assefa M. Melesse for giving me the opportunity to endure with the Ph.D. program. Dr. Melesse, I would like to thank you for believing in me and for your continuous academic support, guidance, and advice. I am grateful for the long hours we spent together in reviewing models, teaching me science, and all the opportunities you gave me to publish papers and book chapters. I found my dream of advancing water resources studies a reality because of your high-level professionalism, thank you!!

I would like to extend my gratitude to Professors René M. Price, Dean Whitman, and Wossenu Abtew for their unlimited guidance and mentorship. I am grateful for all of you not only for your guidance but also for challenging the ideas that help me advance the level of work included in this desertion. I like to command Professors René M. Price; whose guidance gave life to my groundwater model and its application. None of my work would have been possible without the guidance and computational skills I learned from Professors Dean Whitman. I am grateful for Dr. Wossenu Abtew who introduced me to

the hydrology of South Florida and how hydrological modeling can be used to alleviate realistic natural problems. I am also great full for Dr. Hector Fuentes, who served as an external evaluator.

I am profoundly grateful to Drs. Elizabeth P. Anderson and Jennifer S. Rehage, who were excellent mentors and friends to my family and extended hands during challenging days—myself, my wife, and my children are grateful to both of you. I am grateful to the entire department of Earth and Environment staff members.

The Florida International University Graduate School through the Dissertation Evidence Acquisition (DEA) and Dissertation Year Fellowship (DYF) programs supported my research. The Everglades Foundation and FIU for Everglades have provided a prestigious scholarship that supported my research and publications processing. Further, the CREST CAChE, FC-LTER, Institute of Environment, FIU Department of Earth and Environment, and the College of Arts Science and Education has provided financial support for specialized training, publications processing, and conference participation. I am extensively grateful to the respective institutions and the kind leadership behind these decisions. I acknowledge Professors Leonard Scinto, Todd Crowl, and Evelyn E. Gaiser and several, great, high level leaders and their offices that work diligently to make FIU a home to everyone.

ABSTRACT OF THE DISSERTATION

MODELING DROUGHT, DROUGHT TELECONNECTION, AND ITS EFFECT ON GROUNDWATER LEVEL DYNAMICS IN THE BISCAYNE AQUIFER

by

Anteneh Zewdie Abiy

Florida International University, 2020

Miami, Florida

Professor Assefa M. Melesse, Major Professor

Developing a self-sufficient water supply system in Southeast Florida is one input to the success of the ongoing restoration effort in the Everglades. Maintaining a high groundwater level in the urban side of the Biscayne Aquifer (BA) is important to sustain the urban water supply. However, the long-term groundwater table condition in the Biscayne Aquifer (BA) is threatened by a combination of drought, groundwater pumping, and sea-level rise. Further, the long-term drought pattern, drought drivers, and the aquifer's response to drought and other stress conditions are not well known. As a result, options that would help to maintain a high groundwater table condition in the urban section of the aquifer without being dependent on recharge from the Everglades water are not outlined. In this study, long-term drought and the causes of drought variability in the area, the effect of drought on the groundwater table condition, and the contribution of

potential groundwater management options are assessed. The study results indicated that the drought in Southeast Florida was driven by a combination of ENSO fluctuation (short-term drought variability) and AMO fluctuation (long-term drought variabilities). Since the early 1990s, the area has been receiving rainfall higher than the long-term average (by 16%). The combination of higher rainfall in August and lower rainfall in May and October results in uni-modality in the previously bi-modal rainfall regime in Southeast Florida. By modeling the groundwater table dynamics in the BA, we found that drought, causing groundwater recharge limitation and a decline of surface water stag in canals, has a regional influence on the position of the groundwater table. Sea-level rise and groundwater pumping have a more substantial impact over the groundwater table in the coastal region and close to the well-field areas, respectively. Given that drought has a regional influence over the groundwater table, its effect on long-term freshwater availability is sizeable. Application of a hypothetical artificial recharge zone in the western margin of the model domain indicated a promising potential to mitigate the groundwater table decline attributed to drought and pumping pressure. However, the feasibility of the recharge zone must be studied further.

TABLE OF CONTENTS

LIST OF TABLES

TABLE PAGE

LIST OF FIGURES

FIGURE PAGE

ABBREVIATIONS AND ACRONYMS

AMO	Multi Decadal Oscillation.
BA	Biscayne Aquifer.
ENSO	El Niño–Southern Oscillation.
PDO	Pacific Decadal Oscillation.
SFWMD	South Florida Water Management District.
SI	Saltwater Intrusion.
SPI	Standardized Precipitation Index

1. CHAPTER I: INTRODUCTION

1.1. Background

Coastal aquifers are subjected to stress conditions that threaten the wellbeing and sustainability of the freshwater ecosystem and ecosystem services (Konikow and Kendy, 2005; Ogden et al., 2005; Werner et al., 2013). Among others, the effect of limited groundwater recharge, groundwater pumping, and sea-level rise instigate hydrological stress on coastal aquifers that often compromise the quality and quantity of freshwater resources in coastal regions. More than 60% of the world's population resides within 100 km of a coast, and coastal regions are increasingly urbanized. A high level of urbanization increases surface imperviousness and prevents groundwater recharge. The expansion of urban infrastructure is associated with increased surface imperviousness, and thus, a high level of surface runoff.

Furthermore, by decreasing rainfall volume, the incidence of drought has an additional effect in limiting recharge to coastal aquifers (D'Odorico and Bhattachan, 2012). By increasing the groundwater demand and high surface imperviousness, urbanization promotes enhanced aquifer mining. Sea level rise is another stress condition that impedes water quality in coastal freshwater systems (Ferguson and Gleeson, 2012; Langevin and Zygnerski, 2013; Werner and Simmons, 2009). As limited groundwater recharge and groundwater pumping provoke groundwater table decline, urbanized coastal aquifers and related freshwater dependent ecosystems in coastal regions remain vulnerable to the adverse effect of sea-level rise. Therefore,

understanding how limited groundwater recharge, pumping pressure, and sea-level rise influence a given coastal groundwater dynamics is an essential input for sustainable freshwater water management, planning, and decision making.

Hydrological drought is a rainfall deficit below the long-term normal, leading to adverse effects on surface and groundwater resource availability (Palmer, 1965; Tallaksen and Van Lanen, 2004). Regionally, hydrological drought is driven by the combined effects of ocean and atmosphere interaction modes. Prolonged gain or loss of rainfall is a reflection of the Pacific Decadal Oscillation (PDO) and Atlantic Multidecadal Oscillation (AMO) (Obeysekera et al., 1999). Driven by the sea surface temperature changes in the Atlantic Ocean from 0° to 60° N and the Pacific Ocean poleward of 20° North, AMO and PDO are the principal drivers to long-term regional hydroclimatic variability (Kiem et al., 2003). When combined, El Niño Southern Oscillation (ENSO) plus AMO and PDO trigger hydrological extremes, leading to dryness or flooding. ENSO defines the changes in sea surface temperature in the equatorial region of the Pacific Ocean. Short term hydrological drought in South Florida is driven by the La-Nina phase of ENSO (Abtew and Trimble, 2010; Obeysekera et al., 1999).

In South Florida, the incidence of drought limits surface water availability and decrease groundwater recharge (Abtew and Huebner 2002). For example, a rainfall decline by 30 inches was observed in the 1980 to 1982 drought (Abtew and Huebner 2002). The 1980 to 1982 drought caused a significant decrease in the surface water levels in Lake Okeechobee and the Everglades, inflow along canals, and in

groundwater head in the Biscayne Aquifer (BA). A decline in freshwater and groundwater head enhances drainage from the Everglades to the aquifer. Even so, high groundwater pumping causes a water table decline that, in combination with sea-level rise, are crucial drivers of Saltwater Intrusion (SI) in the BA (Hughes and White, 2014; Renken et al., 2005). As the water table in the aquifer declines, the water level in the Everglades also decreases. As a result, the overall hydrological stress conditions in the aquifer (drought, groundwater pumping, and sea-level rise) have extended control to freshwater availability in the Everglades and the BA by limiting groundwater recharge that would otherwise lead to an accelerated SI in the area.

Located in the Sothern Florida Peninsula (Figure 1-1), the BA is the sole source of water supply for more than seven million people in South East Florida (Marella and Berndt, 2005). In Miami-Dade County alone, water supply for more than 2.5 million residents relies on this aquifer (Prinos et al. 2014). Although the BA receives recharge from rainfall and leakage of water from canals, the hydrological stress in the aquifer is increasing over time. Like any other coastal aquifer, the BA is subject to a high level of hydrological tress conditions derived from the incidence of drought, groundwater pumping, and sea-level rise. Although the BA is considered as a highly productive groundwater reservoir, the position of the groundwater table is greatly influenced by the volume of recharge the aquifer receives from the Everglades wetland. Because of the high population pressure, groundwater pumping remains high. The incidence of drought and extensive surface imperviousness decreases

groundwater recharge decline. Furthermore, the effects of sea-level rise, including SI and coastal flooding, are issues of concern for the area. Together, these stress conditions imposed on the BA are threatening the wellbeing and sustainability of the freshwater dependent ecosystem, municipal, and agricultural uses of water in South Florida.

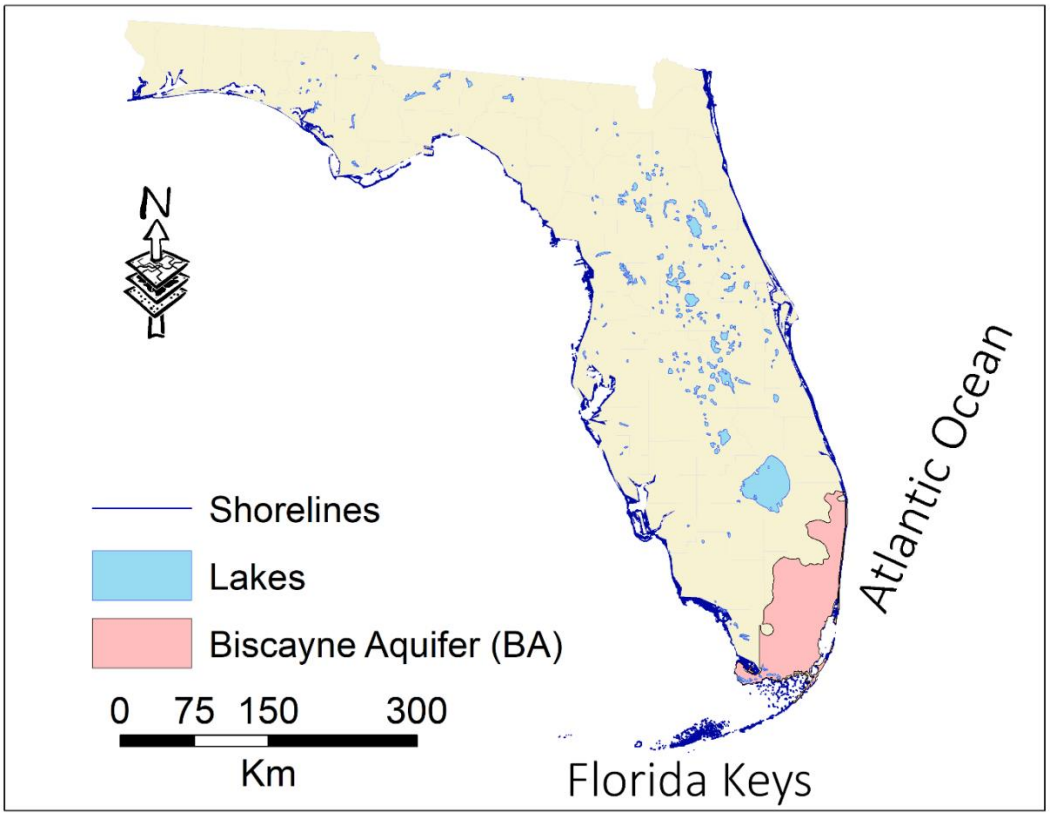

Figure 1- 1. The spatial extent of the BA (Source of the shapefile is the South Florida Water Management District, SFWMD).

The effect of hydrological stress conditions in South Florida results in water level decline in the BA, drying up of the Everglades wetland, and saltwater intrusion, when combined, can facilitate cause peat collapse. With peat collapse, the release of greenhouse gases, such as methane, is reported (Chambers et al., 2014; Orem et al.,

2015). Therefore, the overall effects of hydrological stress in the area can propagate into a global scale by adding more greenhouse gas into the atmosphere, as illustrated below (Figure 1-2). Such positive feedback allows unavoidable water demand units, such as public water supply, to overwhelm the system.

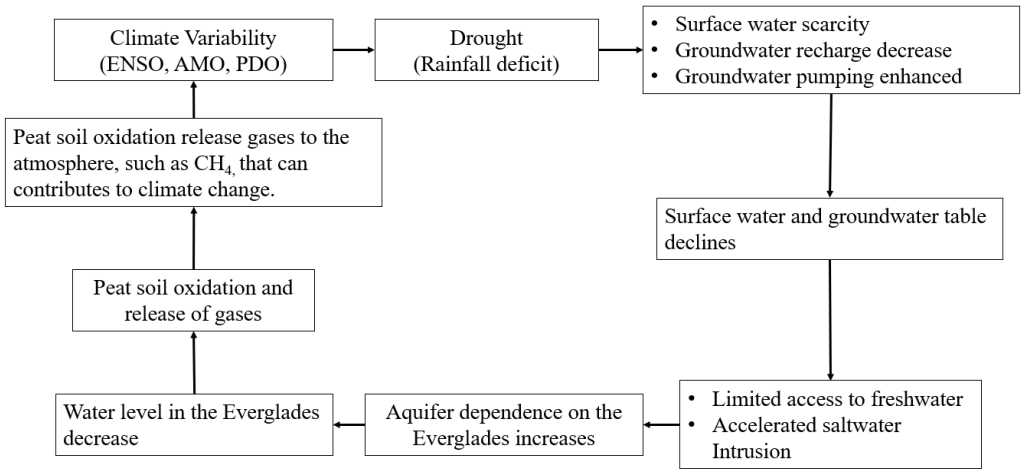

Figure 1- 2. Hypothetical feedback loop structure of natural climate variability and its effect on freshwater resources in the Everglades and the BA.

One of the world's largest environmental management and restoration projects, the Comprehensive Everglades Restoration Plan (CERP), is part of a healthy hydrologic regime in the Everglades. The CERP (USACE,1999) attempts to find a balance between restoring water levels and flows in the contemporary Everglades wetland while preventing flooding in the urban/agricultural areas to the east (Price et al., 2019). However, increasing hydrological stress conditions in the BA causes high dependence on groundwater recharge from the Everglades. So, the water supply system and undermining hydrological stress conditions in the BA are bottlenecks to the successful implementation of the CERP. Therefore, for a successful implementation of the CERP, one of the key strategies could be to enable a self-

resilient water supply system that is not dependent on the Everglades as a source of aquifer recharge. Such strategic design should be based on a thorough understanding of the aquifer system responds to changes in the above-mentioned stress conditions, as well as the testing of alternative water resources management options.

1.2. Previous studies

The link between ocean-atmospheric interaction modes and rainfall pattern has been a focus of several studies on a regional scale (Allan et al., 1996; Cullen and Grierson, 2009; Ding and Wang, 2005; Enfield et al., 2001; Feng and Hu, 2004; Hidalgo and Dracup, 2003; McCabe et al., 2004; Oglesby et al., 2012). These studies indicated that PDO, AMO, and ENSO are elated to rainfall distribution in the United States. In Florida, coupled AMO-ENSO fluctuations influence rainfall, so that AMO (cold) and ENSO (El Niño) create wetter conditions than AMO (warm) and El Niño combination (Goly and Teegavarapu, 2014). The effect of ENSO on rainfall variation in south Florida is well established (Abtew and Trimble, 2010; Drinkwater et al., 2014; McCabe et al., 2004; Obeysekera et al., 1999). Moses et al. (2013) indicated that the dry season rainfall distributions in South Florida are correlated to ENSO and that AMO influences wet season rainfall. Also, the influence of AMO fluctuations has been shown to alter water clarity in Lake Annie in Central Florida; water clarity was higher during the AMO cold phase (decreased rainfall) and lowered during the AMO warm phase (increased rainfall) (Gaiser et al., 2009). Although these ocean-atmosphere interaction modes are regional processes with a broad global influence, the net effect of these processes on rainfall distribution varies by region and time

scale. Therefore, for a regional water resource management system, understanding the link between the individual and combined effects of the drivers at the regional scale is essential.

A large volume of research and modeling work has been conducted on the geology and hydrology of the BA. Southeast Florida is characterized by a sequence of terrigenous and biogenic sedimentary depositions associated with fluctuations in sea-level during the late Pleistocene era (Cunningham and Florea, 2009; Parker et al., 1955; Reese and Cunningham, 2000; Wacker et al., 2014). Because the presence of primary porosity is highly enhanced by latter stage dissolution, the BA has high groundwater transmissivity (Fish and Stewart, 1991; Reese and Cunningham, 2000; Wacker et al., 2014). This highly permeable karstic aquifer (mean hydraulic conductivity of 9,000 m/d) also contains a considerable amount of freshwater (Cunningham, 2004; Wacker et al., 2014). As part of the surficial aquifer system in South Florida (Cunningham and Florea, 2009; Fish and Stewart, 1991; Meyer, 1989; Parker et al., 1955), the BA is defined by multiple stratigraphic layers (Causaras, 1985; Reese and Cunningham, 2000).

The importance of understanding the groundwater head dynamics of BA is recognized. A study conducted as part of the US geological survey to simulate the groundwater head for the water years 1945 to 1989 (Merritt, 1996) demonstrated that the groundwater head significantly changes if rainfall and evapotranspiration changes by greater than 20%. The effect of groundwater pumping is associated with the expansion of the radius of influence that ultimately leads to a decline in the

groundwater head (Brakefield et al., 2013). The water level in canals and rainfall conditions are reported to have a direct link with the groundwater level of the aquifer (Lohmann et al., 2012). A comprehensive modeling work with multiple scenarios has indicated the impact of pumping, sea-level rise, and leakage from canals on the position of the freshwater saltwater interface (Hughes and White, 2014). This latest study reports that changes to the saltwater interface at the base of the BA for the period 1996 to 2010 are associated with changes in pumping, sea-level rise, and leakage from canals. Despite all these modeling and research findings, the complicated nature of the surface water-groundwater interaction, the highly controlled flow system, and the location in juxtaposition to the Atlantic Ocean has hindered our complete understanding of the area. Questions like, "how does the groundwater table respond to combined stress conditions?", and "what are plausible long-term water resource management options to sustain freshwater availability in the area?" remain unanswered.

1.3. Objectives

Although the geology, hydrology, and hydrogeology of the BA are well studied and documented, the long-term freshwater supply and sustainability of the aquifer system are not well defined. Neither the impact of hydroclimate variabilities and prolonged drought nor the fate of the aquifer under various stress conditions has been evaluated in adequate detail. However, groundwater head decline due to drought-driven limitation of recharge and ever-increasing groundwater pumping is evidence that the hydraulic gradient between the freshwater and sea surface can

decrease. The decreasing gradient will enhance the already on-going SI problem in the aquifer. Current groundwater management practices do not provide clear insight into what could happen to SI given decadal and multi-decadal hydroclimate variabilities, persistent drought, and high levels of groundwater pumping. Hence, SI remains a threat to freshwater availability in the BA. A fully integrated knowledge base on the BA's groundwater table fluctuation is vital to develop a sustainable freshwater management strategy for South Florida. It is now necessary to study how long-term hydroclimate variability and hydrological stress affect the groundwater level (at the regional scale). Therefore, the general objective of this research was to define a groundwater management option for the BA from the perspective of improving the resilience of public water supply without compromising ecosystem services. Accordingly, the specific objectives of the study are:

- to understand historical rainfall trend and drought variability in southeast Florida;
- to evaluate the links between drought variability in South Florida and different global ocean-atmospheric interaction modes;
- to simulate the dynamic response of groundwater level to hydrological stress conditions; and
- to assess the potential contribution of groundwater management options to mitigate the adverse effect of hydrological stress conditions.

1.4. Significance of the research

The goal of this research is to realize a sustainable freshwater dependent ecosystem by effectively minimizing the dependence of public water supply systems from recharge to groundwater from the Everglades wetland system. Understanding how the BA responds to the stress conditions is a crucial part of achieving the goals outlined in the Comprehensive Everglades restoration plan (CERP).

As part of this dissertation research, the long-term rainfall trend and drought variability, as well as the drivers of drought, are assessed. Also, groundwater modeling and the analysis of the water table responses to varied and combined stress conditions are included. As part of the rainfall and drought study, the dissertation offers information that indicates the state of the contemporaneous rainfall regime and the potential of drought recurrence in short- and long-term time scales.

This study includes a successful simulation of the groundwater table fluctuation of the BA under different stress conditions and combined stress conditions. The groundwater modeling work offers vital information on the spatial distribution of hydrologically sensitive areas to varied stress conditions. This novel simulation of how the groundwater table responds to combined stress conditions provides a unique perspective towards our understanding of how the water table in the BA responses to combined stress conditions. This kind of combined stress-based simulation has not been previously reported, and it is thought to offer highly realistic hydrological stress conditions that the aquifer could face. Furthermore, the

application of a hypothetical recharge zone is another unique contribution that of this research offers. The assessment of groundwater management potential using regional groundwater recharge offers new insight into understanding the aquifer, and therefore, highlights the possibility of developing a self-resilient water supply system that would be reliable and sustainable without compromising the Everglades ecosystem. Accordingly, this research has addressed essential hydrological information and groundwater table fluctuations scenarios under various plausible scenarios.

1.5. Dissertation organization

This dissertation consists of six chapters. Chapter 1 is this introduction. Chapters 2, 3, 4, and 5 each address specific objectives of the dissertation. In Chapter 2, the results of the long-term rainfall trends and drought variability in Southeast Florida (Chapter 2) (Abiy et al., 2019b) are presented, together with a published manuscript (PLoS One). The study indicated that Southeast Florida is receiving rainfall higher than the long-term normal (by about 20%), while the previously bimodal rainfall regime is shifting to unimodality.

Chapter 3 presents the rainfall anomalies and drought in South Florida are connected to ENSO, AMO, and PDO. Applying a combination of statistical modeling techniques, this study has discovered that ENSO fluctuations define short-term drought fluctuations in Southeast Florida. In contrast, long-term variations are

significantly influenced by AMO fluctuations. The findings presented in Chapter 3 have been published in the Atmosphere Journal (Abiy et al., 2019a).

Chapter 4 presents a groundwater flow model of the BA developed using the USGS Modular Three Dimensional Groundwater Flow Model, MODFLOW 2000 (Harbaugh et al., 2000). The chapter details the modeling protocol, model design, and data use for assessing the BA's groundwater dynamic (water table fluctuation) attributed to stress conditions (drought, pumping pressure, and sea-level rise). Chapter 5 is a continuation of Chapter 4, which simulates the effect of individual and combined stress conditions on the groundwater table and assesses how artificial recharge can be used as a mitigation measure to reduce the adverse impact of combined stress conditions. The results show that under combined stress conditions, the inland groundwater table condition is subject to a decline, while the coastal groundwater table rises with sea-level rise. The addition of artificial recharge offers a potential solution to mitigate the adverse effects of drought, pumping pressure, and sea-level rise.

Chapter 6 delivers the conclusions and recommendations for further work. Suggestions for water management strategies and future research directions are also included.

References

Abiy, A.Z., Melesse, A.M., Abtew, W., 2019a. Teleconnection of regional drought to ENSO, PDO, and AMO: Southern Florida and the Everglades. Atmosphere (Basel). https://doi.org/10.3390/atmos10060295

Abiy, A.Z., Melesse, A.M., Abtew, W., Whitman, D., 2019b. Rainfall trend and variability in Southeast Florida: Implications for freshwater availability in the Everglades. PLoS One 14, e0212008. https://doi.org/10.1371/journal.pone.0212008

Abtew, W., Trimble, P., 2010. El Niño-Southern Oscillation Link to South Florida Hydrology and Water Management Applications. Water Resour. Manag. 24, 4255–4271. https://doi.org/10.1007/s11269-010-9656-2

Allan, R., Lindesay, J., Parker, D., 1996. El Niño southern oscillation & climatic variability, CSIRO publishing.

Beckage, B., Platt, W.J., Slocum, M.G., Panko, B., 2003. INFLUENCE OF THE EL NIÑO SOUTHERN OSCILLATION ON FIRE REGIMES IN THE FLORIDA EVERGLADES. Ecology 84, 3124–3130. https://doi.org/10.1890/02-0183

Brakefield, L.K., Hughes, J.D., Langevin, C.D., Chartier, K., 2013. Estimation of capture zones and drawdown at the Northwest and West Well Fields, Miami-Dade County, Florida, using an unconstrained Monte Carlo analysis: recent (2004) and proposed conditions. US Geological Survey.

Causaras, C.R., 1985. Geology of the surficial aquifer system, Broward County, Florida; lithologic logs. US Geological Survey,.

Cullen, L.E., Grierson, P.F., 2009. Multi-decadal scale variability in autumn-winter rainfall in south-western Australia since 1655 AD as reconstructed from tree rings of Callitris columellaris. Clim. Dyn. 33, 433–444. https://doi.org/10.1007/s00382-008-0457-8

Cunningham, K.J., Florea, L.J., 2009. The BA of southeastern Florida. Geogr. Fac. Publ. 20.

Chambers, L.G., Davis, S.E., Troxler, T., Boyer, J.N., Downey-Wall, A. and Scinto, L.J., 2014. Biogeochemical effects of simulated sea level rise on carbon loss in an Everglades mangrove peat soil. Hydrobiologia, 726(1), pp.195-211.

D'Odorico, P., Bhattachan, A., 2012. Hydrologic variability in dryland regions: impacts on ecosystem dynamics and food security. Philos. Trans. R. Soc. B Biol. Sci. 367, 3145–3157. https://doi.org/10.1098/rstb.2012.0016

Dai, A., Trenberth, K.E., Qian, T., 2004. A Global Dataset of Palmer Drought Severity Index for 1870–2002: Relationship with Soil Moisture and Effects of Surface Warming. J. Hydrometeorol. 5, 1117–1130.

Ding, Q., Wang, B., 2005. Circumglobal teleconnection in the Northern Hemisphere summer. J. Clim. 18, 3483–3505. https://doi.org/10.1175/JCLI3473.1

Drinkwater, K.F., Miles, M., Medhaug, I., Otterå, O.H., Kristiansen, T., Sundby, S., Gao, Y., 2014. The Atlantic Multidecadal Oscillation: Its manifestations and impacts with special emphasis on the Atlantic region north of 60°N. J. Mar. Syst. 133, 117–130. https://doi.org/10.1016/j.jmarsys.2013.11.001

Enfield, D.B., Mestas-Nuñez, A.M., Trimble, P.J., 2001. The Atlantic multidecadal oscillation and its relation to rainfall and river flow in the continental U.S. Geophys. Res. Lett. 28, 2077–2080. https://doi.org/10.1029/2000GL012745

Feng, S., Hu, Q., 2004. Variations in the teleconnection of ENSO and summer rainfall in northern China: A role of the Indian summer monsoon. J. Clim. 17, 4871–4881. https://doi.org/10.1175/JCLI-3245.1

Fish, J.E., Stewart, M.T., 1991. Hydrogeology of the surficial aquifer system, Dade County, Florida.

Gaiser, E.E., Deyrup, N.D., Bachmann, R.W., Battoe, L.E., Swain, H.M., 2009. Multidecadal climate oscillations detected in a transparency record from a subtropical Florida lake. Limnol. Oceanogr. https://doi.org/10.4319/lo.2009.54.6.2228

Goly, A., Teegavarapu, R.S. V, 2014. Individual and coupled influences of AMO and ENSO on regional precipitation characteristics and extremes. Water Resour. Res. https://doi.org/10.1002/2013WR014540

Harbaugh, B.A.W., Banta, E.R., Hill, M.C., Mcdonald, M.G., 2000. MODFLOW-2000, The U.S Geological Survey Modular Ground-water Model – User Guide to Modularization Concepts and the Ground-water Flow Process, Open File Report 00-92. https://doi.org/10.3133/ofr200092

Hidalgo, H.G., Dracup, J.A., 2003. ENSO and PDO Effects on Hydroclimatic Variations of the Upper Colorado River Basin. J. Hydrometeorol. 4, 5–23. https://doi.org/10.1175/1525-7541(2003)004<0005:EAPEOH>2.0.CO;2

Hughes, J.D., White, J.T., 2014. Hydrologic conditions in urban Miami-Dade County, Florida, and the effect of groundwater pumpage and increased sea-level on canal leakage and regional groundwater flow.

Kiem, A.S., Franks, S.W., Kuczera, G., 2003. Multi-decadal variability of flood risk. Geophys. Res. Lett. 30. https://doi.org/10.1029/2002GL015992

Konikow, L.F., Kendy, E., 2005. Groundwater depletion: A global problem. Hydrogeol. J. 13, 317–320. https://doi.org/10.1007/s10040-004-0411-8

Lohmann, M.A., Swain, E.D., Wang, J.D., Dixon, J., 2012. Evaluation of effects of changes in canal management and precipitation patterns on salinity in Biscayne Bay, Florida, using an integrated surface-water/groundwater model. US Geol Surv Sci Invest Rep 5009, 94.

Marella, R., Berndt, M., 2005. Water withdrawals and trends from the Floridan aquifer system in the southeastern United States, 1950-2000. USGS Geol. Surv. Circ. 1278.

McCabe, G.J., Palecki, M.A., Betancourt, J.L., 2004. Pacific and Atlantic Ocean influences on multidecadal drought frequency in the United States. Proc. Natl. Acad. Sci. 101, 4136–4141. https://doi.org/10.1073/pnas.0306738101

Merritt, M.L., 1996. Simulation of the water-table altitude in the BA, southern Dade County, Florida, water years 1945-89. US Geol. Surv. Water Supply Pap.

Meyer, F.W., 1989. Hydrogeology, ground-water movement, and subsurface storage in the Floridan aquifer system in southern Florida.

NOAA, 2007. El Niño, La Niña, and ENSO. NOAA Natl. Weather Serv. 1–2.

Obeysekera, J., Browder, J., Hornung, L., Harwell, M. a, 1999. The natural South Florida system I: Climate, geology, and hydrology. Urban Ecosyst. 3, 223–244. https://doi.org/doi: 10.1023/A:1009552500448

Ogden, J.C., Davis, S.M., Jacobs, K.J., Barnes, T., Fling, H.E., 2005. The use of conceptual ecological models to guide ecosystem restoration in South Florida. Wetlands 25, 795–809.

Oglesby, R., Feng, S., Hu, Q., Rowe, C., 2012. The role of the Atlantic Multidecadal Oscillation on medieval drought in North America: Synthesizing results from proxy data and climate models. Glob. Planet. Change 84–85, 56–65. https://doi.org/10.1016/j.gloplacha.2011.07.005

Orem, W., Newman, S., Osborne, T.Z. and Reddy, K.R., 2015. Projecting changes in Everglades soil biogeochemistry for carbon and other key elements, to possible 2060 climate and hydrologic scenarios. Environmental Management, 55(4), pp.776-798.

Palmer, W.C., 1965. Meteorological Drought. U.S. Weather Bur. Res. Pap. No. 45.

Parker, G.G., Ferguson, G.E., Love, S.K., 1955. Water resources of southeastern Florida, with special reference to geology and groundwater of the Miami area. USGPO,.

Price, R. and Schwartz, K. with Anderson, B. Boucek, R. Briceño,H. Cook, M. Fitz, C. Heithaus, M. Onsted, J. Rehage. J. 2019. Chapter 3: Water, Sustainability, and Survival in The Coastal Everglades: The Dynamics of Social-Ecological Transformation in the South Florida Landscape: 34-70. in Childers, D. L., Gaiser, E. and Ogden, L. (Eds). The coastal Everglades: the dynamics of social-ecological transformation in the South Florida landscape. Oxford University Press, NY.

Reese, R.S., Cunningham, K.J., 2000. Hydrogeology of the gray limestone aquifer in southern Florida. USGS,.

Renken, R.A., Cunningham, K.J., Zygnerski, M.R., Wacker, M.A., Shapiro, A.M., Harvey, R.W., Metge, D.W., Osborn, C.L., Ryan, J.N., 2005. Assessing the vulnerability of a municipal well field to contamination in a karst aquifer. Environ. Eng. Geosci. 11, 319–331. https://doi.org/10.2113/11.4.319

Tallaksen, L.M., Van Lanen, H. a J., 2004. Hydrological Drought, Volume 48: Processes and Estimation Methods for Streamflow and Groundwater, Development in Water Science.

Trenberth, K.E., 1996. El Nino definition. CLIVAR-Exchanges 1, 6–8.

U.S. ARMY CORPS OF ENGINEERS. 1999. Central and South Florida Project comprehensive review study. Final Integrated Feasibility Report and Programmatic Environmental Impact Statement, vols. 1–10. U.S. Army Corps of Engineers, Jacksonville District, Jacksonville, Florida, USA.

Wacker, M.A., Cunningham, K.J., Williams, J.H., 2014. Geologic and hydrogeologic frameworks of the BA in central Miami-Dade County, Florida. US Geol. Surv. Investig. Rep. 5138.

Werner, A.D., Bakker, M., Post, V.E.A., Vandenbohede, A., Lu, C., Ataie-Ashtiani, B., Simmons, C.T., Barry, D.A., 2013. Seawater intrusion processes, investigation and management: Recent advances and future challenges. Adv. Water Resour. 51, 3–26. https://doi.org/10.1016/j.advwatres.2012.03.004

2. CHAPTER II: RAINFALL TREND AND VARIABILITY IN SOUTHEAST FLORIDA: IMPLICATIONS FOR FRESHWATER AVAILABILITY IN THE EVERGLADES.

Abiy, A.Z., Melesse, A.M., Abtew, W., Whitman, D., 2019b. Rainfall trend and variability in Southeast Florida: Implications for freshwater availability in the Everglades. PLOS ONE 14, e0212008. https://doi.org/10.1371/journal.pone.0212008.

2.1. Abstract

Freshwater demand in Southeast Florida is predicted to increase over the next few decades. However, shifting patterns in the intensity and frequency of drought create considerable pressure on local freshwater availability. Well-established water resources management requires evaluating and understanding long-term rainfall patterns, drought intensity and cycle, and related rainfall deficit. In this study, the presence of rainfall monotonic trends was analyzed using linear regression and Mann–Kendal trend tests. Pettit's single point detection test examined the presence of an abrupt change of rainfall. Drought in Southeast Florida is assessed using the Standardized Precipitation Index (SPI) in a 3-, 6-, 12-, and 24-months scale, and the Fast Fourier Transform is applied to evaluate the frequency of each drought intensity. There was an increase of rainfall in most of the wet season months, the total wet season, and the annual total. The wet season duration showed a decrease driven by a decrease in October rainfall. Since 1990, the wet season and total annual rainfall exhibited an abrupt increase. The SPI analysis has indicated that extended wetness characterizes the contemporary rainfall regime since 1995, except for the incidence of

intermittent dry spells. Short-term droughts have 3-year to 5-year recurrence intervals, and sustained droughts have a 10-year and 20-year recurrence intervals. In Southeast Florida, prolonged drought limits freshwater availability by decreasing recharge, resulting in a longer hydro-period to maintain the health of the Everglades Ecosystem, and to control saltwater intrusion. The increasing dry season duration suggests the growing importance of promoting surface water storage and demand-side management practices.

Key words: Drought, South Florida, Hydrology, Data analysis, SPI, Spectral analysis.

2.2. Introduction

The increasing incidence of extreme hydroclimatic conditions, particularly drought, plays a vital role in regulating water resource availability. In Southeast Florida, rainfall is a significant component of the local hydrologic budget (Abtew et al., 2007; Obeysekera et al., 1999), with rainfall deficit limiting surface and groundwater availability. As water resources are entirely allocated, any change in the precipitation regime has a substantial impact on the local water management system (Abtew et al., 2007). The incidence of drought in the area forces water managers to revise water allocation practices and management criteria that are specific to drought. However, these revisions do not present long-term solutions. Improving freshwater availability in the area requires preparedness for water resource planning and management in the face of drought.

Natural hydroclimate reduces atmospheric moisture availability, resulting in meteorological drought (Mishra and Singh, 2011, 2010; Palmer, 1965; Wilhite and Glantz, 1985). Meteorological drought decreases soil water content, promoting slow plant growth, and directly affecting agricultural productivity (agricultural drought). Extended atmospheric dryness results in a prolonged but small-scale rainfall deficit (D'Odorico and Bhattachan, 2012; Tallaksen and Van Lanen, 2004) that can reduce surface water flow, groundwater recharge, and water in storage (hydrological drought).

In Southeast Florida, the incidence of drought has historically caused a decrease in surface water levels (Obeysekera et al., 1999; Swain, 2012; Wilcox et al., 2004). As surface water level decreases, groundwater recharge decreases, leading to groundwater level decline, which can trigger saltwater intrusion (Harvey and McCormick, 2009; Swain, 2012; Wilcox et al., 2004). Ultimately, drought in the area creates a complex challenge that limits freshwater availability, threatening the Everglades' vulnerable Ecosystem (DeAngelis et al., 1998; Perry, 2008). To curb the adverse effects of drought on the hydrological system, we must understand the evolution of drought in the area by analyzing and evaluating long-term historical rainfall trends and reconstructing historical drought cycles. Such an understanding can enhance our knowledge of the local drought variability at a different time domain, a key input to long-term resource allocation and strategic planning. Because the study of drought's hydrological impact in the area has limited coverage and is limited to the

short-term, it is necessary to conduct long-term drought analysis and identify implications to current and future water resource availability.

The objectives of this study are to 1) evaluate long-term (111 years) rainfall patterns, 2) describe historical drought conditions at different time scales, and 3) assess the frequency of different classes of drought in Southeast Florida. We have analyzed historical regionalized monthly rainfall data in Southeast Florida from 1906 to 2016. For such long-term historical hydrological drought evaluation, evapotranspiration and soil moisture are scarce. Therefore, by considering drought as a system continuum (Mishra and Singh, 2011, 2010; Swain, 2012; Wilcox et al., 2004), we have evaluated the local rainfall data using the Standardized Precipitation Index (SPI). Drought frequency is examined by using a Fast Fourier Transformation (FFT). Based on the overall analyses, we have evaluated and presented potential implications for regional freshwater availability.

2.3. Description of the study area

The Southeast Florida peninsula has a flat topography that rises from 0.0 m to 7.0 m above NAVD 88. The average elevation in the area is 1.5m (Figure 2-1). Around 25% of the area is urbanized land cover with a predominantly impervious surface. The Everglades wetland covers most of the study area, extending from the water conservation area southeast of Lake Okeechobee to the Florida Bay (DeAngelis et al., 1998; Perry, 2008; Renken et al., 2005; Sklar et al., 1999).

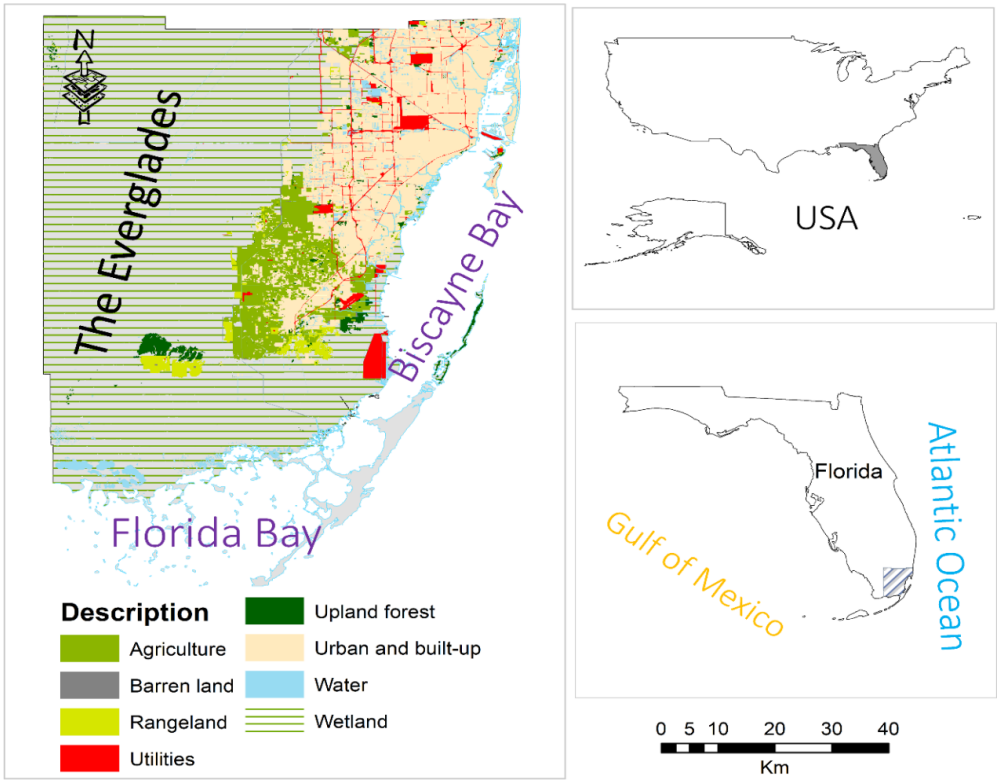

Figure 2- 1. Location map of the study area. Cartographic Boundary Shapefiles are freely available at US Census Bureau.

In Southeast Florida, the primary source of freshwater for more than 6 million people is the BA (Marella and Berndt, 2005). Surface water in lakes and the Everglades helps to maintain high groundwater head and control saltwater intrusion by providing groundwater recharge. The freshwater in the area is optimally allocated, and any shift in the hydrologic regime requires considerable readjustment on water allocation and management criteria (Marella and Berndt, 2005; Renken et al., 2005; Sklar et al., 1999). Increased groundwater pumping, the recurrence of drought, and sea-level rise threaten freshwater availability in Southeast Florida (Renken et al., 2005; Swain, 2012).

2.4. Hydrometeorology

Southeast Florida has a tropical monsoon climate characterized by hot and humid rainy summer and mild winters. The annual average minimum, mean, and maximum temperatures in the area are 15 °C, 26 °C, and 32 °C, respectively. A wide range of temperature records with a standard deviation of 3°C -6 °C is reported. Southeast Flori has a bi-modal rainfall distribution with a long-term total annual average of 1507 mm. The total annual average potential evapotranspiration (ETP) loss in the area ranges from 1220 mm to 1320 mm per year (Figure 2-2).

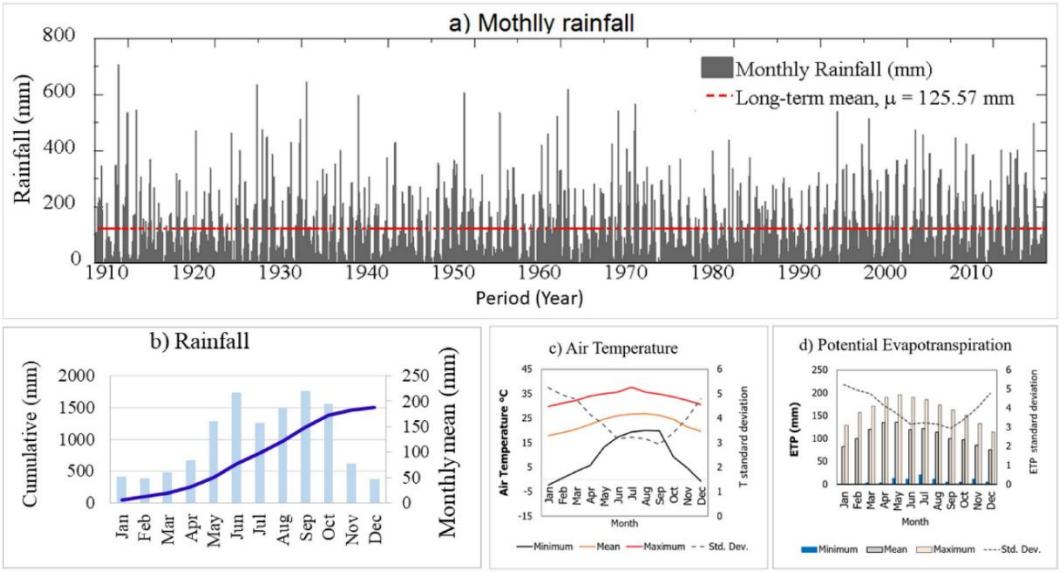

Figure 2- 2. (a) Monthly rainfall distribution in Southeast Florida from 1906-2016, (b) Histogram and cumulative rainfall monthly rainfall of Southeast Florida (1906-2016), C) Monthly composite air temperature, and d) potential evapotranspiration. Monthly composite data for air temperature and ETP are collected from the S331W climatological measurement station of the South Florida Water Management District.

Rainfall in Southeast Florida is highly variable and is driven by local and regional hydroclimatic factors (Obeysekera et al., 1999). The area receives rainfall from a convective, tropical cyclone, and frontal rainfall systems (Ali et al., 2000). Its

topography, geographic location adjacent to the ocean, and degree of urbanization have a significant effect on the spatial and temporal distribution of rainfall. A wide range of precipitation intensity characterizes the warm and humid summer season. There is a high range of variation in local long-term rainfall between months within a year. Likewise, specific months show a wide range of rainfall variation across different years (Table 2-1). Overall, the hydrologic regime in the area is divided into dry (November through April) and wet seasons (May through October) (Figure 2-2).

Table 2- 1. Descriptive statistics of mean monthly rainfall record from 1906 to 2016; where, STDEV and CV stand for the standard deviation and coefficient of variation, respectively.

Description	Dry						Wet					
Month	Nov	Dec	Jan	Feb	Mar	Apr	May	Jun	Jul	Aug	Sep	Oct
Mean Rainfall (mm)	77.2	46.9	52.0	48.9	60.5	85	160.8	217	157.4	186	220.4	194.6
STDEV (mm)	75.1	45.9	45.2	39.1	54.4	73.3	106.3	125.3	69.2	84.8	113.1	145.3
CV (%)	97.3	97.8	86.6	80	90	86.2	66.1	57.7	44	45.6	51.3	74.7

Around 75% of the total precipitation falls in the wet season, which comes from convective rainfall and tropical systems. The dry season rainfall is from frontal systems. Discharge from regional groundwater circulation and controlled release from upstream canals provide a considerable volume of freshwater input to the water balance in the area (Abtew et al., 2007).

Extreme hydroclimate conditions such as heavy rainfall leading to flooding, and precipitation deficit causing drought, are common in Southeast Florida. Sustained decline of rainfall below the long-term normal was reported in 1932,1955-57,1961-63, 1971-72, 1973-74, 1980-82, 1985, 1988-89, 1990, 2000-2001, 2006-2007, 2011-

2012 (Abtew et al., 2007; Obeysekera et al., 1999). These drought events have a strong association with the La-Nina phase of the ENSO events (Abtew and Trimble, 2010). When drought occurs, a decline in surface water level is observed in reservoirs, such as Lake Okeechobee. Furthermore, increasing intensity and duration of drought have caused a significant disturbance in the Everglades ecosystem (DeAngelis et al., 1998; Gentile et al., 2001; Obeysekera et al., 1999). The increasing incidence of drought is a critical challenge to the current and future water resources management in Southeast Florida, by decreasing freshwater supply. In contrast, the demand for freshwater in the area will remain high.

2.5. Dataset and Methodology

2.5.1. Rainfall data

Regional monthly rainfall data from 1906 to 2016 was obtained from the Florida Climate Center (FCC) (http://climatecenter.fsu.edu/products-services/data/precipitation/miami), who acquired their data from the National Weather Service's Cooperative Observation (NWSCO) network and the Automated Surface Observing System (ASOS). The rainfall station at Miami International Airport (MIA) was the most comprehensive data source used by the FCC to develop the regional monthly rainfall data. NWSCO and ASOS data fill the gaps left by the MIA rainfall records. Studies in South Florida indicate that a station can represent the monthly regional rainfall within an 80 km distance (Abtew et al., 1993; Ali et al., 2000). Therefore, this data is representative of Southeast Florida regionalized rainfall.

2.5.2. Rainfall trend evaluation

The rainfall trend was evaluated in three categories. The first group is the sequential time series rainfall data based on a month-by-month record. The second category is the analysis of interannual variability, which uses annual maximum, minimum, and mean, and the total rainfall of wet (MJJASO) and dry (NDJFMA) seasons. The last category constitutes an evaluation of the total yearly rainfall trend.

Monotonic and stepped trend detection approaches to evaluate rainfall trends. The presence of a monotonic rainfall trend was examined using linear regression and Mann–Kendal (MK) trend tests (Abdi, 2007; Kendall and Gobbons, 1990; Mann, 1945). The linear regression test has the advantage of evaluating linear temporal trends. The t-test statistics evaluate the statistical significance of the monotonic trend defined by linear regression. The MK test is a robust non-parameter, ranked, monotonic trend test that indicates the presence of an upward or downward trend. Z-score is used to assess the significance of the trend detected by the MK test. The rate of change of the trend detected by the MK test is calculated using the Sen-Theil trend line slope estimate (Sen's slope). Sen's slope defines the rate of long-term rainfall data's monotonic trend (Irizarry-Ortiz et al., 2013; Sen, 1968; Theil, 1992; Vujica Yevjevich, 1972). The details of the algorithms for the MK test and Sen's slope are well explained elsewhere (Mayowa et al., 2015). Pettitt's single point change detection test assesses the presence of an abrupt change of the mean of the long-term rainfall record (Katz et al., 2002; Mayowa et al., 2015; Storch and Zwiers, 1999). The detection test estimates the change of the mean between successive points in the

sequential time series data (Pettitt, 1979). All the analysis is calculated at a 95 % confidence interval.

2.5.3. Drought Evaluation

The historical drought in Southeast Florida was evaluated using two approaches. The first drought analsysi is based on the monthly rainfall residual as compared to the mean rainfall of the respective monthly rainfall and the second method of drought analysis is the application of SPI (Edwards and McKee, 1997; Mckee et al., 1993).

I. Drought evaluation with rainfall residual analysis

The difference of each month's rainfall record from the long-term mean of each corresponding month is calculated to evaluate the long-term monthly rainfall residual. The residual represents the overall wetness or dryness of each month as compared to the long-term mean of each corresponding month. With this approach, a year-month matrix of the rainfall residual is interpolated by using the Empirical Bayesian Kriging (EBK) package in ArcGIS 10.4. EBK was selected because it includes more accurate standard errors of forecasting by developing an interpolated surface. Geostatistical evaluation by kriging is among the best interpolation methods for evaluating monthly rainfall distribution in the South (Abtew et al., 1993; Ali et al., 2000; Krivoruchko, 2012).

II. Drought evaluation with Standardized Precipitation Index (SPI).

The regionalized rainfall record from 1906 to 2016 is used to compute SPI (Edwards and McKee, 1997; Mckee et al., 1993; Wu et al., 2007). SPI can establish the incidence of drought using rainfall data and has the flexibility to calculate droughts in different time windows, such as 3-, 6-, 12-, and 24-months. Therefore, it can effectively evaluate drought duration and magnitude. SPI results can be used to establish the frequency of different intensities of drought (Guttman, 1999; Wu et al., 2007). The use of 30 to 50 years of monthly information is recommended for SPI-3 to SPI-24 analyses. For drought evaluation over a longer time window, SPI-24 or longer, more than 60 years of data is recommended (Wu et al., 2007). SPI calculation requires normally distributed rainfall data. However, long-term monthly rainfall data is not normally distributed. For rainfall data with a gamma probability distribution function, an approach to estimating SPI by using cumulative probability is analytically solved (Edwards and McKee, 1997; Mckee et al., 1993) with the following equation:

$$\mathrm{SPI} = \begin{cases} -\left(t - \frac{c_0 + c_1 + c_2 t^2}{1 + d_1 t + d_2 t^2 + d_3 t^3}\right), \\ t = \sqrt{\ln\left(\frac{1}{H(x)^2}\right)}, \quad 0 < H(x) \leq 0.5 \\ t - \frac{c_0 + c_1 + c_2 t^2}{1 + d_1 t + d_2 t^2 + d_3 t^3}, \\ t = \sqrt{\ln\left(\frac{1}{1 - H(x)^2}\right)}, \quad 0.5 < H(x) < 1 \end{cases} \tag{2-1}$$

where x is a continuous random variable, and in this case, x is the observed rainfall data in a given time window (the running sum in 3-,6-,12-, and 24-moths time window). H(x) is a modified cumulative probability as a function of the probability of no rainfall at x=0, and the constant values are given as:

$c_0 = 2.515517$, $c_1 = 0.802853$, $c_2 = 0.010328$,

$d_1 = 1.432788$, $d_2 = 0.189269$, $d_3 = 0.001308$.

The equation is valid only if the rainfall has a gamma probability distribution (Guttman, 1999). For effective implementation of the above equation, evaluation of the rainfall data distribution is required. A MATLAB function that solves equation (1) is used to evaluate SPI in 3-, 6-, 12-, and 24-months.

III. Drought severity analysis

Drought severity (D_s) is a measure of the continuation of an event drought over time. In this case, D_s is the cumulative negative SPI values, given as:

$$D_s = \sum_{i=1}^{n} SPIi \qquad \forall\ SPI < 0 \qquad (2\text{-}2)$$

where D_s is the drought severity, n is drought duration, and i is SPI values of successive months of the given SPI-x such that the SPI is negative.

IV. Drought frequency analysis

The Fourier transform is used to calculate the frequency of wet-dry cycles evaluated by SPI-x (Fleming et al., 2002). For such hydrological data with equal sampling interval and specific period, the Discrete Fourier Transform (DFT) frequency analysis is commonly applied (Fleming et al., 2002; Press et al., 1992):

$$X_j = \sum_{k=0}^{N-1} x_k e^{-i\frac{2\pi}{N}kj} \quad (2\text{-}3)$$

$$k = 0,1,\dots,N-1 \text{ and } j = 0,1,\dots,N-1$$

where X_j is the j^{th} discrete frequency component of the SPI-x time sequence x_k, N is the total number of the data, and -*i* is a complex number, $i = \sqrt{-1}$.

Alternatively, the transform result can be interpreted by using the amplitude spectra or power spectral density (PSD). The amplitude spectra is a normalized absolute value of the complex array, and the PSD is a standardized product of the frequency-domain signal and its complex conjugate, given as:

$$A = \frac{|X_i|}{N}, \text{ and} \quad (2\text{-}4)$$

$$P_j = \frac{X_j X_j^*}{N*N} = \frac{|X_j|^2}{N^2} \quad (2\text{-}5)$$

where A is the scaled amplitude spectra, and P_j is the power spectral density.

2.6. Results and discussion

This section contains the trend analyses of monthly, interannual, and yearly rainfall evaluated by linear regression and MK trend tests. We present the results of long-term rainfall homogeneity for seasonal and total annual records, the historical drought evaluation, drought severity, and drought frequency, and we discuss the implications of rainfall trend and drought to freshwater availability.

2.6.1. Monthly rainfall trend and homogeneity

There is a decreasing pattern in the monthly rainfall for October, November, January, and May, and an increasing pattern for February, March, April, July, December, June, August, and September (Figure 2-3).

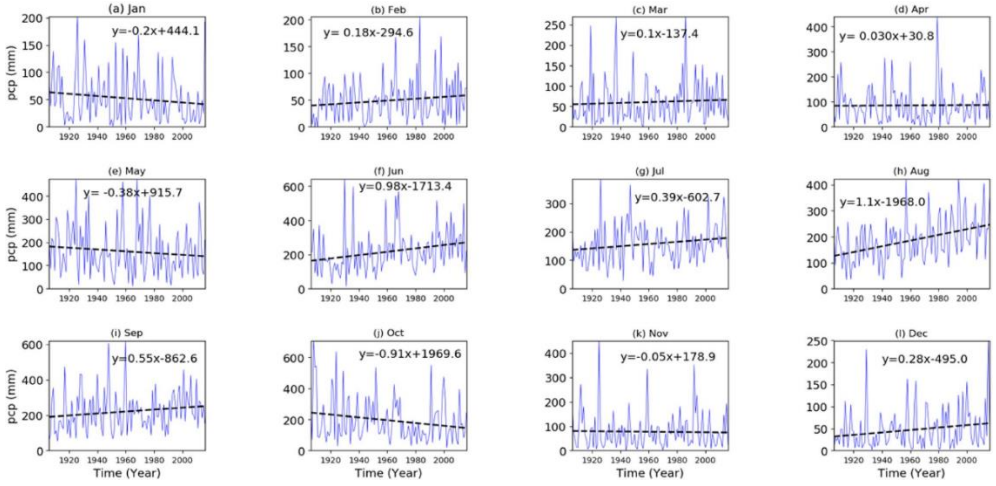

Figure 2- 3. Monthly rainfall regression analysis.

However, only the rainfall trends in October, June, and August are statistically significant (Table 2-2). The decreasing trend in October is 0.91mm/year, while the

rainfall for June and August are increasing 0.98 mm/year, and 1.1 mm/year, respectively (Table 2-2).

Table 2- 2. Test statistics of monthly rainfall trend test. For a 95% confidence interval, the computed p-value of less than 0.05 indicates the presence of trend, and the MK test statistics |Z| >1.96 indicates the presence of a significant trend.

Month	Jan	Feb	Mar	Apr	May	Jun	Jul	Aug	Sep	Oct	Nov	Dec
m	-0.2	0.18	0.1	0.03	-0.38	0.98	0.39	1.1	0.55	-0.91	-0.05	0.28
t	-1.50	1.52	0.62	0.13	-1.22	2.73	1.91	4.79	1.66	-2.14	-0.23	2.06
P(t)	0.14	0.13	0.53	0.90	0.22	**0.007**	0.058	< **0.0001**	0.099	**0.035**	0.82	**0.042**
mu	52	48.9	60.5	85	160.8	217	157.4	185.95	220.4	194.6	77.2	46.9
Kendall's tau	-0.11	0.08	0.08	0.00	-0.08	0.22	0.13	0.27	0.14	-0.09	0.02	0.12
p-value	0.09	0.25	0.21	0.98	0.20	0.00	0.04	< 0.0001	0.03	0.16	0.77	0.05
Z	-1.69	1.16	1.26	-0.03	-1.28	3.50	2.10	4.27	2.21	-1.40	0.30	1.93
Sen's slope	-0.17	0.12	0.01	0.00	**-0.36**	**1.00**	**0.41**	**1.02**	**0.71**	**-0.42**	0.03	0.17
w	3.45	3.25	4.01	5.64	**10.67**	**14.4**	**10.45**	**12.34**	**14.63**	**12.91**	5.12	3.11

m= slope of the regression line (mm/year), mu= average rainfall (mm), and w= rainfall contribution (percent).

The rainfall for June, July, and August showed increases by 1.003mm/year, 0.408 mm/year, 1.025 mm/year, and 0.711 mm/year, respectively. The calculated test statistics of rainfall for June (3.5mm), July (2.1mm), August (4.3mm), and September (2.2mm) indicates the presence of a significantly increasing rainfall trend over the recorded period (Table 2-2).

The months of May through October contribute the most rainfall to the area (Table 2-2). Individually, June and August contribute almost 30% of the total annual precipitation. Hence, an increasing trend of rainfall for these months can have a significant impact on the total wet season rainfall. Because the increase in earlier months balances it, the decreasing precipitation trend in October might not influence

the total annual rainfall but may contribute to the shortening of the overall wet season duration (Table 2-2).

2.6.2. Interannual rainfall trend and homogeneity

Analysis of the interannual rainfall variabilities showed increasing rainfall trends for the mean annual (t=2.196, and p (t) =0.030) and wet season (t=2.192, p (t) =0.031) rainfall (Figure 2-4). The maximum and minimum monthly rainfall records did not exhibit a statistically significant trend.

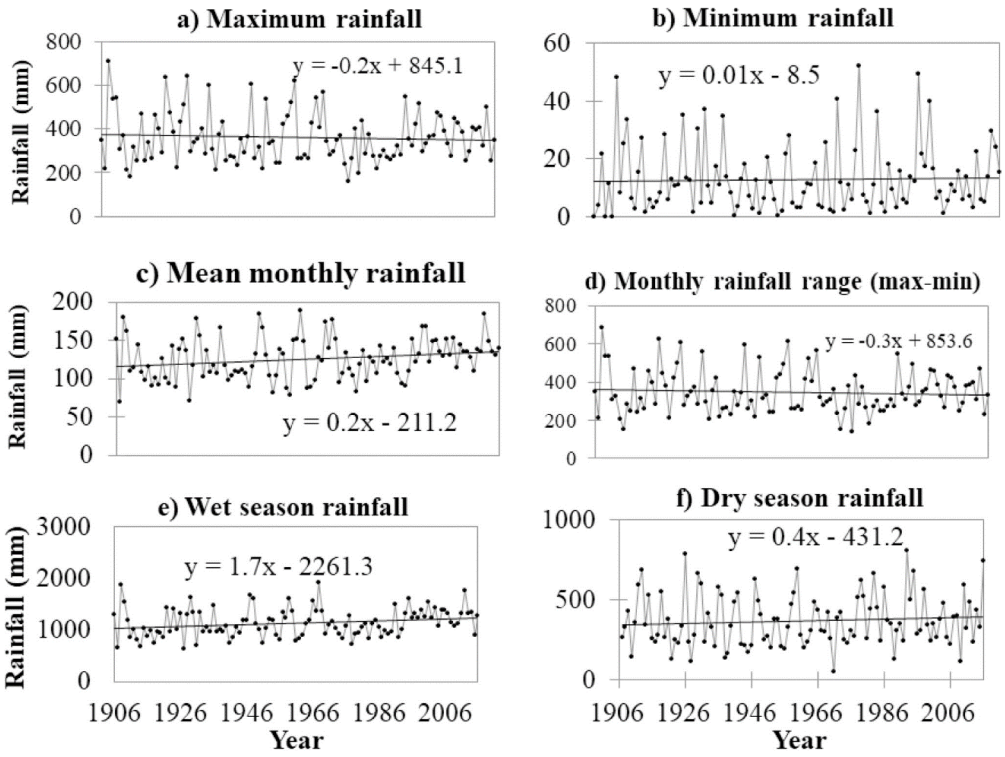

Figure 2- 4. Linear regression of rainfall data: (a) the maximum and (b) the minimum monthly values for each year; (c) The mean monthly values for each year; (d) Rainfall range: the difference between the maximum and minimum monthly value of each year; (e) Wet season rainfall: the sum of the monthly rainfall for May to October; and (f) Dry season rainfall: the sum of rainfall from November to April.

Under this category, we found a statistically significant trend (Z>1.96) for the annual average (Z=2.43) and wet season (Z=2.7) rainfall. The annual average and wet season total rainfall increased by 0.22m/year and 2.23mm/year, respectively. An abrupt change was spotted for the mean monthly and wet season total rainfall, only. Both changes were spotted in 1990 (Figure 2-5). The monthly mean exhibited an abrupt change of 15% rainfall increase, and the wet season rainfall showed an increase of 19%.

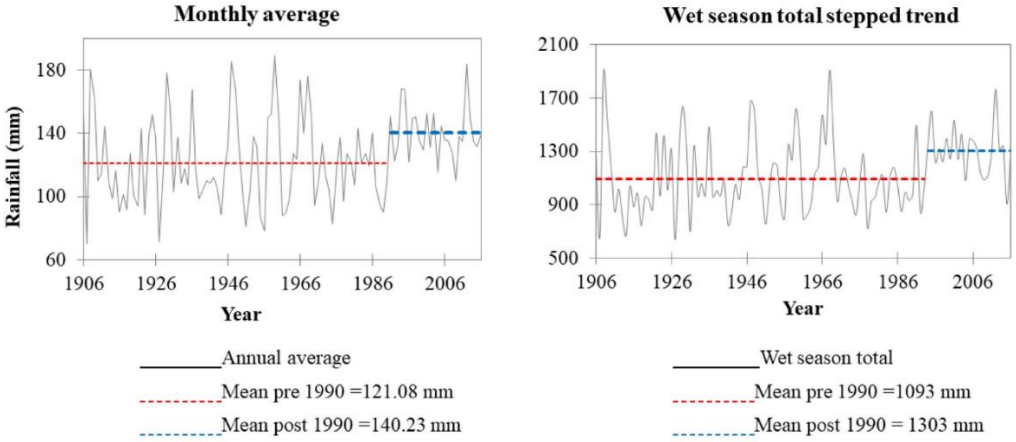

Figure 2- 5. The steeped trend of the long-term monthly average and wet season rainfall. Both have indicated the presence of an abrupt increase in the mean rainfall since 1990.

The total annual rainfall is increasing by 2.1mm/year (at t=2.2, and p (t) = 0.03). An overall increase of the monthly average and wet season total rainfall is attributed to the increase of rainfall in June and August. Like the mean annual and wet season rainfall, the total annual rainfall has shown an abrupt increasing trend since 1990 (Figure 2-6b). Therefore, we associate the increase in total annual rainfall with the observed increased rainfall for June and August. Interpolation of the observed monthly data as a year-month matrix indicates the decreasing trend of the

wet season duration (Figure 2-6-I), and this narrowing of the wet season duration is attributed to the decrease for October.

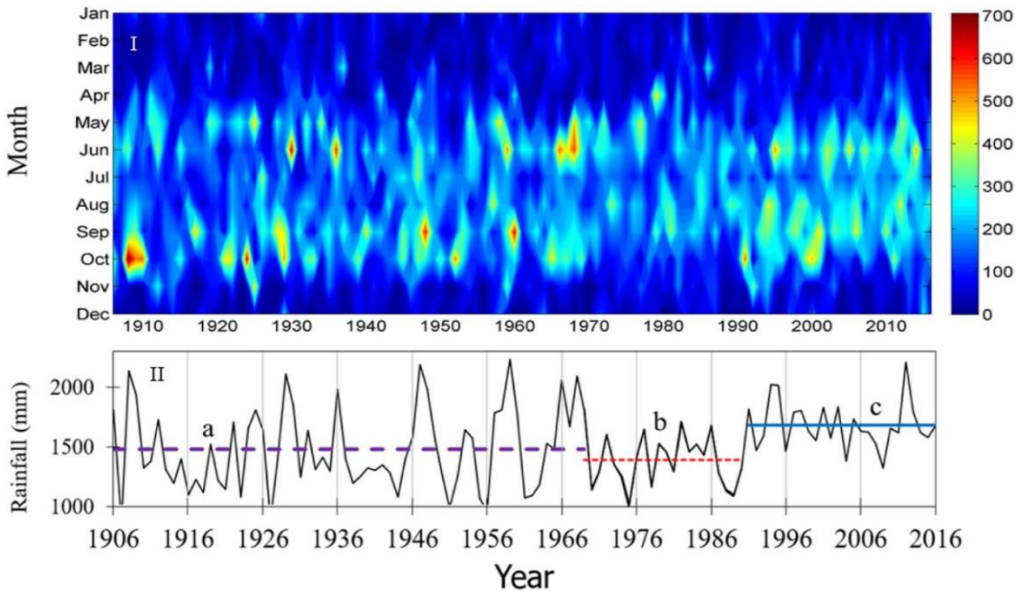

Figure 2- 6. I) Chart of the month-year data matrix and II) stepped trend of the total annual rainfall.

Through the study period (1906 - 2016), Southeast Florida experienced at least two statistically significant abrupt changes of the mean annual rainfall, spotted in 1969/70 and 1990. The mean rainfall pre-1969 was 1481mm (Figure 2-6-II-line a). From 1969 to 1990, the mean rainfall dropped to 1368mm (Figure 2-6-II, line b), and post-1990 it abruptly increased 1685mm (Figure 2-6-II, line c), accounting for an increase of 16%. This total annual rainfall increase is more or less consistent with the 15% increase of mean monthly rainfall. Although more than 75% of the rainfall in the area is received during the wet season, the post-1990 19% increase of rainfall in the wet seasons has not contributed much to the total annual rainfall increase. In essence, this is because of the decreasing rainfall trend in October.

July and August's rainfall increase and October's rainfall decline have led to an increasing amount of rainfall and a decreasing duration of the wet season. The increasing rainfall in August is gradually altering the rainfall regime from bimodal to unimodal. The abrupt increase of rainfall, the relative narrowing of wet season duration, and the alteration of bimodal rainfall distribution to unimodal distribution are indicated in the year-month matrix chart (Figure 2-6-I).

2.6.3. Drought evaluation

I. Drought evaluation with rainfall residual analysis

Three distinct patterns of dry and wet fluctuations are portrayed (Figure 2-7). The first condition is when all months in a year and successive years have more than average rainfall. The second condition is when the dry season becomes dryer, and the wet season becomes wetter. The third condition is defined as that all months are dry. The three patterns explain that the rainfall variability in the area is a function of rainfall quantity, timing, and duration. Further, it suggests the exposure of the area in a dryer dry season, or wetter wet season or vice versa and the potential of drought propagation through interannual, annual and multiple years scale.

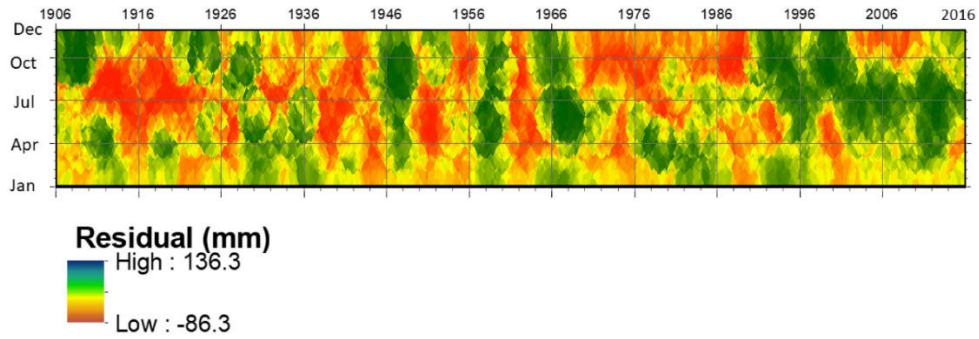

Figure 2- 7. Residual map of monthly rainfall. The deviation of the recorded monthly rainfall from the respective long-term mean monthly value, residual map.

There was a high degree of dryness over a range of years from 1910 to 1925, 1940 to 1947, 1952 to 1958, 1963 to 1966, and 1973 to 1980. Periods from 1908 to 1910, 1928 to 1931, 1945 to 1949, and 1964 to 1969 were wet years. With its distinct fluctuations of the wet and dry phases, the contemporary rainfall pattern in Southeast Florida since 1990 indicates the presence of sustained wetness.

The advantage of the rainfall residual analysis method is that it allows visual interpretation of the rainfall variability in two dimensions, enabling evaluation of the timing and extent of the rainfall deviation from the long-term mean value. The residual map (Figure 2-7) indicates the magnitude of the monthly rainfall deviation and the temporal propagation of rainfall deficit.

II. Drought evaluation with SPI

Drought evaluation with SPI begins with defining the probability distribution of the rainfall data. The normality test using Anderson-Darling ($A^2 = 40.9$) suggests that the regionalized long-term monthly rainfall data is not normally distributed. Evaluation of the regionalized long-term rainfall data with the gamma probability

distribution indicates that the two parameters have positive values (alpha = 1.3 and beta =96.8), confirming that the rainfall has a gamma distribution (Figure 2-8). Studies in South Florida indicate that the monthly rainfall in the area follows a gamma distribution (Abtew et al., 1993; Ali et al., 2000; Irizarry-Ortiz et al., 2013). Therefore, the SPI index can be used to evaluate drought effectively (Wu et al., 2007).

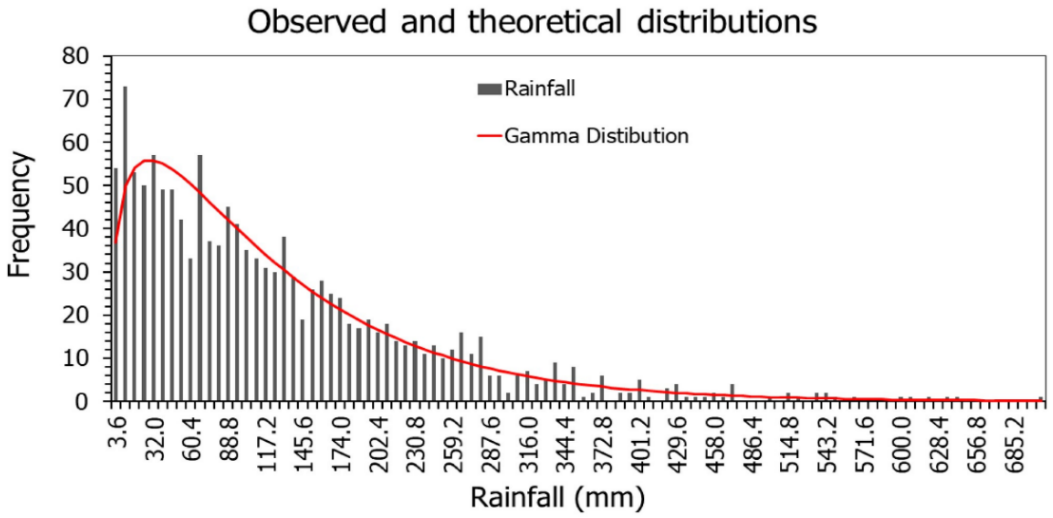

Figure 2- 8. Probability density function and fitted theoretical distribution.

The depth of rainfall deficit due to the propagation of drought is evaluated using the SPI in different time windows. SPI value has a mean of zero, and positive (negative) values indicate the presence of wet (dry) total rainfall within the time window under consideration (Edwards and McKee, 1997; Mckee et al., 1993). The different time window SPI (Figure 2-9) indicated seasonal and long-term precipitation variabilities. The SPI-3 and SPI-6 plots (Figures 2-9a and b) indicate interannual fluctuations, whereas the SPI-12 and SPI-24 (Figures 2-9c and d) indicate the long-term rainfall variability.

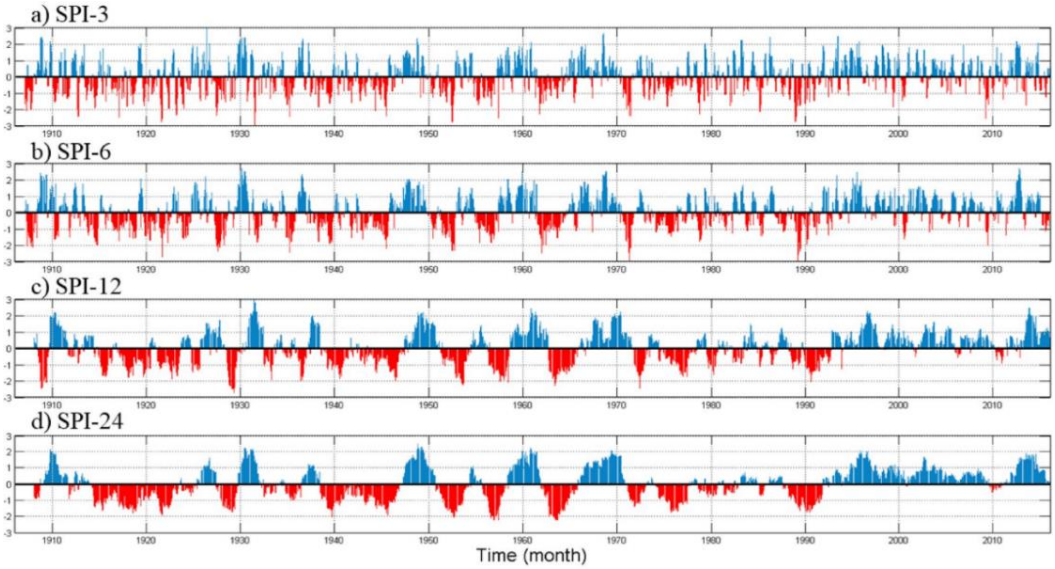

Figure 2- 9. Time series plot of the (a) SPI-3, (b) SPI-6, (c) SPI -12, and (d) SPI-24. The SPI value is the standard normal random variable of the sequential time series data with a positive value indicating wetness, and negative values representing dryness.

Besides the seasonal variations, the SPI-3 and SPI-6 reflect changes in the length of wet and dry seasons within a given year. The SPI-12 and -24 indicated that the area is in the wettest stage of the long-term natural wet and dry cycles.

Apart from incidences of dry spells, Southeast Florida has received prolonged wetness since 1990. However, the SPI analysis indicated that the effect of drought before 1990 was continued until 1994/5. The area has been in an extended wet phase since this time (plots SPI-12 and SPI-24). The prolonged contemporary SPI coincides with the sudden post-1990 increase of the total annual rainfall. Overall, the SPI analysis indicated the temporal propagation of drought, implying a delayed recovery of the hydrologic system after a sustained drought.

For a given time window, SPI ≥2.0 is referred to as an extreme wet condition, and SPI value of 1.5 and 1.0 are upper limits for very wet and moderately wet rainfall periods (Edwards and McKee, 1997; Mckee et al., 1993). SPI value between 1.0 and -1.0 refers to a neutral condition. SPI value between -1.5 and -1.0 indicates moderate drought, -2.0 to -1.5 indicates severe drought, and less than -2.0 indicates extremely severe drought (Edwards and McKee, 1997; Mckee et al., 1993). The rainfall deficit for these drought intensities is computed by combining the probability distributions of the rainfall and the corresponding cumulative distribution SPI value (Figure 2-10). Hence, the rainfall deficit for a given drought intensity in a specific time window can be outlined by projecting from the cumulative distribution of the SPI to the corresponding cumulative rainfall plot (Figure 2-10).

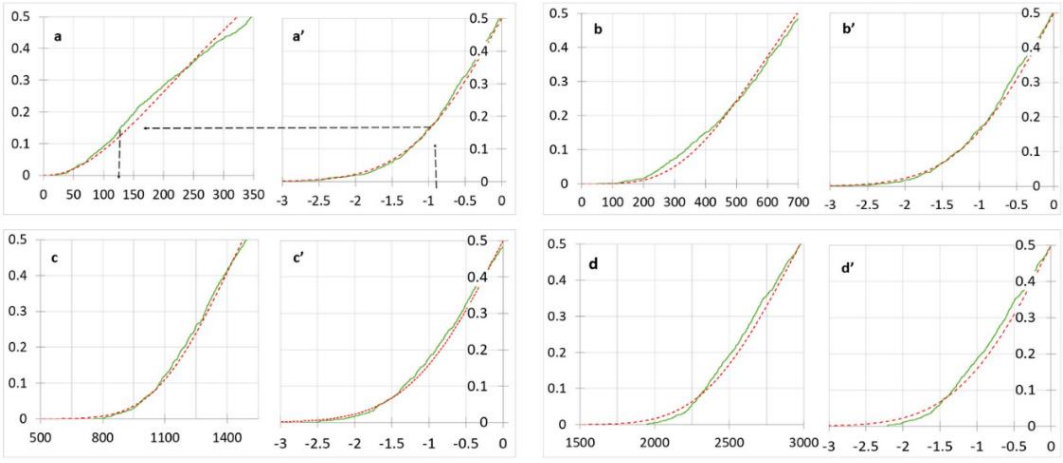

Figure 2- 10. Cumulative histograms for total rainfall and corresponding SPI's in different time window: a and a') 3-month total rainfall and SPI-3; b and b') 6-month total rainfall and SPI-6; c and c') 12-month total rainfall and SPI-12; and d and d') 24-month total rainfall and SPI-24.

The SPI cumulative frequency distribution and the corresponding rainfall cumulative histogram can be used to define the volume of rainfall deficit at different time windows. According to the proposed drought intensity classification using SPI, we tabulate a range of rainfall deficit that corresponds to various intensities of drought in different time windows (Table 2-3). Such a depth of rainfall deficit refers to the net loss of the total rainfall within the given time window.

Table 2- 3. Range of total rainfall deficit (mm) for different drought categories in various SPI time windows.

Drought Category	SPI range	3 months	6 months	12 months	24 months
Moderate drought	$-1.5 \leq SPI < -1$	130 to 80	416 to 300	1160 to 1030	2530 to 2290
Severe drought	$-2.0 \leq SPI < -1.5$	80 to 56	300 to 232	1030 to 910	2290 to 2040
Extreme drought	$SPI < -2.0$	>56	> 232	>910	>2040

For drought monitoring and applications to water use, allocation, and management, the relative incidence of rainfall deficit should be monitored in the different time windows. Consideration of drought timing is especially important for rainfall deficit in the 3-month to 6-month time windows. Such droughts make dry

seasons drier, and the cumulative effects could pause the hydrological drought. The dryness in the dry period limits the freshwater head in the Everglades. In general, seawater from the ocean intrudes inland during the dry season, and it is discharged back to the sea during the wet season. Monitoring and evaluation results in the BA (BA) indicate that only 20% of the intruded water is discharged back into the ocean (Kohout, 1960). The rest remains as a diluted solute in the coastal aquifer. Hence, the repeated occurrence of small-scale dry season droughts can promote a gradual buildup of salinity in the aquifer.

III. Drought severity

Hydrological system evaluations should be based on the effect of cumulative rainfall deficit in a given time window (Guttman, 1999; Wu et al., 2007). Drought intensity is the measure of the cumulative effect of uninterrupted negative SPIs. The study area has seen different phases of drought within various magnitudes and durations (Figure 2-11).

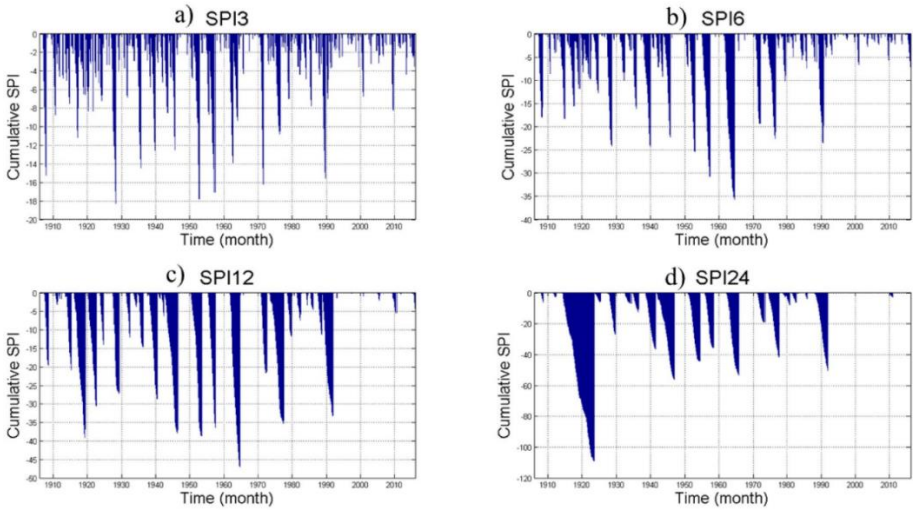

Figure 2- 11. Cumulative values of the (a) SPI-3, (b) SPI-6, (c) SPI-12, and (d) SPI-24.

Drought from 1910 to 2016 is an accumulated long-held but small-scale drought traced by SPI-3. Because the short-term droughts that are shown in SPI-3 from 1990 to 2016 are intermittent, the SPI-12 and SPI-24 plots do not show the incidence of drought in this period. Short ranged, but high magnitude drought events that are recorded by SPI-3 in 1928/29, 1952, 1957, and 1999 have indicated only limited propagation effect in an annual and two-year period. Since the repeated occurrence of small intensity droughts can have a cumulative effect, it potentially causes a significant impact on the local water resource system.

IV. Drought frequency

Application of the Fourier transformation requires a detrended input data. SPI is an index value with mean zero and standard deviation of one, which permits its use in this analysis. Droughts that persist between 3 and 6 months (SPI-3 and SPI-6) have 2 to 3 years of the cycle, while droughts that persist between 1 and 2 years (SPI-12

and-24) have 3 different frequency ranges (5 to 6, 9 to 10, and 10 to 20) (Figure 2-12).

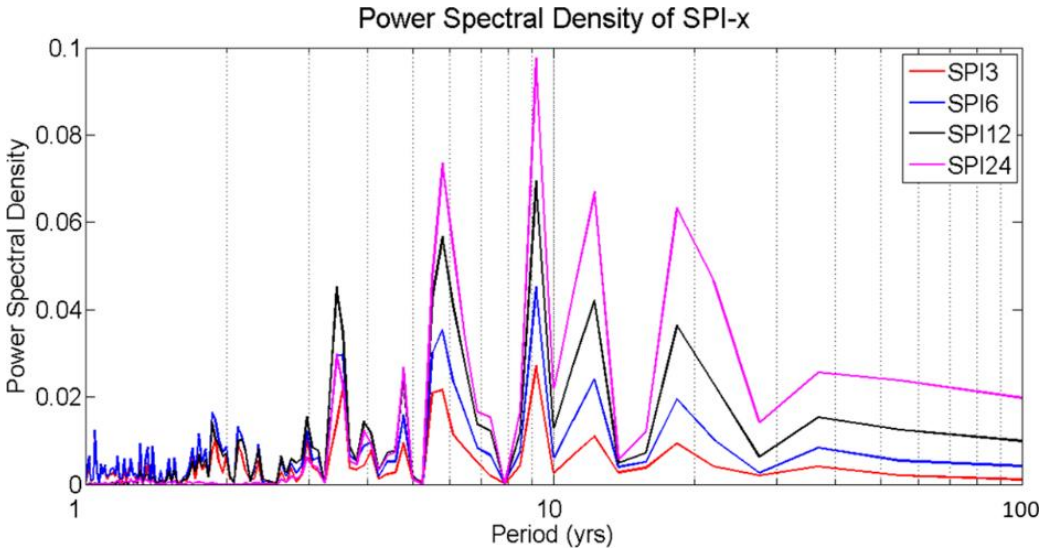

Figure 2- 12. Power spectral density of the SPI-3, -6, -12, and -24 values.

2.7. Implications for freshwater availability

The impact of hydroclimate variability on the freshwater availability in Southeast Florida is described based on the implications of increasing rainfall intensity and the incidence of drought. Freshwater in the area is stored in lakes, the Everglades wetland, and the aquifer systems. The human-made modifications in the area have amplified the high natural hydrologic connectivity among different reservoirs. In general, surface water reservoirs have a quick response to stress conditions, however, in Southeast Florida, the groundwater and surface water system are highly connected (Abtew et al., 2007; Obeysekera et al., 1999). As a result, the

feedback of the entire hydrologic system has quick response to any sustained stress or pulses.

The BA (BA) is highly dependent on recharge from the Everglades. For example, the rainfall decline of 30 inches (762 mm) due to drought in 1980 to 1982 caused a significant decline in the water level at Lake Okeechobee, the Everglades, flow along canals, and groundwater head in the BA (Abtew et al., 2007; Obeysekera et al., 1999). Rainfall deficit increases irrigation water demand, increases the dependence on groundwater pumping, leading to groundwater head decline in the BA.

The BA is a highly permeable karstic system with the hydraulic conductivity of 9,000 m/d that has a rapid response to rainfall recharge (Figure 2-13). Conversely, the groundwater table is highly elastic to hydrological stress conditions (Abtew et al., 2007). However, a decline in recharge reduces in the underlining aquifer's hydraulic pressure, increasing the hydraulic gradient along the coastal boundaries and the potential for saltwater intrusion into the freshwater system.

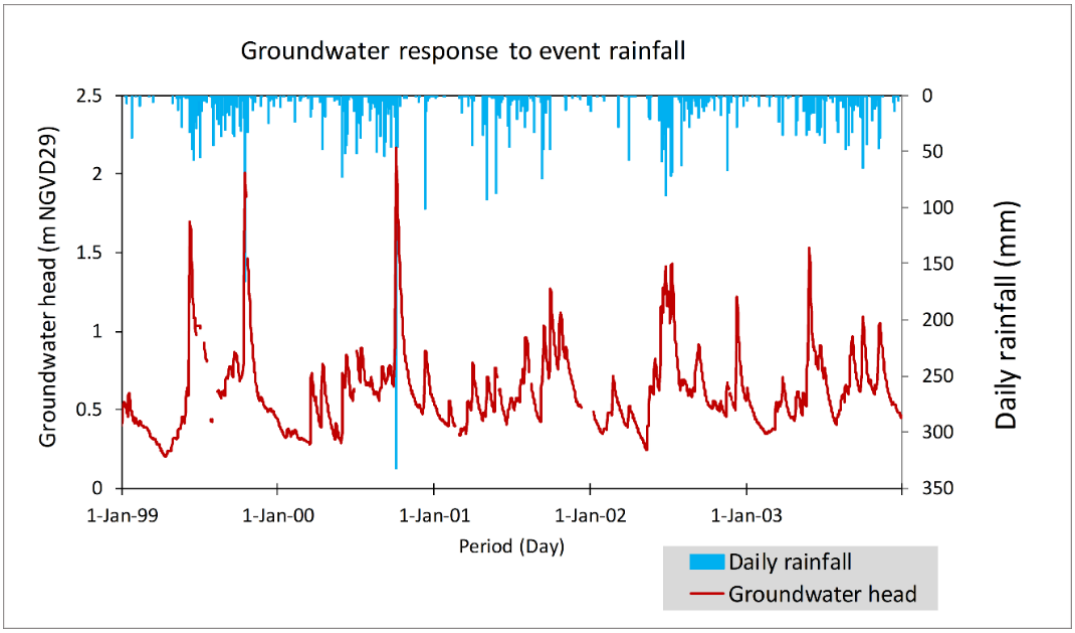

Figure 2- 13. The quick response of the BA groundwater table to event rainfall. The rainfall and groundwater measurements are collected from a station close to S331W (Figure 2-14).

Evaporative loss is another threat to freshwater sustainability in the Everglades. The Everglades have year-round evaporation that is higher than the rainfall it receives (Figure 2-14). Although the urban side has a positive balance, the net water balance is profoundly affected by groundwater pumping.

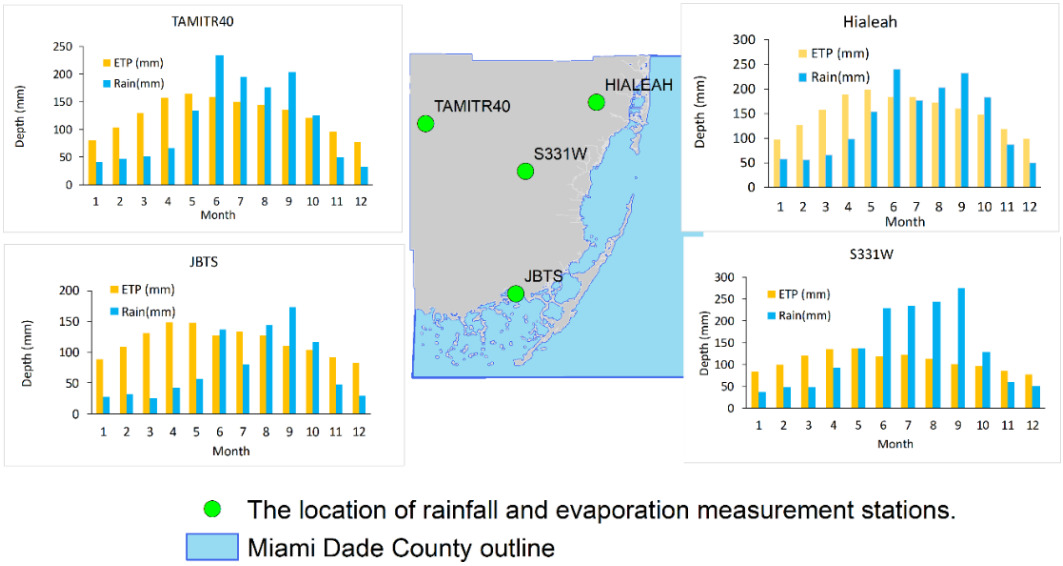

Figure 2- 14. Rainfall and ET record comparison between the coastal and Everglades sides of the study area. JBTS and Hialeah stations represent the coastal region, and TAMITR40 is located in the Everglades. S331W represents the central region of the study area.

The other perspective of hydroclimate variability in the area is the impact of decreasing wet-season duration. The decreasing wet season duration can cause a decrease in groundwater recharge. The elongation of the dry season increases the water user's dependence on water supply from storage and groundwater pumping. To better address such drought-driven freshwater availability deficits, appropriate water conservation practice is necessary.

Evaluation and selection of best water conservation practices to enhance the self-resilience of the BA will decrease the dependence of the BA on recharge from the Everglades. Water management options that can increase freshwater head in the Everglades and promote groundwater recharge into the BA have will reduce the hydrological stress on the Everglades. Also,

regulations to limit the groundwater demand in the area can decrease the susceptibility of freshwater supply to short and long-term hydrological stress conditions.

Promoting high freshwater head and expanding water storage mechanisms in the Everglades are promising hydrological water management options. This requires constructing an expansion of water storage that can enhance freshwater flow to the Everglades. The hydrological management measures benefit both the Everglades Ecosystem and water supply infrastructures. Conservation practices that discourage groundwater pumping can be of practical importance to maintain adequate groundwater head. In the face of high uncertainty to drought predictions, water resources planning in Southeast Florida shall consider multiple scenarios commensurate to different levels of stress conditions. However, an in-depth evaluation of the fate of the BA in the face of prologue drought and saltwater intrusion is a substantial input to review the existing water supply management system.

2.8. Conclusion and recommendation

From the analyses of the trend of monthly rainfall records from 1906 to 2016, results indicate an increase in the total wet season, the mean annual, and total annual rainfall. The wet season duration is decreasing due to a decrease in October rainfall. Rainfall in August is increasing, promoting a gradual shift of the local rainfall pattern from bimodal to a unimodal regime. The emergence of a uni-modal rainfall regime,

decreasing wet season duration, and an increased total annual rainfall suggest the increasing importance of freshwater storage and water harvesting in the area.

Given the persistent positive values of the SPI-12 and SPI-24 since 1994/5, Southeast Florida is in the wet phase of the long-term hydroclimate variabilities. The area is receiving rainfall much above the long-term average. Drought frequency analysis indicates that short-ranged drought events have a 3- to 5-years cycle, and sustained drought has a cycle of 10- to 20-years. Thus, Southeast Florida is prone to a minimum of one small-scale drought every three years and a minimum of one large-scale drought every ten years.

With the increasing dry season duration, it is possible that small-scale droughts can propagate over a more extended period. Prolonged small-scale drought tends to accumulate its effect gradually and unnoticed, and eventually compromising the sustainable water resource system. This can affect freshwater availability in the Everglades, disrupting the local ecosystem and ecosystem services.

Acknowledgment

This research is partially supported by the Everglades Foundation, FIU for Everglades fellowship, the Department of Earth and Environment, and the NSF CREST-CACHE project. The funders had no role in study design, data collection and analysis, decision to publish, or preparation of the manuscript. We would like to acknowledge our data sources the Florida Climate Center and the South Florida

Water Management District. The manuscript was proof read and polished in Center for Excellence in Writing at Florida International University; specifically, we are grateful to Charles A. Donate, Kay-Ann L., and Manny for arranging extra time to proofreading the manuscript. The authors are thankful to the journal editor and anonymous reviewers for providing substantial comments. This is contribution number 898 from the Southeast Environmental Research Center in the Institute of Water & Environment at Florida International University.

References

Abdi, H., 2007. The Kendall Rank Correlation Coefficient. Encycl. Meas. Stat. 508–510. https://doi.org/http://dx.doi.org/10.4135/9781412952644

Abtew, W., Obeysekera, J., Shih, G., 1993. Spatial Analysis for Monthly Rainfall in South Florida1. JAWRA J. Am. Water Resour. Assoc. 29, 179–188. https://doi.org/10.1111/j.1752-1688.1993.tb03199.x

Abtew, W., Pathak, C., Huebner, R.S., Ciuca, V., 2007. Chapter 2: Hydrology of the South Florida environment. South Florida Environ. Rep. 1, 2.1-2.72.

Abtew, W., Pathak, C., Huebner, R.S., Ciuca, V., n.d. 2010 South Florida Environmental Report Chapter 2: Hydrology of the South Florida Environment.

Abtew, W., Trimble, P., 2010. El Niño-Southern Oscillation Link to South Florida Hydrology and Water Management Applications. Water Resour. Manag. 24, 4255–4271. https://doi.org/10.1007/s11269-010-9656-2

Ali, A., Abtew, W., Van Horn, S., Khanal, N., 2000. Temporal and spatial characterization of rainfall over Central and South Florida. J. Am. Water Resour. Assoc. 36, 833–848.

D'Odorico, P., Bhattachan, A., 2012. Hydrologic variability in dryland regions: impacts on ecosystem dynamics and food security. Philos. Trans. R. Soc. B Biol. Sci. 367, 3145–3157. https://doi.org/10.1098/rstb.2012.0016

DeAngelis, D.L., Gross, L.J., Huston, M. a., Wolff, W.F., Fleming, D.M., Comiskey, E.J., Sylvester, S.M., 1998. Landscape Modeling for Everglades Ecosystem Restoration. Ecosystems 1, 64–75. https://doi.org/10.1007/s100219900006

Edwards, D.C., McKee, T.B., 1997. Characteristics of 20th Century drought in the United States at multiple time scales. Atmos. Sci. Pap. No. 634, May 1–30 174.

Fleming, S.W., Marsh Lavenue, A., Aly, A.H., Adams, A., 2002. Practical applications of spectral analysis of hydrologic time series. Hydrol. Process. 16, 565–574. https://doi.org/10.1002/hyp.523

Gentile, J.., Harwell, M.., Cropper Jr, W., Harwell, C.., DeAngelis, D., Davis, S., Ogden, J.., Lirman, D., 2001. Ecological conceptual models: a framework and case study on ecosystem management for South Florida sustainability. Sci. Total Environ. 274, 231–253.

Guttman, N.B., 1999. Accepting the Standardized Precipitation Index: a Calculation Algorithm1. JAWRA J. Am. Water Resour. Assoc. 35, 311–322. https://doi.org/10.1111/j.1752-1688.1999.tb03592.x

Harvey, J.W., McCormick, P. V., 2009. Groundwater's significance to changing hydrology, water chemistry, and biological communities of a floodplain ecosystem, Everglades, South Florida, USA. Hydrogeol. J. 17, 185–201. https://doi.org/10.1007/s10040-008-0379-x

Irizarry-Ortiz, M.M., Obeysekera, J., Park, J., Trimble, P., Barnes, J., Park-Said, W., Gadzinski, E., 2013. Historical trends in Florida temperature and precipitation. Hydrol. Process. 27, 2225–2246. https://doi.org/10.1002/hyp.8259

Katz, R.W., Parlange, M.B., Naveau, P., 2002. Statistics of extremes in hydrology. Adv. Water Resour. 25, 1287–1304. https://doi.org/10.1016/S0309-1708(02)00056-8

Kendall, M.G., Gobbons, J.D., 1990. Rank Correlation Methods, Science Forum.

Kohout, F.A., 1960. Cyclic flow of salt water in the BA of southeastern Florida. J. Geophys. Res. 65, 2133–2141. https://doi.org/10.1029/JZ065i007p02133

Krivoruchko, K., 2012. Empirical Bayesian Kriging. ESRI Press Fall 2012, 6–10.

Mann, H.B., 1945. Nonparametric Tests Against Trend. Econometrica 13, 245. https://doi.org/10.2307/1907187

Marella, R., Berndt, M., 2005. Water withdrawals and trends from the Floridan aquifer system in the southeastern United States, 1950-2000. USGS Geol. Surv. Circ. 1278.

Mayowa, O.O., Pour, S.H., Shahid, S., Mohsenipour, M., Harun, S. Bin, Heryansyah, A., Ismail, T., 2015. Trends in rainfall and rainfall-related extremes in the east coast of peninsular Malaysia. J. Earth Syst. Sci. 124, 1609–1622. https://doi.org/10.1007/s12040-015-0639-9

Mckee, T.B., Doesken, N.J., Kleist, J., 1993. The relationship of drought frequency and duration to time scales. AMS 8th Conf. Appl. Climatol. 179–184. https://doi.org/citeulike-article-id:10490403

Mishra, A.K., Singh, V.P., 2011. Drought modeling - A review. J. Hydrol. https://doi.org/10.1016/j.jhydrol.2011.03.049

Mishra, A.K., Singh, V.P., 2010. A review of drought concepts. J. Hydrol. https://doi.org/10.1016/j.jhydrol.2010.07.012

Obeysekera, J., Browder, J., Hornung, L., Harwell, M. a, 1999. The natural South Florida system I: Climate, geology, and hydrology. Urban Ecosyst. 3, 223–244. https://doi.org/doi: 10.1023/A:1009552500448

Palmer, W.C., 1965. Meteorological Drought. U.S. Weather Bur. Res. Pap. No. 45.

Perry, W.B., 2008. Everglades restoration and water quality challenges in south Florida. Ecotoxicology 17, 569–578. https://doi.org/10.1007/s10646-008-0240-y

Pettitt, A.N., 1979. A Non-Parametric Approach to the Change-Point Problem. Appl. Stat. 28, 126. https://doi.org/10.2307/2346729

Press, W.H., Teukolsky, S. a, Vetterling, W.T., Flannery, B.P., 1992. Numerical recipes in C (2nd ed.): the art of scientific computing, Technometrics. https://doi.org/10.2307/1269484

Renken, R.A., Dixon, J., Koehmstedt, J., Lietz, A.C., Ishman, S., Marella, R., Telis, P., Rogers, J., Memberg, S., 2005. Impact of anthropogenic development on coastal ground-water hydrology in Southeastern Florida, 1900-2000. US Geol. Surv. Circ. 1–87.

Sen, P.K., 1968. Estimates of the Regression Coefficient Based on Kendall's Tau. J. Am. Stat. Assoc. 63, 1379–1389. https://doi.org/10.1080/01621459.1968.10480934

Sklar, F., McVoy, C., Zee, R. Van, Gawlik, D., Swift, D., Park, W., Fitz, C., Wu, Y., Rudnick, D., Fontaine, T., Miao, S., Ferriter, A., Krupa, S., Armentano, T., Tarboton, K., Rutchey, K., Dong, Q., Newman, S., 1999. Chapter 2 : Hydrologic needs : The effects of altered hydrology on the Everglades. Everglades Interim Rep. 2:1–68.

Storch, H. Von, Zwiers, F.W., 1999. Statistical Analysis in Climate Research. J. Am. Stat. Assoc. 95, 1375. https://doi.org/10.1017/CBO9780511612336

Swain, E., 2012. Stochastic analyses to identify wellfield withdrawal effects on surface-water and groundwater in Miami-Dade County, Florida. J. Environ. Manage. 113, 15–21. https://doi.org/10.1016/j.jenvman.2012.08.033

Tallaksen, L.M., Van Lanen, H. a J., 2004. Hydrological Drought, Volume 48: Processes and Estimation Methods for Streamflow and Groundwater, Development in Water Science.

Theil, H., 1992. A Rank-Invariant Method of Linear and Polynomial Regression Analysis, in: Henri Theil's Contributions to Economics and Econometrics. pp. 345–381. https://doi.org/10.1007/978-94-011-2546-8_20

Vujica Yevjevich, 1972. Probability and Statistics in Hydrology, Water Resources pubblications.

Wilcox, W.M., Solo-Gabriele, H.M., Sternberg, L.O.R., 2004. Use of stable isotopes to quantify flows between the Everglades and urban areas in Miami-Dade County Florida. J. Hydrol. 293, 1–19. https://doi.org/10.1016/j.jhydrol.2003.12.041

Wilhite, D.A., Glantz, M.H., 1985. Understanding: The drought phenomenon: The role of definitions. Water Int. 10, 111–120. https://doi.org/10.1080/02508068508686328

Wu, H., Svoboda, M.D., Hayes, M.J., Wilhite, D.A., Wen, F., 2007. Appropriate application of the Standardized Precipitation Index in arid locations and dry seasons. Int. J. Climatol. 27, 65–79. https://doi.org/10.1002/joc.1371

3. CHAPTER III: TELECONNECTION OF REGIONAL DROUGHT TO ENSO, PDO, AND AMO: SOUTHERN FLORIDA AND THE EVERGLADES.

Abiy, A.Z., Melesse, A.M., and Abtew, W., 2019. Teleconnection of Regional Drought to ENSO, PDO, and AMO: Southern Florida and the Everglades. Atmosphere, 10(6), p.295. https://www.mdpi.com/2073-4433/10/6/295/htm.

3.1. Abstract

Drought variability is associated with global oceanic and atmospheric teleconnections driven by the Pacific Decadal Oscillation (PDO), the Atlantic Multidecadal Oscillation (AMO), the El Niño–Southern Oscillation (ENSO) and others. Climate teleconnections are impacted by a region's rainfall including drought and flooding implications and should be part of short- and long-term water management planning and operations. In this study, the link between drought and climatic drivers was assessed by using historical data from 110 years of regional rainfall in southern Florida and the Everglades. The objective of this study is to evaluate historical drought and its link with global oceanic and atmospheric teleconnections. The Standardized Precipitation Index (SPI) assesses regional historical drought in 3-, 6-, 12-, 24-, 36-, 48-, and 60-month periods. Each of the SPIs was used to analyze the association of different magnitudes of drought with ENSO, AMO, and PDO. Historical droughts were evaluated in different time windows indicating that there is a wet and dry cycle in the regional hydrology. The area is currently in the wet phase of the fluctuation since 1995 with some drought years in between. Regional historical rainfall anomalies and drought index relationships with

each driver and combination of drivers were statistically evaluated. The impact of ENSO fluctuation is limited to short-period rainfall variability whereas the long-period influence is from AMO and PDO.

Keywords: teleconnection; drought; Standardized Precipitation Index; SPI; South Florida hydrology; the Everglades; ENSO; AMO; PDO.

3.2. Introduction

Ocean–atmosphere interactions can regulate global energy flow and influence rainfall amounts and distribution on a regional scale (Abtew and Trimble, 2010; McCabe et al., 2004; Rayner, 2003). The link between these drivers, rainfall patterns, and general hydroclimate variability has been a focus of several studies on a regional scale (Allan et al., 1996; Cullen and Grierson, 2009; Ding and Wang, 2005; Enfield et al., 2001; Feng and Hu, 2004; Hidalgo and Dracup, 2003; McCabe et al., 2004; Oglesby et al., 2012). For example, the magnitude as well as spatial, and temporal distribution of rainfall in the United States are a function of different modes of ocean-atmosphere interaction processes as well as other global and regional conditions.

In Southeast Florida, the Pacific Decadal Oscillation (PDO), the Atlantic Multidecadal Oscillation (AMO), and El Niño–Southern Oscillation (ENSO) influence rainfall variation (Abtew and Trimble, 2010; Drinkwater et al., 2014; McCabe et al., 2004; Obeysekera et al., 1999). A detailed study based on 11 stations in Florida including Southeast Florida showed that AMO–ENSO influenced rainfall and concluded that AMO (cold) and ENSO (El Niño) created wetter conditions than

AMO (warm) and El Niño combination (Goly and Teegavarapu, 2014). A study of precipitation and climate teleconnections in the Greater Everglades and South Florida reported that the dry season is correlated to ENSO and that AMO influences wet season rainfall (Moses et al., 2013). A study using historical water clarity and climate teleconnections in Lake Annie in Central Florida reported that water clarity was higher during the AMO cold phase and lower during the AMO warm phase with a decrease and an increase in rainfall, respectively (Gaiser et al., 2009).

Although these ocean-atmosphere interaction modes are regional processes with a broad global influence, the net effect of these processes on rainfall distribution varies by region. Therefore, for a regional water resource management system, understanding the link between the individual and combined effects of the drivers at the regional scale is essential. The Everglades wetland system is a unique and complex ecohydrology facing stress from water quality degradation and changes in the magnitude and distribution of supply. As a result, state- and federally-supported ecological restoration programs were initiated in the early 1990s (Perry, 2004). In southern Florida, the water supply of the Everglades wetland system and the highly populated Miami-Dade County (Figure 3-1) is subject to hydroclimate variations.

South Florida is home to more than 6 million people and the Everglades ecosystem. The Everglades is a unique freshwater marsh with ecological and water supply importance covering over 5500 km^2 in its current reduced state. The public water source is the Biscayne Aquifer (BA). The BA is a shallow unconfined freshwater aquifer that provides water supply to Palm Beach, Broward, Miami-Dade,

and Monroe counties in Southeast Florida. Groundwater recharge to the aquifer is from rainfall and runoff, canal recharge, and the Everglades. Due to increased pumping to meet the increasing water demand, the recurrence of droughts is frequently compromising the sustainability of the aquifer. This has increased the dependence of the aquifer on recharge from the Everglades and upstream canals. Groundwater head decline due to pumping pressure and declining rainfall conditions is threatening the sustainability of the aquifer, as well as the Everglades ecosystem from increased salinity.

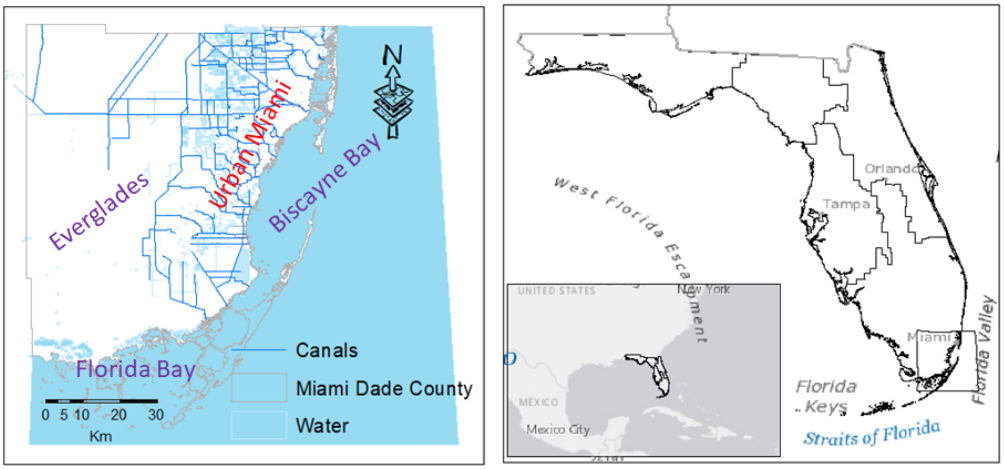

Figure 3- 1. Location map of the study area, Miami-Dade County and the Everglades. Source: SFWMD (South Florida Water Management District)-20004 and regional layers are from the ESRI (Environmental Systems Research Institute) base map.

Rainfall is a significant source of freshwater input into the region's freshwater balance. Precipitation is driven by local and regional hydroclimate factors (Obeysekera et al., 1999). In addition to regional ocean-atmosphere interaction, the region's geographic location in juxtaposition to the Atlantic ocean (Figure 3-1) and the presence of the Everglades wetland hydrologic system have a significant

influence over the local rainfall distribution in the area (Abtew and Melesse, 2016). As a result, the area receives rainfall driven from local and regional climate circulation factors, convective rain, tropical depressions and storms, and frontal rainfall systems (Ali et al., 2000).

Extreme hydrologic events, such as droughts, high-intensity rainfall, and floods are common. Droughts and other water demands pose a particularly strong challenge to the continuous supply of freshwater to the Everglades. Apart from intense competition for the use of the fully allocated water resource system, drought presents a threat to sustained freshwater availability in the Everglades. In South Florida, drought has been recorded in the years 1932, 1955–1957, 1961–1963, 1971–1972, 1973–1974, 1980–1982, 1985, 1988–1989, 1990, 2000–2001, 2006–2007, and 2011–2012 (Abtew, n.d.; Benson MA, n.d.; Verdi et al., 2006). These drought events have caused a remarkable decline in surface and groundwater head and a significant disturbance to the Everglades ecosystem (Abtew et al., 2009, 2007, n.d.; Beckage et al., 2003; Duever et al., 1994). In general, short- and long-term drought has been observed in different periods whose effect varies with the duration and magnitude of the rainfall deficit (Abiy et al., 2019; Abtew et al., 2007; Obeysekera et al., 1999).

The teleconnections between ENSO and rainfall in South Florida is well known and accepted. Short-term drought events have a strong association with La Niña (Abtew and Trimble, 2010; Beckage et al., 2003). El Niño increases dry season rainfall. However, small-scale and persistent rainfall deficit is a function of low-frequency ocean-atmosphere interaction modes: PDO, AMO, and others. Regional

rainfall variability is a function of the interaction between low-frequency and high-frequency ocean-atmosphere interaction modes. Therefore, evaluating rainfall deficit in different time windows and the association between rainfall deficit and individual and combined effects of the ocean-atmosphere interaction modes is necessary to manage regional water sustainably in South Florida (Abtew and Melesse, 2013). Concerning the degree of rainfall associated with the different ocean-atmosphere interaction modes, the current state of the fluctuation in the region has been well evaluated; however, the possible implications for long-term freshwater availability at the regional scale have not yet been sufficiently assessed. Therefore, the objectives of this study were to (1) assess historical droughts in the region, (2) evaluate the link between each of the regional hydroclimate drivers (ENSO, AMO, and PDO) and rainfall variability in the region, and (3) define the combined effects of the ocean-atmosphere interaction modes on regional drought. An understanding of the relationship between regional droughts with the regional ocean-atmosphere interaction modes aids short- and long-term water resource management planning and decision-making.

Furthermore, such knowledge can be applied to promote long-term drought preparedness and response. Accordingly, in this study, the correspondence between regional rainfall anomaly and each of the drivers' indices is presented as a pairwise correspondence analysis. Historic droughts in the region for different time scales are shown. Finally, the combined effect of the drivers on drought in the region is presented. Implications for the current and future water resource availability, water

resource management alternatives, and management priorities under drought conditions are discussed.

3.3. Dataset and Study Area

3.3.1. Rainfall

Long-term monthly regional rainfall data from 1906 to 2016 (Figure 3-2a) were accessed from the Florida climate center (Langevin, 2003). These regionalized monthly rainfall data were derived from several ground-based rainfall measurement stations. The regionalization has combined historical records from the National Weather Service's Cooperative Observation (COOP) network and the Automated Surface Observing System (ASOS). In South Florida, monthly rainfall measurement can be represented by a station for an area having an approximately 80 km radius (Abtew et al., 1993; Ali et al., 2000). Monthly rainfall variation has a wide range, i.e., a 10–100 km spatial scale (Moses et al., 2013). Therefore, these data are considered the representative monthly rainfall for the Southeast Florida region. The mean annual rainfall in the study area is 1507 mm (Figure 3-2b) compared to the mean rainfall for the Everglades National Park of 1386 mm (1941–2016).

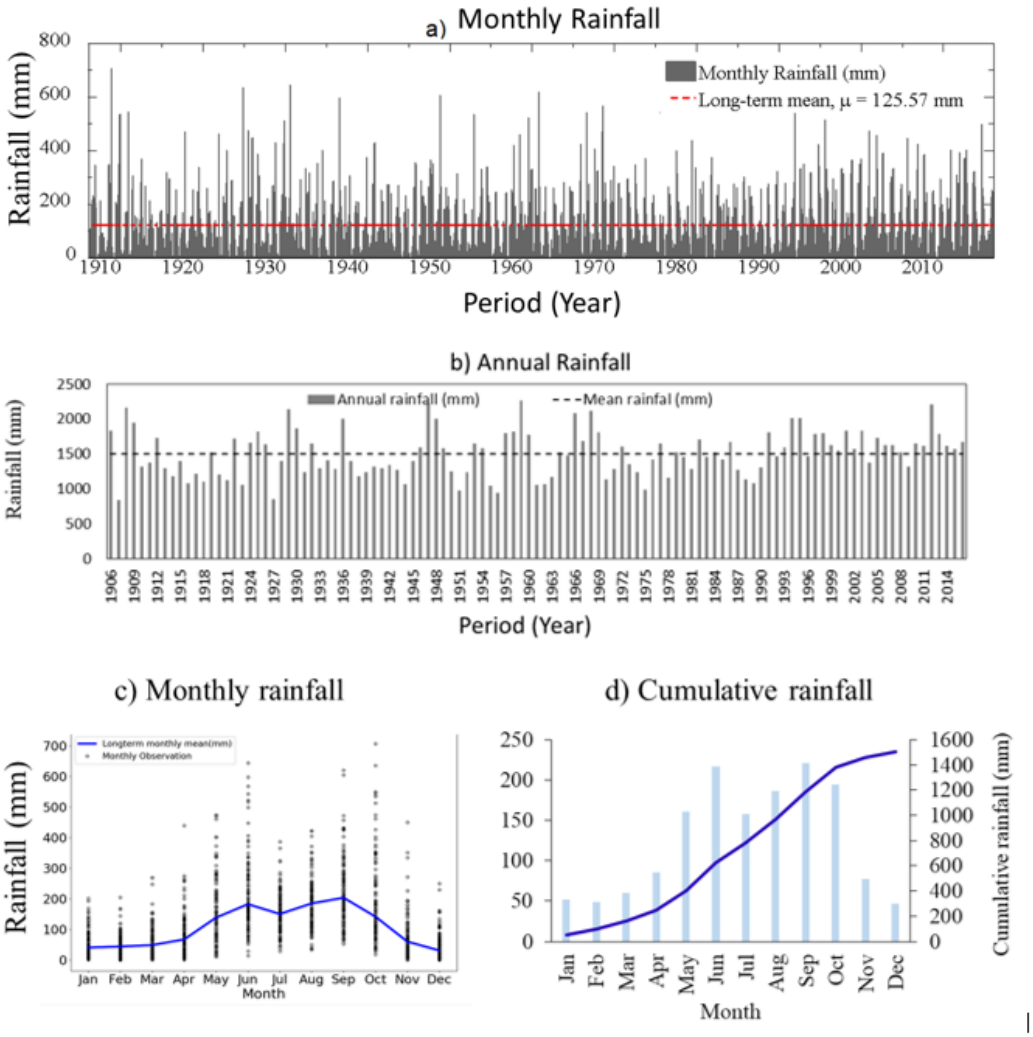

Figure 3- 2. (a) Total monthly rainfall distribution for southern Florida from 1906 to 2016, (b) total annual rainfall and its deviation from the long-term average rainfall, (c) observations by month, and (d) mean monthly and cumulative rainfall histogram.

The long-term mean monthly rainfall in South Florida is 125.57 mm per year (Figure 3-2a); 75% of the annual rain in the region occurs in the wet season (Abiy et al., 2019). The mean monthly long-term rainfall is characterized by a bimodal rainfall distribution (Figure 3-2c, d). The high volume of rain falling in June and September forms the two peaks on the bi-modal distribution. The cumulative mean monthly

precipitation indicates that November–April is the dry season while May–October is the wet season (Figure 3-2c). A thorough statistical evaluation of the same dataset shows a decreasing trend of the wet season duration leading to the emergence of a unimodal rainfall regime (Abiy et al., 2019).

3.3.2. ENSO, PDO, and AMO Dataset

ENSO is a natural ocean-atmosphere interaction process defined by sea surface temperature (SST) variations measured in the eastern and central equatorial Pacific. The SST anomaly in the tropical Pacific region (5° N to 5° S, 170° W to 120° W) refers to NINO 3.4 (Figure 3-3), which influences hydrological variation in the USA (Gershunov and Barnett, 1998; Palmer, 1965; Pielke and Landsea, 1999).

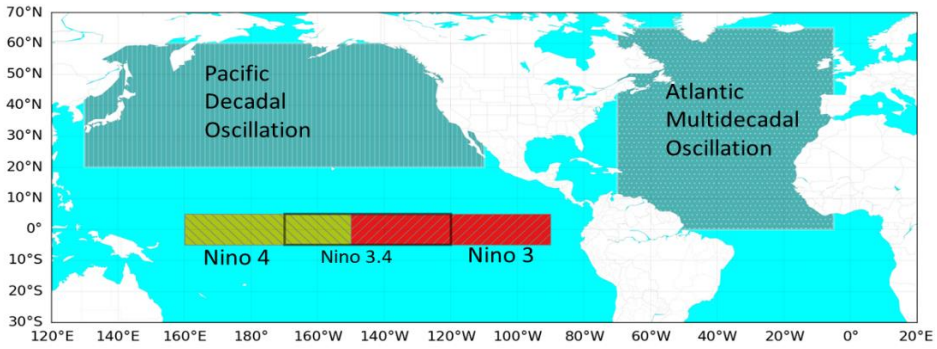

Figure 3- 3. Location of the different modes of ocean-atmosphere interaction.

ENSO has three phases: The El Niño phase of ENSO refers to the weakening of the easterly trade winds that allows the development of a positive SST anomaly in the eastern equatorial Pacific Ocean. The persistence of easterly trade winds pushes the warm pool to the west causing upwelling of colder water in the eastern equatorial Pacific Ocean. The upwelling results in colder than average SST in the east and

central tropical Pacific (negative SST anomaly) resulting in a La Niña condition. The presence of equatorial SST close to normal within ±0.5 °C is a neutral phase of ENSO. In Southeast Florida, the positive SST anomaly, El Niño (SST > 0.5 °C), is associated with an increase in dry season precipitation whereas La Niña (SST < −0.5 °C) is associated with drought in the dry season (Abtew et al., 2007). ENSO has a 3- to 7-year cycle, whereas the effect of El Niño or La Niña can persist for 6 to 18 months (Abiy et al., 2019).

The standard format monthly Nino 3.4 data was accessed from the National Oceanic and Atmospheric Administration's Climate Prediction Center (Rayner, N. A., Parker, D. E., Horton, E. B., Folland, C. K., Alexander, L. V., Powell, D. P., 2003) (Figure 3-4a). In this study, the monthly and total annual ENSO anomalies (Figure 3-4b) are calculated as residual from the long-term normal.

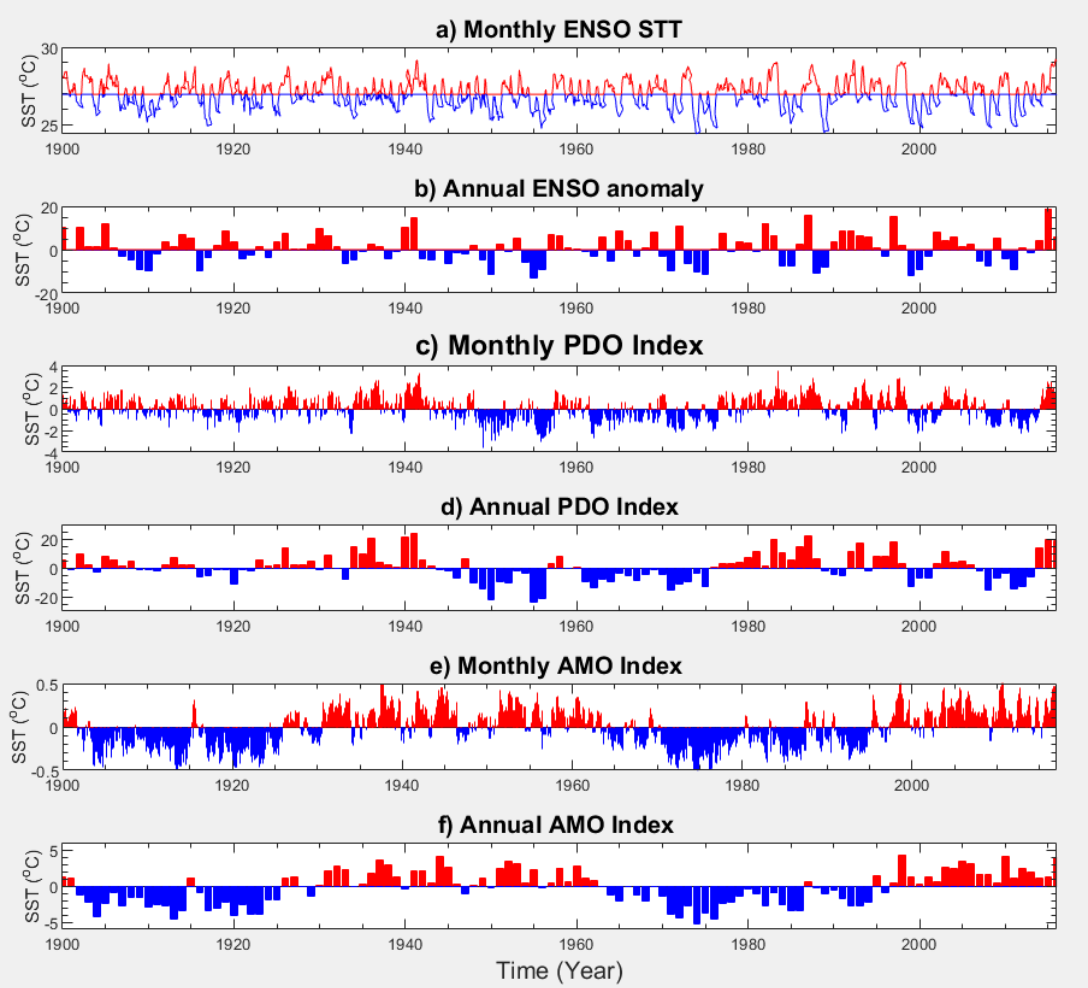

Figure 3- 4. Long-term monthly and annual record of the three ocean-atmosphere interaction modes. (a) Monthly El Niño–Southern Oscillation (ENSO) sea surface temperature (SST): mean SST measured at NINO 3.4; (b) Annual ENSO anomaly: annual cumulative of the monthly SST anomaly; (c) Monthly Pacific Decadal Oscillation (PDO) index: monthly SST variability in the northern Pacific region; (d) Annual PDO index: cumulative of the monthly SST variability within a year; (e) Monthly Atlantic Multidecadal Oscillation (AMO) index: mean of the monthly SST anomalies in the North Atlantic Basin; and (f) Annual AMO index: the sum of the monthly SST anomalies in a year.

PDO is an index of the SST change in the Pacific Ocean poleward of 20° North. Like ENSO, the changes in SST, sea-level pressure, and wind pattern in the northern Pacific Ocean influence a greater area in continental North America and the rest of the world. PDO with a 5- to 30-year cycle has an effect similar to ENSO on

the rainfall distribution in the continental U.S. (Enfield et al., 2001; G. J. McCabe et al., 2004). PDO is rare unlike ENSO. Therefore, the effect of PDO over an area in a given time is a function of ENSO phases. For example, studies indicate that when PDO and ENSO are in phase, PDO can be constructive to the effects of ENSO (Gershunov and Barnett, 1998; Wang et al., 2008).

For this study, the PDO index data from 1906 to 2016 (Figure 3-4c,d) were accessed from the Joint Institute for the Study of the Atmosphere and Ocean (JISAO) at the University of Washington (Mantua et al., 1997). This database exhibits the standardized PDO index derived from monthly SST anomalies.

Representing the mean SST changes in the North Atlantic Ocean from 0° to 60° N, AMO is characterized by multi-decadal variability with 40-year cycles with a maximum full duration of up to 70 years (Dijkstra et al., 2006; Drinkwater et al., 2014; Enfield et al., 2001; Oglesby et al., 2012). Therefore, an essential hydroclimate variable controls the long-term precipitation pattern. The AMO anomaly has an inverse relation with precipitation amount in some regions of the U.S. where the warm (cold) phase of AMO is associated with dryness (wetness) (Enfield et al., 2001). The AMO index is a measure of the 10-year running average of SST anomalies in the North Atlantic Ocean. The AMO index (Figure 3-4e,f) used here was accessed from the Kaplan SST dataset available online (https://www.esrl.noaa.gov/psd/data/timeseries/AMO/) (Enfield et al., 2001)).

3.4. Methodology

3.4.1. Correspondence of Regional Rainfall Anomaly to ENSO, AMO, and PDO

The monthly rainfall anomaly is the deviation from the long-term normal of each corresponding month. The monthly rainfall residual was used to develop a year–month matrix that was plotted using empirical Bayesian kriging (EBK) as indicated in previous studies (Abiy et al., 2019). The pattern of the residual rainfall chart was compared to ENSO, PDO, and AMO charts developed by the same approach.

The quadrant-based paired point-count approach was used to evaluate the degree of correspondence or synchronicity between the total annual and dry season rainfall anomaly and ENSO, PDO, and AMO. The method was used to statistically evaluate the significance of the correspondence portrayed in the monthly rainfall anomaly analysis chart. The yearly and dry season rainfall anomalies were plotted against ENSO, PDO, and AMO. The resulting diagram indicates the location of each contemporaneous pair in one of the four quadrants (QI to QIV). The correspondence is the count of positive–positive (QI-true positive) and negative–negative (QIV-true negative) pairs. The true positive counts indicate the increase in rainfall with the positive anomaly of each of the drivers, and the true negative counts indicate the decrease in rainfall with the negative anomaly. The pairs at quadrant II (QII, false negative) and quadrant III (QIII, false positive) indicate that the change in the drivers does not represent the rainfall anomaly.

The strength of the association between rainfall anomalies with each of the drivers was computed and compared using chi-squared test statistics (Abtew and Melesse, 2013; Abtew and Trimble, 2010). Using this approach, one can assess the degree of correspondence between the cumulative annual anomalies (sum of the monthly anomaly) of ENSO with the total dry season (November to May) rainfall anomaly. The results used a test of significance for the binomial proportions and chi-square test (Equation 3-1). This chi-square analysis is based on the hypothesis that there is a correspondence between the cumulative dry month's rainfall and each of the drivers (Abtew and Trimble, 2010):

$$\chi^2 = \frac{\sum_{i=1}^{2}(f_i - F)^2}{F} \qquad (3\text{-}1)$$

where χ^2 is the chi-square of the binomial proportions; $f_1 + f_2$ is the number of years of the analysis; f_1 is the number of years where the rainfall anomaly corresponds to each of the drivers (total counts in QI and QIII); f_2 is the number of years where the rainfall anomaly does not correspond to each of the drivers (total counts in QII and QIV); and F is the expected frequency of random correspondence assuming a probability (p) of 0.5, ($F = (f_1 + f_2)\, P$). Term F is also the expected number of years where the rainfall anomaly does not correspond with any events as p is 0.5.

3.4.2. Drought Evaluation with the Standardized Precipitation Index (SPI)

The regionalized monthly rainfall record from 1906 to 2016 was used to evaluate the drought variability using the SPI in 3-month to 60-month time windows. Monthly regional rainfall data in the region have a gamma probability (Abiy et al., 2019). Similar results were shown in the previous chapter of this dissertation. Rainfall with a gamma probability distribution can be effectively used to calculate the SPI as given by (Edwards and McKee, 1997; Guttman, 1999; Mckee et al., 1993; Wu et al., 2007):

$$\mathrm{SPI} = \begin{cases} -\left(t - \frac{c_0 + c_1 t + c_2 t^2}{1 + d_1 t + d_2 t^2 + d_3 t^3}\right), t = \sqrt{\ln\left(\frac{1}{H(x)^2}\right)}, 0 < H(x) \leq 0.5 \\ t - \frac{c_0 + c_1 t + c_2 t^2}{1 + d_1 t + d_2 t^2 + d_3 t^3}, t = \sqrt{\ln\left(\frac{1}{1 - H(x)^2}\right)}, 0.5 < H(x) < 1 \end{cases} \quad (3\text{-}2)$$

where c_0 = 2.515517, c_1 = 0.802853, c_2 = 0.010328, d_1 = 1.432788, d_2 = 0.189269, and d_3 = 0.001308.

The SPI (Equation 3-2) calculates the incidence of drought over different time windows using the running total rainfall of the respective time windows. For such long-term studies, drought evaluation with the SPI is feasible as it uses rainfall data only (Wu et al., 2007). The SPIs (Equation (2)) in different time windows were calculated in the MATLAB (R2018b, MathWorks Inc, Natick, MA, USA) interface. The evaluation of the drought index for an extended period (such as 48 and 60

months) is credible only if the study applies long-period monthly rainfall data (Wu et al., 2007). In this study, 110 years of monthly rainfall data were used.

The SPI calculated at 3-, 6-, 12-, 24-, 36-, 48-, and 60-month time windows was used to evaluate the combined effects of ENSO, AMO, and PDO on drought. The SPI analysis result was normally distributed; therefore, the regression analysis could be used. Each of the sequential time series drought indices calculated by the SPI was used as dependent variables whereas ENSO, AMO, and PDO were collectively used as independent variables. The significance of the strength of each of the independent variables as a driver for regional drought was assessed by t-test statistics evaluated at 95% confidence interval.

3.4.3. Frequency analysis

Analysis of the frequencies of the SPI-x values and ENSO, AMO, and PDO was conducted using the Fast Fourier Transform function in MATLAB (Fleming et al., 2002). The Fast Fourier Transform fiction is given as:

$$X_j = \sum_{k=0}^{N-1} x_k e^{-i\frac{2\pi}{N}kj} \qquad (3\text{-}3)$$

$$k = 0,1,\dots,N-1 \text{ and } j = 0,1,\dots,N-1$$

where Xj is the jth discrete frequency component of the SPI-x time sequence xk, N is the total number of the data, and -i is a complex number, $i = \sqrt{-1}$. (Fleming et al., 2002; Press et al., 1992).

The transform result is interpreted Power Spectral Density (PSD), calculated as a standardized product of the frequency-domain signal and its complex conjugate given as:

$$A = \frac{|X_i|}{N}, \text{ and} \quad (3\text{-}4)$$

$$P_j = \frac{X_j X_j^*}{N * N} = \frac{|X_j|^2}{N^2} \quad (3\text{-}5)$$

where A is the scaled amplitude spectra, and Pj is the power spectral density (Fleming et al., 2002; Press et al., 1992).

3.5. Results and Discussion

3.5.1. Pairwise Correspondence Test

Rainfall deviation from the long-term normal is a preliminary indicator of rainfall variability in the area (Figure 3-5). The residual map represents the difference between the recorded total monthly rainfall and the respective long-term mean monthly value. The residual embodies the overall wetness or dryness of each month versus the long-term mean of the respective individual month. Likewise, the plots of ENSO, AMO, and PDO show the coincidence of residual rainfall pattern with ocean-atmosphere interaction modes.

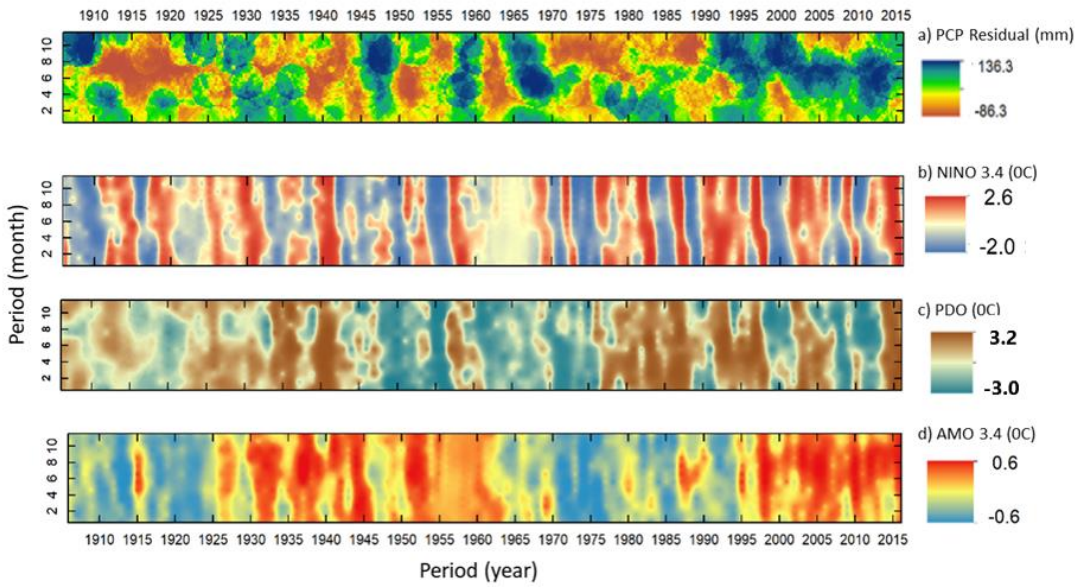

Figure 3- 5. Year–month matrix map of (a) monthly rainfall deviation from the long-term average rainfall of the corresponding month, (b) NINO 3.4, (c) AMO, and (d) PDO indices. The vertical axis refers to months from January (1) to December (12).

The residual rainfall chart presents three patterns of the rainfall deviation from the normal. The first pattern is when all months in a year and successive years are wetter than average. The second pattern is when the dry season becomes wet and the wet season wetter. The third pattern is when all months are dry. Dryness is seen from 1911 to 1923, 1937 to 1945, 1950 to 1958, 1961 to 1963, and 1970 to 1990 are indicated (Figure 3-5a). On the other hand, the periods from 1908 to 1910, 1928 to 1931, 1945 to 1949, and 1964 to 1969 were wet, and the contemporary rainfall pattern since the early 1990s indicates sustained wetness except for short droughts.

The regional rainfall residual chart is poorly correlated to the ENSO variability. The lack of one-to-one correspondence between rainfall deviation and ENSO variability signifies that the rainfall pattern in the area is the cumulative effect

of other drivers and external factors. Unlike the correspondence between ENSO and rainfall anomaly, there is relatively less correspondence between PDO and rainfall anomaly (Figure 3-5a, c, and d). On a longer timescale, the rainfall residual has high similarity to AMO (Figure 3-5c). For example, the dryness in early 1911 to 1923 and 1970 to 1990 corresponds to the negative phase of AMO. The long-held wetness from 1990 onward corresponds to the positive phase of AMO. However, the high-frequency rainfall variability between 1925 and 1970 does not show similarity with the long-held positive phase of AMO.

Plotting the rainfall anomalies against the cumulative SST anomalies of each of the indices define the level of correspondence between rainfall and the drivers (Figure 3-6). South Florida is profoundly affected by tropical storms causing rainfall outliers. Therefore, one should use dry season rainfall anomalies. Nevertheless, an additional analysis for total annual rainfall deviations evaluates how much of the variation can be attributed to the climate indices.

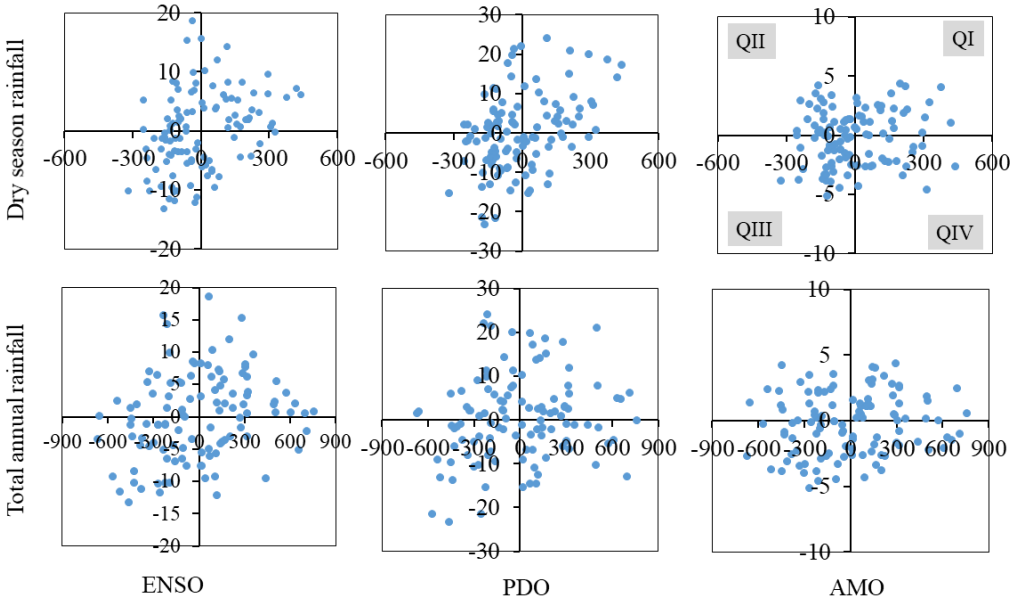

Figure 3- 6. Quadrant-based correspondence test of total annual and dry season rainfall deviation to ENSO, PDO, and AMO. The x-axis refers to the rainfall deviation (mm), and the vertical axis refers to the cumulative SST anomaly (°C) of the respective drivers.

Dry season anomaly correspondence with ENSO is 73 events out of 110 (QI + QIII), and annual anomaly has a correspondence of 70 events out of 111 (QI + QIII) (Tables 3-1 and 3-2). Accordingly, this correspondence between the rainfall anomaly and ENSO index signifies that ENSO is 63.4% and 63.1% for the dry season and annual rainfall variation, respectively. AMO is the second primary driver for the rainfall variability in the region. The dry season and annual rainfall anomaly correspondences with the AMO index are 54 out of 110 events and 56 out of 111 events (49% and 50.1%), respectively. The rainfall anomaly correspondence with the PDO index shows a correspondence of only 52 out of 110 events (43.3%) for dry season rainfall and 55 out of 111 events for annual rainfall (50%). The total annual and dry season rainfall is weakly associated with PDO.

Table 3- 1. Quadrant counts of the overlaps of total annual and dry season rainfall anomalies with cumulative SST anomalies of ENSO, AMO, and PDO.

Quadrant	ENSO		AMO		PDO	
	Dry	Annual	Dry	Annual	Dry	Annual
I	33	36	27	32	27	28
II	23	21	26	21	28	28
III	40	34	37	34	35	27
IV	14	20	20	24	20	28
Total	110	111	110	111	110	111

The binomial proportions statistics test assesses the possibility that the paired events are random or have a cause-and-effect relation showing that the chi-squared measures the significance of the binomial proportion (correspondence) (Abtew and Melesse, 2013; Abtew and Trimble, 2010). This analysis shows that ENSO has a statistically significant correspondence to both the total annual and the dry season rainfall anomalies (Table 3-2). Furthermore, ENSO fluctuations have the highest chi-square value for the dry season rainfall (with 95% confidence interval). The dry season negative rainfall anomaly has the most frequent overlap with ENSO on the true negative quadrant of the paired plot. Likewise, the annual rainfall variability is significantly associated with ENSO variability. Accordingly, the significant driver for the regional rainfall variability is the ENSO fluctuation.

Table 3- 2. Test statistics for the correspondence of rainfall anomaly to ENSO, AMO, and PDO. As indicated in equation 3.1, n is the total number of data observation, f=h refers to the number pairs that fall in quadrant I and III, F=np, refers to the expected frequency of random correspondence, and p refers to the probability of random correspondence. It is customary to report the tabular chi-square values to define the significance level of the data analysis. A tabular chi-square is used at 1 degree of freedom (DF).

Parameter	ENSO		AMO		PDO	
	Dry Season	Annual Rainfal l	Dry Season	Annual Rainfall	Dry Season	Annual Rainfall
n	110	111	110	111	110	111
h	73	70	64	66	62	55
n-h	37	41	46	45	48	56
p	0.50	0.50	0.50	0.50	0.50	0.50
F=np=nq	55.00	55.50	55.00	55.50	55.00	55.50
Computed Chi-square	5.89	3.79	1.47	1.99	0.89	0.00
Tabular Chi-square[1]	5.02	2.71	2.71	2.71	2.71	2.71
Significance level	0.025	0.10	0.10	0.10	0.10	0.10

In Table 3-2, the calculated expected random correspondence of the dry season or annual rainfall has a probability of greater than 50% with a chi-square significance value of 5% at one degree of freedom. The AMO index shows a higher degree of correspondence to the total annual rainfall (with 80% confidence interval and tabular chi-square of 1.64) than the dry season rainfall in the region. The chi-square value for the correspondence between PDO and rainfall anomalies in the region indicates a general weaker relationship. The lower level of confidence (80%) for correspondence between dry season rainfall and AMO, and annual precipitation and AMO events suggest that AMO events failed to explain the overall short-term rainfall variability in the area. The comparison of AMO and PDO effects suggests that rainfall variability in Southeast Florida is driven more by AMO than PDO fluctuations.

Overall, the rainfall deviation indicates high- and low-frequency signals. The ENSO fluctuation influences the short-term variability whereas the long-held low-frequency signal has high similarity to AMO (Figure 3-5). An insignificant correspondence between PDO and rainfall anomaly suggests that there is a minimal PDO effect on short-term rainfall variability in the region. This analysis confirms the need to evaluate the degree of correspondence between the rainfall deviation and each of the drivers. Knowledge of the level of correspondence between each of the drivers is necessary for short-term water management decision-making. However, for sustained long-term water management planning, it is important to understand the combined effect of the drivers on regional drought.

3.5.2. Combined Effects of Drivers on Regional Rainfall Variability

The results of the SPI indices in 3-, 6-, 12-, 24-, 36-, 48-, and 60-month windows were used for multiple regression analysis of each of the indices against all drivers. The SPI-3, SPI-6, and SPI-12 represent the link between rainfall variability and the drivers whereas SPI-24, SPI-36, SPI-48, and SPI-60 represent the link between long-term drought and the combined effect of the drivers.

The SPI analysis (Figure 3-7) agrees with monitoring-based reported droughts in 1932, 1955–1957, 1961–1963, 1971–1972, 1973–1974, 1980–1982, 1985, 1988–1989, 1990, and 2000–2001 (Abtew et al., 2007). Even though the incidence of droughts such as in 2010–2012, 2014, and 2015, the current hydrology of the area is a wet phase relative to the of the long-term cycles. An analysis of the drought cycle

using fast Fourier transform and input data of the monthly SPI indices indicated that the regional drought has periodicities of 2 to 3, 5 to 6, 9 to 10, and 10 to 20 years (Abiy et al., 2019). Such cycles coincide with the known cycles of ENSO, AMO, and PDO.

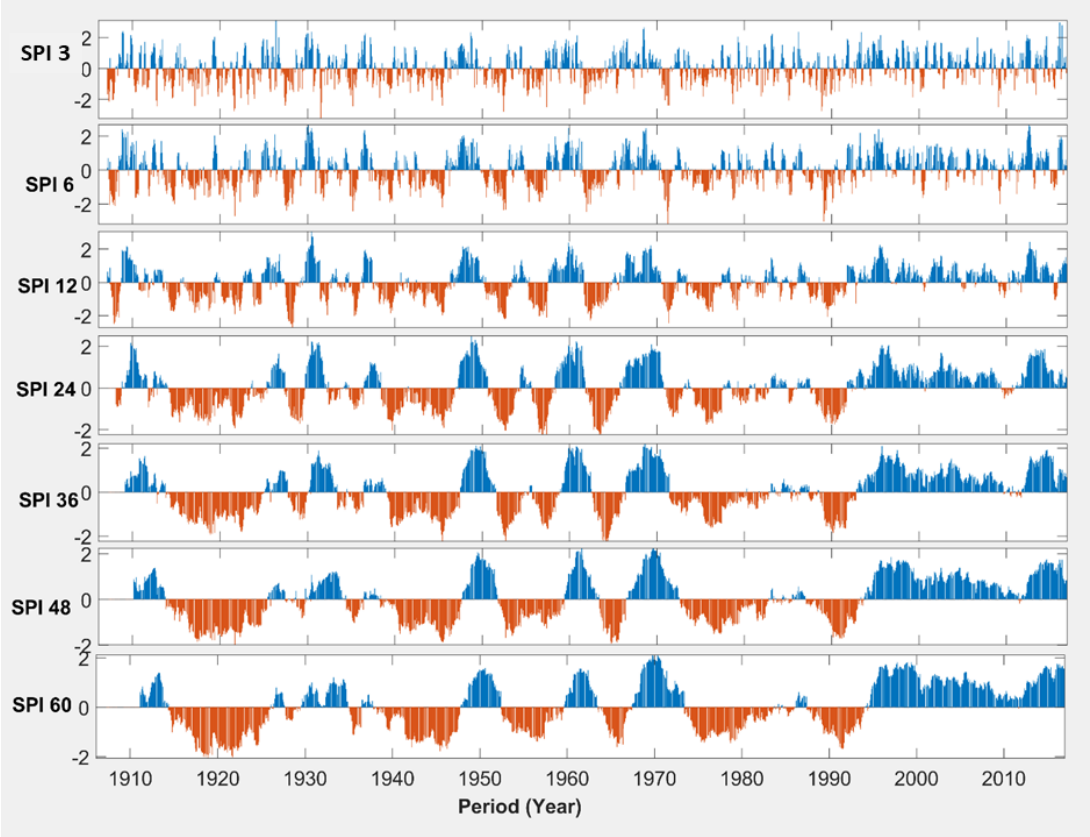

Figure 3- 7. Time series plot of the Standardized Precipitation Index (SPI)-x evaluated by different time windows from 3- months to 60-months.

As depicted in SPI-24 to SPI-60 (Figure 3-7), major extended droughts are observed from 1914 to 1927 and from the early 1970s to 1995/1996. Between 1940 and the early 1970s, the SPI indicates a clear cyclic pattern representing the presence of sustained wet/dry events fluctuations in the area. The multiple regression analysis

used to evaluate the combined effect of the drivers on different intensities of drought indicates that the ENSO fluctuation has a strong association with SPI-3, SPI-6, and SPI-12 (Table 3-3). Rainfall variability evaluated by SPI-3 and SPI-6 is a reflection of seasonal fluctuations whereas negative (positive) values of the SPI-12 refer to the presence of yearly sustained dryness (wetness), respectively. Hence, the effect of ENSO fluctuation in the regional hydrological variability is significant relative to all drivers. This line of analysis corroborates with the pairwise correspondence test whereby the dry season rainfall has the highest degree of correspondence to the ENSO variability. Hence, the overall dry season rainfall gain or loss attributed to ENSO fluctuation is a function of the impact on the dry season rainfall. If the dry season has more rainfall (ENSO positive), then the overall annual precipitation is at or above average.

Table 3- 3. Multiple regression test statistics of SPI-3, SPI-6, SPI-12, SPI-24, SPI-36, SPI-48, and SPI-60 against ENSO, PDO, and AMO. The significance of the t-test statistics is evaluated at a 95% confidence interval. Two-tailed t-test statistics are applied; therefore, a computed p-value of less than 0.025 suggests the significance of the relation between the driver and SPI. In relative terms, a higher variance inflation factor (VIF) implies a high level of multi-collinearity.

SPI-Time Window	Independent	Coefficient	Std. Error	t	p	VIF
SPI-3	Constant	−4.84	0.93	−5.23	<0.001	
	ENSO	0.18	0.03	5.24	<0.001	1.22
	PDO	0.04	0.03	1.54	0.125	1.22
	AMO	0.27	0.13	2.04	0.042	1
SPI-6	Constant	−3.86	0.92	−4.18	<0.001	
	ENSO	0.14	0.03	4.19	<0.001	1.22
	PDO	0.09	0.03	3.05	0.002	1.22
	AMO	0.4	0.13	3.06	0.002	1
SPI-12	Constant	−3.77	0.93	−4.08	<0.001	
	ENSO	0.14	0.03	4.09	<0.001	1.22
	PDO	0.1	0.03	3.65	<0.001	1.22
	AMO	0.58	0.13	4.45	<0.001	1
SPI-24	Constant	−1.91	0.94	−2.04	0.042	
	ENSO	0.07	0.03	2.03	0.042	1.22
	PDO	0.07	0.03	2.62	0.009	1.22
	AMO	0.99	0.13	7.5	<0.001	1
SPI-36	Constant	0.16	0.94	0.18	0.861	
	ENSO	−0.01	0.03	−0.19	0.85	1.22
	PDO	0.04	0.03	1.3	0.194	1.22
	AMO	1.28	0.13	9.68	<0.001	1
SPI-48	Constant	−0.85	0.92	−0.93	0.353	
	ENSO	0.03	0.03	0.92	0.359	1.22
	PDO	−0.01	0.03	−0.41	0.684	1.22
	AMO	1.56	0.13	12.02	<0.001	1
SPI-60	Constant	−0.87	0.91	−0.96	0.338	
	ENSO	0.03	0.03	0.95	0.343	1.22
	PDO	−0.02	0.03	-0.6	0.547	1.22
	AMO	1.68	0.13	13.18	<0.001	1

AMO fluctuation has a statistically significant correlation with SPI-6 to SPI-60. Only AMO has a statistically significant relationship with the regional rainfall variabilities for over 3 to 5 years, i.e., SPI-36, SPI-48, and SPI-60. As indicated in the pairwise association test, AMO has shown the strongest association with the total annual rainfall variability than with the dry season rainfall variability—this is in contrast to ENSO. The region receives more than 70% of the total annual rainfall in the wet season. Therefore, the fact that AMO has a statistically significant correlation

with the long-term total annual rainfall in the area indicates that AMO variability is an essential driver of the long-term rainfall variability in the region (low frequency but sustained impact).

The overall drought analysis used SPI-12 and higher time windows to show that the region is in an extended wet phase of the rainfall variabilities. Furthermore, the multiple regression indicates that the long-term rainfall variabilities are related to AMO fluctuations where the positive AMO favors wetness in the region. However, studies indicate the emergence of negative AMO (Frajka-Williams et al., 2017).

The spectral evaluation of the calculated SPI-x, ENSO, AMO and PDO values (Figure 3-8) indicates that the ENSO fluctuation constantly overlay with short range drought index values (SPI-3 to SPI-36). The droughts that persist between 1 and 2 years (SPI-12 and-24) have 3 different frequency ranges (5 to 6, 9 to 10, and 10 to 20). In the latter drought cycle, the power spectral density of ENSO has a higher energy and is higher than the PSD of AMO and PDO (Figure 3-8b) for the timeline less than 3 years duration—these findings imply that ENSO has a bigger impact on shorter droughts.

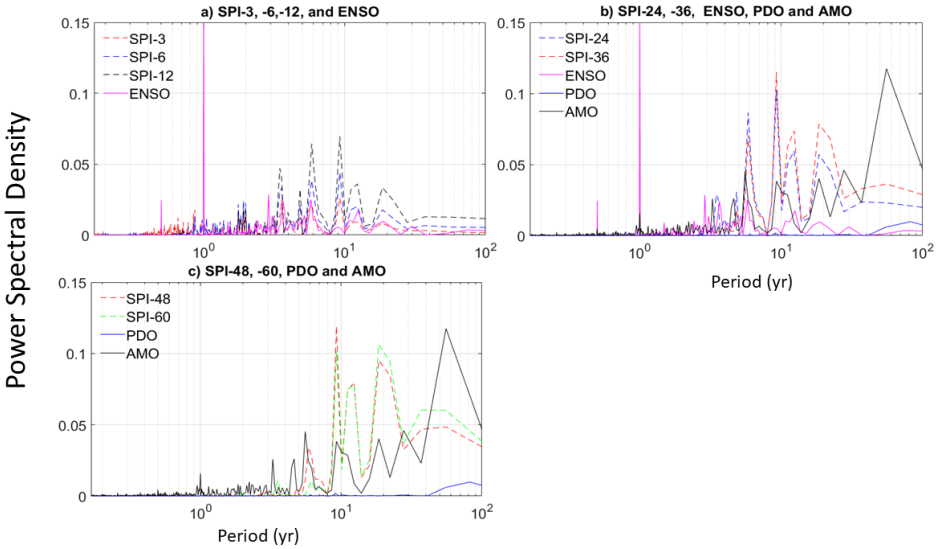

Figure 3- 8. Power spectral density of the a) SPI-3, -6, -12, and ENSO; b) SPI-24, -36, and ENSO, PDO and AMO; and c) SPI-48, -60, PDO, and AMO.

For a period, greater than ten years, the PSD value of AMO increased whereas the PSD of PDO remains much lower than both ENSO and AMO. The PSD comparison of the PDO and AMO with long term drought indices (SPI-48, and -60) adds an additional representation: AMO's higher PSD values at 10- and 20-years match both the periodicity of the long-term drought indices. The PDS of PDO is only slightly above zero for periodicity values greater than 50 years.

The PSD analysis shows that the short-term drought is in phase and overlaps with ENSO fluctuations; long-term droughts are associated with AMO. This line of analysis substantiates with the correspondence and regression analysis explained above.

3.5.3. Implications for Long-Term Freshwater Management

A sustainable freshwater management system in this area requires one to know the combined effects of AMO and ENSO interactions on the hydrometeorology. Four combinations of AMO and ENSO anomalies can control the rainfall and freshwater input to the regional system. The first is the combination of a positive AMO and positive ENSO (El Niño) conditions. The interaction of the positive–positive index is a wet hydrologic regime in the region. This first scenario can be associated with flooding and high-intensity rainfall. The second scenario is a combination of a negative ENSO given positive AMO. A negative ENSO given positive AMO can imply a short drought. In general, the second scenario can be defined by the recurrence of droughts in the area. Given the long-held positive AMO and frequent fluctuation of ENOS between negative and positive phases, the first two scenarios represent the contemporary hydrologic regime in the region particularly since the early 1990s. Within these two scenarios, the region receives much more rainfall than average. However, a negative ENSO corresponds to observed droughts.

Major extended drought episodes in the area coincide with the cold phase of AMO; likewise, the extended wetness from 1994–1995 overlaps with the warm phase of AMO. The third and fourth scenarios are associated with the potential emergence of a negative AMO (Gershunov and Barnett, 1998). The highly likely scenario of the future hydroclimate regime in the region is a balance between long-term droughts induced by negative AMO moderated by the frequent recurrence of positive ENSO. Negative AMO affects the declining regional rainfall regime. The positive ENSO

during negative AMO might help to minimize the adverse effects of rainfall deficit. The occurrence of negative ENSO and negative AMO is the worst-case scenario where drought can be persistent.

Given the possibility of AMO shifting to a negative phase (Caesar et al., 2018; Frajka-Williams et al., 2017), the rainfall regime in the region can shift to moderate to severe drought for an extended period. There is a high potential for the emergence of long periods of small-scale droughts. Prolonged small-scale droughts have gradually increased and eventually influence the sustainability of the water resource system. This can affect freshwater availability in the Everglades and disrupt the regional ecosystem and ecosystem services. Furthermore, long-term drought can reduce the groundwater head of the Biscayne Aquifer, compromise the sustainable yield of the aquifer, and promote saltwater intrusion. Therefore, considering climate teleconnection in regional water management planning and decision-making is critical. The South Florida Water Management District has been incorporating climate predictions into its weekly water management decision process using weekly reported climate teleconnection indices (Abiy et al., 2019; Wu et al., 2007).

3.6. Conclusions and Recommendations

The evaluation of the correspondence between the dry season and annual rainfall with ENSO, AMO, and PDO indicated that ENSO fluctuations have a direct relation to short-term dry season rainfall variability in southern Florida. The multiple regression tests further explained the fact that regional short-term rainfall variability

is associated with ENSO fluctuation. ENSO variability has a limited impact on long-term rainfall variability; this value was averaged over more than two years (≥ SPI-24). The short-term effect of ENSO can trigger droughts or flooding. Therefore, the impact of ENSO fluctuation is limited to short-term rainfall variability.

AMO fluctuations indicate a significant correlation with the long-term rainfall variability in the region. AMO has a direct relation with rainfall and with the positive (negative) phase of AMO associated with a sustained wet (dry) phase of the rainfall variability in the region. Given the significant correlation of ENSO with the short-term rainfall variability, the net effect of a given phase of AMO on rainfall is a combined effect of high-frequency ENSO fluctuations and low-frequency AMO fluctuations.

According to the SPI-x analysis, the hydrologic period from 1994–1995 is defined by a persistent wet phase with frequent dry spells. The short-term SPI indices— SPI-3, SPI-6, and SPI-12—show frequent droughts during this period. However, the long-term SPI indices (SPI-24, SPI-36, SPI-48, and SPI-60) indicate that the long-term hydrologic system is in a sustained wet phase. This long-held wet period in the area coincides with the current stage of positive AMO, and the prevalence of droughts are associated with the negative phase of ENSO. Overall, the long-term rainfall variability in the region is strongly associated with AMO. However, the emergence of a negative phase of AMO has been reported. As a result, the current wet phase of the hydrologic regime could gradually decline to below average.

An increase in surface water storage can enhance groundwater water levels and storage in the Everglades. Construction of new storage reservoirs can reduce runoff loss into the ocean and increase water retention to increase the Everglades' hydro-period. Demand-side management options, restricted use of groundwater for specific applications, and promotion of institute- and household-level rainwater harvesting can significantly decrease freshwater dependence. In addition to hydrologic forecasting and structural water resource management measures, integrated water resource management in the region requires a rigorous policy for promoting demand-side water management. The overall aspects of demand-side water management benefit from active citizen engagement, policy advocacy, and communication.

Acknowledgments

We acknowledge the Everglades Foundation, the Department of Earth and Environment Florida, International University, and the National Science Foundation (NSF) for financial support. This material is based upon work partially supported by the National Science Foundation under Grant No. HRD-1547798. This NSF grant was awarded to Florida International University as part of the Centers for Research Excellence in Science and Technology (CREST) Program. This is contribution number 907 from the Southeast Environmental Research Center in the Institute of Water & Environment at Florida International University. This material was also developed in collaboration with the Florida Coastal Everglades Long-Term Ecological Research program under National Science Foundation Grant No. DEB-

1832229. The authors would like to acknowledge their data sources: The National Oceanic and Atmospheric Administration's Climate Prediction Center, the Joint Institute for the Study of the Atmosphere and Ocean (JISAO) at the University of Washington, the Florida Climate Center, and the South Florida Water Management District.

References

Abiy, A.Z., Melesse, A.M., Abtew, W., Whitman, D., 2019. Rainfall trend and variability in Southeast Florida: Implications for freshwater availability in the Everglades. PLOS ONE 14, e0212008.

Abtew, W. and V.C., n.d. Chapter 2: South Florida Hydrology and Water Management. 2018 South Florida Environmental Report South Florida Water Management District, West Palm Beach, FL I.

Abtew, W., Melesse, A.M., 2013. Climate teleconnections and water management. In: Nile River Basin: Ecohydrological Challenges, Climate Change and Hydropolitics.

Abtew, W., Melesse, A.M., 2016. Landscape changes impact on regional hydrology and climate. In: Springer Geography.

Abtew, W., Obeysekera, J., Shih, G., 1993. Spatial Analysis for Monthly Rainfall in South Florida1. JAWRA Journal of the American Water Resources Association 29, 179–188.

Abtew, W., Pathak, C., Huebner, R.S., Ciuca, V., 2007. Chapter 2: Hydrology of the South Florida environment. South Florida Environmental Report 1, 2.1-2.72.

Abtew, W., Pathak, C., Huebner, R.S., Ciuca, V., 2009. Hydrology of the South Florida environment. South Florida Environmental Report 1, 1–2.

Abtew, W., Pathak, C., Huebner, R.S., Ciuca, V., n.d. 2010 South Florida Environmental Report Chapter 2: Hydrology of the South Florida Environment.

Abtew, W., Trimble, P., 2010. El Niño-Southern Oscillation Link to South Florida Hydrology and Water Management Applications. Water Resources Management 24, 4255–4271.

Ali, A., Abtew, W., Van Horn, S., Khanal, N., 2000. Temporal and spatial characterization of rainfall over Central and South Florida. Journal of the American Water Resources Association 36, 833–848.

Allan, R., Lindesay, J., Parker, D., 1996. El Niño southern oscillation & climatic variability, CSIRO publishing.

Beckage, B., Platt, W.J., Slocum, M.G., Pank, B., 2003. Influence of the El Nino Southern Oscillation on fire regimes in the Florida everglades. Ecology 84, 3124–3130.

Benson MA, G.R., n.d. The 1971 drought in South Florida and its effect on the hydrologic system. US Geological Survey; 1974.

Caesar, L., Rahmstorf, S., Robinson, A., Feulner, G., Saba, V., 2018. Observed fingerprint of a weakening Atlantic Ocean overturning circulation. Nature.

Cullen, L.E., Grierson, P.F., 2009. Multi-decadal scale variability in autumn-winter rainfall in south-western Australia since 1655 AD as reconstructed from tree rings of Callitris columellaris. Climate Dynamics 33, 433–444.

Dijkstra, H.A., Te Raa, L., Schmeits, M., Gerrits, J., 2006. On the physics of the Atlantic Multidecadal Oscillation. Ocean Dynamics 56, 36–50.

Ding, Q., Wang, B., 2005. Circumglobal teleconnection in the Northern Hemisphere summer. Journal of Climate 18, 3483–3505.

Drinkwater, K.F., Miles, M., Medhaug, I., Otterå, O.H., Kristiansen, T., Sundby, S., Gao, Y., 2014. The Atlantic Multidecadal Oscillation: Its manifestations and impacts with special emphasis on the Atlantic region north of 60°N. Journal of Marine Systems 133, 117–130.

Duever, M.J., Meeder, J.F., Meeder, L.C., McCollom, J.M., 1994. The climate of south Florida and its role in shaping the Everglades ecosystem, Everglades: the ecosystem and its restoration.

Edwards, D.C., McKee, T.B., 1997. Characteristics of 20th Century drought in the United States at multiple time scales. Atmospheric Science Paper No 634, May 1–30 174.

Enfield, D.B., Mestas-Nuñez, A.M., Trimble, P.J., 2001. The Atlantic multi-decadal oscillation and its relation to rainfall and river flows in the continental U.S. Geophysical Research Letters 28, 2077–2080.

Feng, S., Hu, Q., 2004. Variations in the teleconnection of ENSO and summer rainfall in northern China: A role of the Indian summer monsoon. Journal of Climate 17, 4871–4881.

Fleming, S.W., Marsh Lavenue, A., Aly, A.H., Adams, A., 2002. Practical applications of spectral analysis of hydrologic time series. Hydrol. Process. 16, 565–574. https://doi.org/10.1002/hyp.523

Frajka-Williams, E., Beaulieu, C., Duchez, A., 2017. Emerging negative Atlantic Multidecadal Oscillation index in spite of warm subtropics. Scientific Reports 7.

Gaiser, E.E., Deyrup, N.D., Bachmann, R.W., Battoe, L.E., Swain, H.M., 2009. Multi-decadal climate oscillations detected in a transparency record from a subtropical florida lake. Limnology and Oceanography.

Gershunov, A., Barnett, T.P., 1998. Interdecadal Modulation of ENSO Teleconnections. Bulletin of the American Meteorological Society 79, 2715–2725.

Goly, A., Teegavarapu, R.S. V, 2014. Individual and coupled influences of AMO and ENSO on regional precipitation characteristics and extremes. Water Resources Research.

Guttman, N.B., 1999. Accepting the Standardized Precipitation Index: a Calculation Algorithm1. JAWRA Journal of the American Water Resources Association 35, 311–322.

Hidalgo, H.G., Dracup, J.A., 2003. ENSO and PDO Effects on Hydroclimatic Variations of the Upper Colorado River Basin. Journal of Hydrometeorology 4, 5–23.

Langevin, C.D., 2003. Simulation of Submarine Ground Water Discharge to a Marine Estuary: Biscayne Bay, Florida. Ground Water.

Mantua, N.J., Hare, S.R., Zhang, Y., Wallace, J.M., Francis, R.C., 1997. A Pacific Interdecadal Climate Oscillation with Impacts on Salmon Production. Bulletin of the American Meteorological Society 78, 1069–1079.

McCabe, Gregory J., Palecki, M.A., Betancourt, J.L., 2004. Pacific and Atlantic Ocean influences on multi-decadal drought frequency in the United States. Proceedings of the National Academy of Sciences 101, 4136–4141.

McCabe, G. J., Palecki, M.A., Betancourt, J.L., 2004. Pacific and Atlantic Ocean influences on multi-decadal drought frequency in the United States. Proceedings of the National Academy of Sciences 101, 4136–4141.

Mckee, T.B., Doesken, N.J., Kleist, J., 1993. The relationship of drought frequency and duration to time scales. AMS 8th Conference on Applied Climatology 179–184.

Moses, C.S., Anderson, W.T., Saunders, C., Sklar, F., 2013. Regional climate gradients in precipitation and temperature in response to climate teleconnections in the Greater Everglades ecosystem of South Florida. Journal of Paleolimnology.

Obeysekera, J., Browder, J., Hornung, L., Harwell, M. a, 1999. The natural South Florida system I: Climate, geology, and hydrology. Urban Ecosystems 3, 223–244.

Oglesby, R., Feng, S., Hu, Q., Rowe, C., 2012. The role of the Atlantic Multidecadal Oscillation on medieval drought in North America: Synthesizing results from proxy data and climate models. Global and Planetary Change 84–85, 56–65.

Palmer, W.C., 1965. Meteorological Drought. US Weather Bureau, Res Pap No 45.

Perry, W., 2004. Elements of south Florida's comprehensive Everglades restoration plan. Ecotoxicology 13, 185–193.

Pielke, R.A., Landsea, C.N., 1999. La Niña, El Niño, and Atlantic Hurricane Damages in the United States. Bulletin of the American Meteorological Society 80, 2027–2033.

Press, W.H., Teukolsky, S. a, Vetterling, W.T., Flannery, B.P., 1992. Numerical recipes in C (2nd ed.): the art of scientific computing, Technometrics. https://doi.org/10.2307/1269484

Rayner, N. A., Parker, D. E., Horton, E. B., Folland, C. K., Alexander, L. V., Powell, D. P., 2003. Global analyses of sea surface temperature, sea ice, and night marine air temperature since the late nineteenth century. Journal of Geophysical Research 108, 4407.

Rayner, N.A., 2003. Global analyses of sea surface temperature, sea ice, and night marine air temperature since the late nineteenth century. Journal of Geophysical Research 108, 4407.

Verdi, R.J., Tomlinson, S. a, Marella, R.L., Florida. Dept. of Transportation., Florida. Dept. of Environmental Protection., Geological Survey (U.S.), 2006. The drought of 1998-2002 impacts on Florida's hydrology and landscape, Circular 1295.

Wang, L., Chen, W., Huang, R., 2008. Interdecadal modulation of PDO on the impact of ENSO on the east Asian winter monsoon. Geophysical Research Letters 35.

Wu, H., Svoboda, M.D., Hayes, M.J., Wilhite, D.A., Wen, F., 2007. Appropriate application of the Standardized Precipitation Index in arid locations and dry seasons. International Journal of Climatology 27, 65–79.

4. CHAPTER IV: GROUNDWATER MODEL SETUP, CALIBRATION AND VALIDATION OF THE BISCAYNE AQUIFER, SOUTHEAST FLORIDA, USA.

4.1. Abstract

The position of the groundwater table in the Biscayne Aquifer (BA) plays a vital role in providing the volume of groundwater available for consumption and the extent of saltwater intrusion in the aquifer. The aquifer is susceptible to many hydrological stressors, including drought, groundwater pumping, and sea level rise. However, the effect of each stressor on the regional groundwater system is not well known. A single layer numerical groundwater-flow model of the BA was developed using the Modular Three-Dimensional Groundwater Flow Model (MODFLOW-2000). The model was calibrated for the period 1996-2000, while model validation and verification were conducted for the periods of 2001 to 2005, and 2006 to 2010, respectively. A highly parameterized Parameter Estimation (PEST) was used to simulate the inversion process for the steady and transient state groundwater flow model calibration. The model was compared with observed groundwater level data recorded over 30 groundwater monitoring station. The model performance was evaluated using BIAS, Coefficient of Determination (R^2), Root Mean Square Error (RMSE), and Nash and Sutcliff (NS) Efficiency model performance evaluation measures for each well. Wells away from canals and coastal areas showed higher performance as indicated by the performance measure indices than wells located by canals and coastal waters. Based on the results of the calibration and validation, the

model is acceptable to evaluate selected scenarios targeting changes in groundwater recharge attributed to drought, increased groundwater pumping and sea level rise.

Keywords: Groundwater, MODFLOW, PEST, Sea level rise, Biscayne Aquifer, South Florida.

4.2. Introduction

The Biscayne Aquifer (BA) is the sole source aquifer for water supply in South Florida. The position of the groundwater table in the aquifer plays a key role in controlling the volume of water available for the domestic water supply, as well as the regulation of water stages in canals, and the control of saltwater intrusion. The BA is a karst aquifer (Cunningham and Florea, 2009; Wacker et al., 2014) with extremely high transmissivity (Fish and Stewart, 1991). The position of the groundwater table in the aquifer is the result of a subtropical climate, a relatively flat topography, highly conductive karst terrain, and the management of a complex water-resource infrastructure (Langevin, 2003; Obeysekera et al., 1999; Renken et al., 2005a; Swain, 2012). However, the position of the groundwater table is controlled by the incidence of various stress conditions, such as hydrological drought, increased groundwater pumping, and sea level rise, which ultimately influence the volume of the public water supply and the health of the freshwater-dependent ecosystem in the area (Abtew et al., 1993; Abtew and Trimble, 2010; Harwell et al., 2000). Understanding the dynamics of the groundwater table in response to stress conditions is crucial for

making decisions regarding water use planning, restoration of the Everglades, and the management of saltwater intrusion.

The BA receives groundwater recharge from both diffuse and localized sources. Rainfall is the primary source of diffuse groundwater recharge across the range of the BA. Return flows from irrigating lawns and croplands also contribute to diffuse recharge (Hughes and White, 2014). Leakage from surface water through canals is a significant source of localized groundwater recharge in the aquifer. Regional groundwater flow provides sub-surface recharge from the Everglades to the urban side of the aquifer (Cunningham and Florea, 2009; Renken et al., 2005b; Wilcox et al., 2004; Cunningham et al., 2004).

The public water supply in Miami-Dade County depends on wellfields located on the urban side of the BA (Figure 4-1). However, the urban side is mostly covered by an impervious surface, which decreases the area capable of receiving diffuse recharge. A decline in rainfall would further decrease the diffuse recharge of the BA and contribute to drought conditions. Drought also affects water levels in canals and potentially decreases water leakage from canals into the BA. Groundwater pumping, urban intensification, and reduced rainfall are all expected to increase. The increase of these hydrological stressors could induce declining groundwater level conditions in the BA. Compounded with the fact that the sea level is rising, the underlying stress conditions could accelerate saltwater intrusion, leading to the decline of the quality and quantity of groundwater resources in the BA.

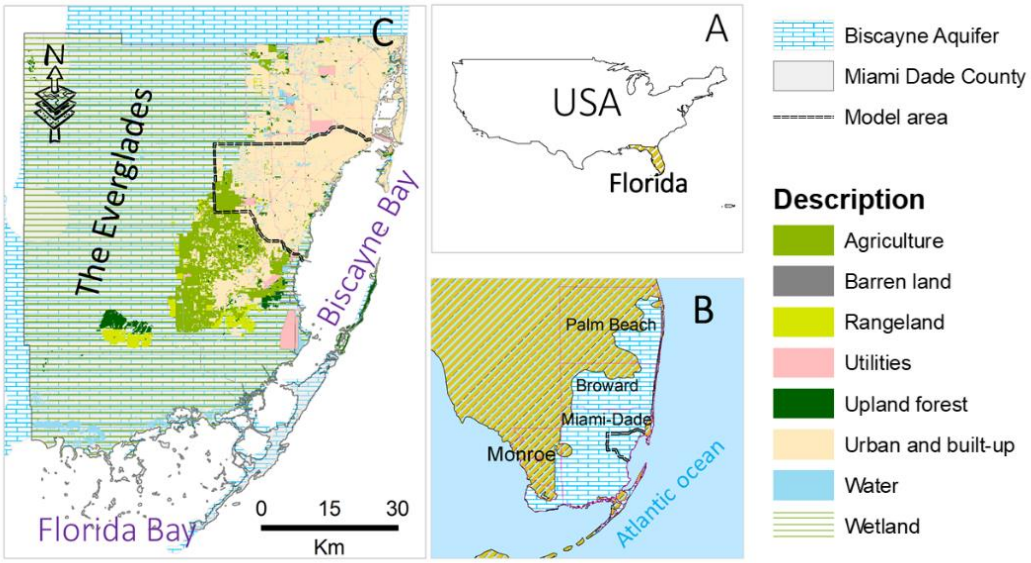

Figure 4- 1. Location map of the study area. A) Location of the Florida Peninsula. B) The four counties in Southeast Florida that depend on groundwater supply from the Biscayne Aquifer and the spatial coverage of the underlining prominently limestone Biscayne Aquifer. C) Land cover in Miami-Dade County, Florida, and the outline of the model domain in this study.

Sustained drought and dry spells, increasing surface imperviousness, and high levels of groundwater pumping are identified as the prominent hydrological stress conditions that affect the groundwater table in the BA (Abiy et al., 2019). These hydrological stress conditions facilitate the decline of the groundwater table. Along with continuously rising sea levels, the decreasing groundwater table affects the quality and quantity of the groundwater, threatening the sustainability of the water supply system in the region.

The need to develop groundwater flow mode of the BA: Various studies have documented the groundwater dynamics of the BA under specific scenarios. For example, a statistical analysis of long-term groundwater table data indicated a correlation of lower water table conditions with the dry season (Prinos, 2005; Prinos

and Dixon, 2016). In another study, groundwater table conditions were found to change when rainfall decreased by more than 20% of the local average values (Merritt, 1996). Water level changes in canals and lower rainfall volumes were reported to have a direct link with the groundwater level of the aquifer (Lohmann et al., 2012).

Brakefield et al. (2013) simulated groundwater well capture zones of two large well fields in Miami-Dade County under wet, dry, and normal canal stages, as well as two proposed hydrological measures to reduce groundwater seepage from the Everglades to urban areas. They concluded that the wellfield capture zones changed slightly under the changing hydrological conditions tested (Brakefield et al. 2013). Hughes and White (2014) conducted a comprehensive modeling effort to understand groundwater–surface-water interactions between the BA with canals and the coastline under current and future scenarios of increased pumping and sea levels (Hughes and White, 2014). They determined that the position of the saltwater interface at the base of the BA changed over the period of 1996 to 2010 with changes in pumping, sea level rise, and leakage from canals (Hughes and White, 2014).

Water table drawdown below the bottom of the top layer can occur when applying hydrological stresses in a multi-layer-based groundwater model of geometrically thin and unconfined or convertible aquifers, like the BA. In MODFLOW-2000, this drawdown causes the MODFLOW grid cells to suffer from a phenomenon often referred to as dewatered or “dry” cells (Painter et al., 2008). MODFLOW–NWT is designed to avoid the occurrence of dry cells in unconfined and

convertible aquifer layers. The Well Package of MODFLOW-NWT reduces the pumping rate to zero if the water table drops below a specified cell thickness of the model (a percentage of the thickness of the top layer) (Niswonger et al., 20110). This adjustment allows for the water table to be maintained above the bottom of the top layer, so no cell will run dry.

However, in the context of the goal of this study, the effect of hydrological stress must be effectively reflected. It is necessary to develop a modeling protocol that incorporates the advantages of MODFLOW-2000 while avoiding its weakness regarding dry cells. Accordingly, after different trials, a single-layer MODFLOW-2000 model was selected as one of the best options to simulate the groundwater table fluctuation under conditions of drought, increased groundwater pumping, and sea level rise.

Under conditions of drought and high groundwater pumping, a single-layer model offers the opportunity to avoid the incidence of dry cells. Development of the MODFLOW-2000 model allows us to use and/or improve the model with little effort. MODFLOW-2000 model can be upgraded to other applications for contaminant transport and saltwater intrusion models using readily available simulation tools, such as MT3DMS and SEAWAT. As such, a complimentary objective for this part of the study is the modeling and the successful simulation of a single-layer MODFLOW-2000 model of the BA.

What is now needed is a comprehensive analysis of groundwater conditions in the BA under individual stress conditions, so the model depicts the effect of higher groundwater pumping and drought conditions. A calibrated and validated groundwater flow model will be an essential tool to evaluate the effect of selected and plausible scenarios (drought, pumping, sea level rise, potential recharge and others) on the groundwater head of the BA. Furthermore, unlike other studies, the scenario analysis that is considered in this study also examines the following questions: a) Which stress conditions have more influence on the groundwater head? b) What is the spatial distribution of the change in the groundwater table in response to the stress conditions? Multiple single and combined scenarios are considered and evaluated in Chapter 5. Accordingly, the objective of this study is to develop, calibrate, and validate a groundwater flow model of the BA capable of evaluating the groundwater table dynamics in response to changes to various stress condition.

4.3. Description of the study area

The study area covers the urban section of Miami-Dade County and covers an area of nearly 500 km^2. More than 85% of the study area has dense urban cover. Part of the Everglades wetland, an agricultural area, grassland, and lawns are located on the west side (Figure 4-1).

4.3.1. Topography and drainage.

A relatively flat plain characterizes Southeast Florida, along with limited variation in physiographic features. The highest elevation in the local topographic is

formed by a carbonate-rich deposit that forms the Atlantic Coastal Ridge (ACR). The NE-SW-trending ACR is crossed by drainage systems that channel water flow from west to east, creating the well-known traverse glades. The highest elevation across the ACR is as high as 7.0 m above NAVD88 (Hughes and White, 2014). The 5-ft mosaic elevation model (Figure 4-2) is the result of the 2018_ITD_LiDAR project for the Miami-Dade County Information Technology Department (ITD).

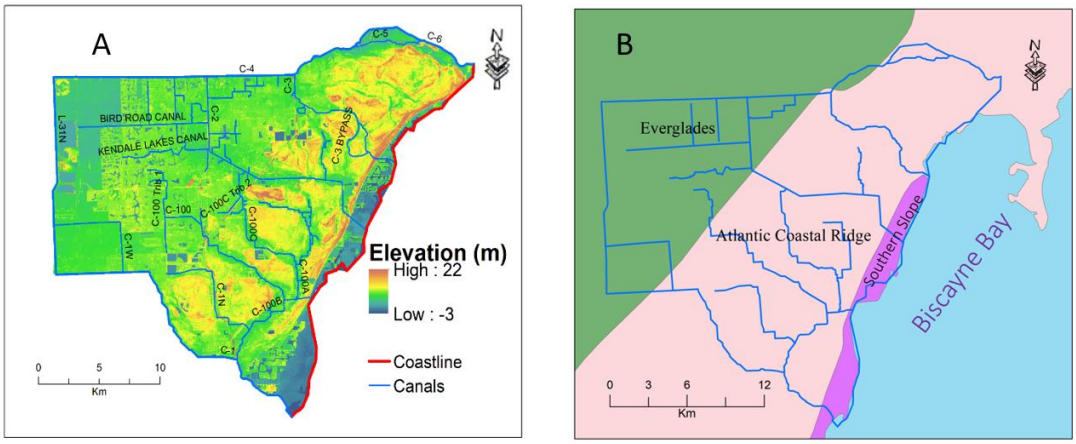

Figure 4- 2. A) Digital elevation model and surface drainage system in the study area. B) Physiography and location of the Atlantic Coastal Ridge in the study area.

The contemporary drainage pattern is a result of a complex network of human-made canals that generally drain water from the Everglades side (west) to the coastal reach (east). Canals were constructed to lower the water table in the Everglades by draining an extensive amount of freshwater to the ocean for the purpose of land acquisition for urban and agricultural development. Since the 1950s, the water table has dropped by 1 to 3 m below the surface (Langevin, 2003). A regulated water flow in canals is used for flood prevention and controlling saltwater intrusion into the BA.

4.3.2. Hydrology

Southeast Florida rainfall has a bimodal distribution. More than 70% of the rain is received in the wet season. The long-term regional rainfall in the area ranges from 1130 to 1640 mm/year, with a long-term average of 1552 mm/year (Abiy et al., 2019). Rainwater in the study area is partitioned into evapotranspiration, infiltration, runoff, and direct storage into the wetland, lakes, and groundwater. Given the sparse vegetation cover, the Everglades wetland is exposed to high evaporation that reaches up to 1317 mm/year. The Everglades loses 70 to 100% of the rainfall via evapotranspiration, while about 10% of the rainfall becomes runoff (Saha et al., 2012; Sandoval et al., 2016). The evaporation rates in the dry season tend to be higher than the amount of rainfall, causing the Everglades to go into a hydrological deficit (Abtew, 2007; Abtew et al., 2003). However, due to the intensive surface imperviousness in the urban area, the rainfall is converted into direct runoff, which is routed to drainage systems that drain water into the Atlantic Ocean (Hughes and White, 2014).

4.3.3. Geology and hydrogeology

There are two large aquifer systems in Southeast Florida: the Surficial Aquifer and the Floridan Aquifer Systems (Meyer, 1989; Parker et al., 1955). The BA is part of the Surficial Aquifer System and is located at the top of it (Cunningham and Florea, 2009; Fish and Stewart, 1991). The BA is composed of multiple stratigraphic layers (Causaras, 1985; Reese and Cunningham, 2000). A dominant part of the

aquifer is covered by a Pleistocene-age sandy, oolitic limestone and bryozoan limestone (Miami Limestone) with alternating beds of freshwater and marine limestone underlying it (Fort Thompson Formation). Cross-bedded layers affected by bioturbation characterize the Miami limestone.

Beneath the Everglades, the Miami Limestone is dominated by sandy, fossiliferous rocks deposited in a lagoon setting (Hoffmeister et al., 1967). The Fort Thompson Formation is composed of highly pervious sand and limestone with some intercalations of marl (Fish and Stewart, 1991). The BA contains intercalations of Pamlico Sand, Anesthesia Formation, and Key Largo Limestone, which also have high permeability (Figure 4-3). Underlying the Fort Thompson Formation, the Tamiami Formation forms the bottom of the BA. Two distinct layers form the Tamiami Formation: the Pinecrest Sand, Ochopee Limestone and underlying Grey Limestone.

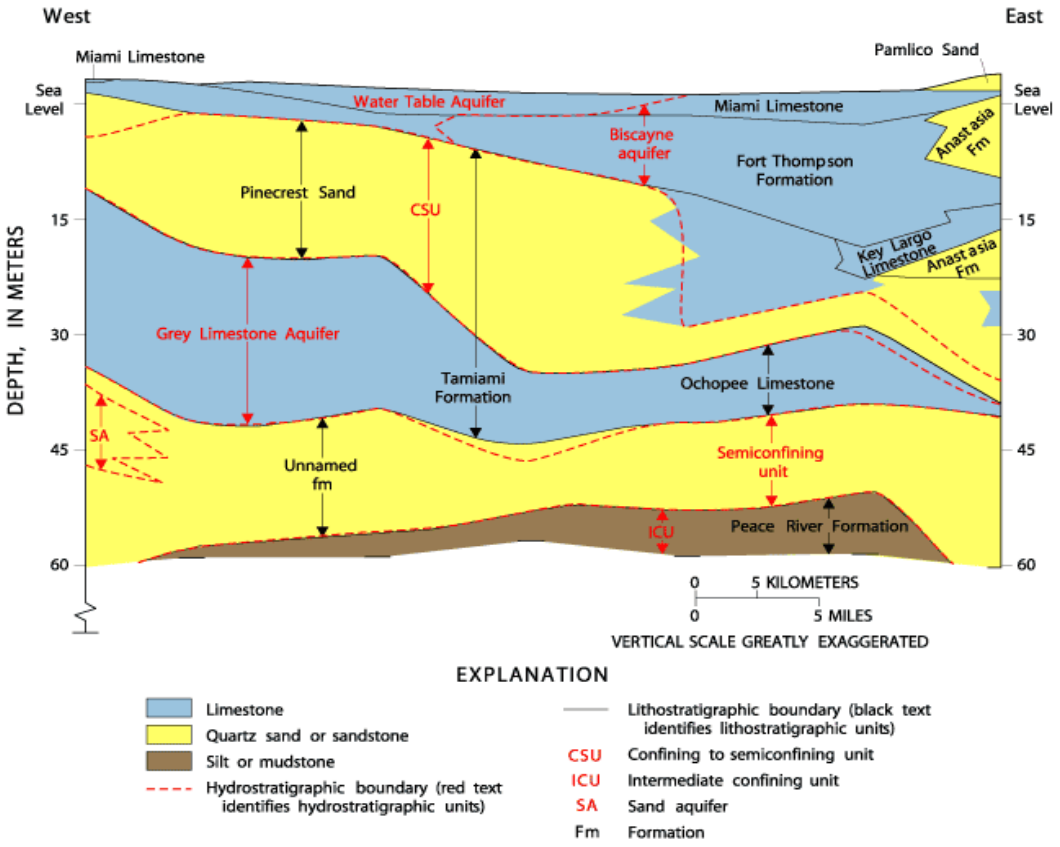

Figure 4-3. Geologic and hydrostratigraphic layers of the BA (Hughes and White, 2014; Reese and Cunningham, 2000).

Together, the Miami Limestone, Fort Thompson Formation, and the Tamiami Formation form the Surficial Aquifer System. A thick layer (over 300 m) of confining silt and sand separates the Surficial Aquifer System from the underlying Floridian Aquifer System (Cunningham and Florea, 2009; Meyers et al., 1993; Parker et al., 1955; Reese and Cunningham, 2000). The top of the Surficial Aquifer System is covered by thin organic soil and marl (Cunningham et al., 2004; Wacker et al. 2014).

Groundwater in the study area generally flows from west to east—from the Everglades to the Atlantic coast (Figure 4-4). Minor variations of east-to-west groundwater flow direction result from the extensive interaction between the aquifer

and surface water in canals. The effect of groundwater pumping is visible in a well-developed cone of depression along the wellfields (Fish and Stewart, 1991). In general, the groundwater table lies above sea level, but in areas where pumping is extensive, the groundwater table level is below sea level (Figure 4-4). The groundwater level near the coastal regions is maintained above sea level by the regulation of water levels in the canals (Hughes and White, 2014).

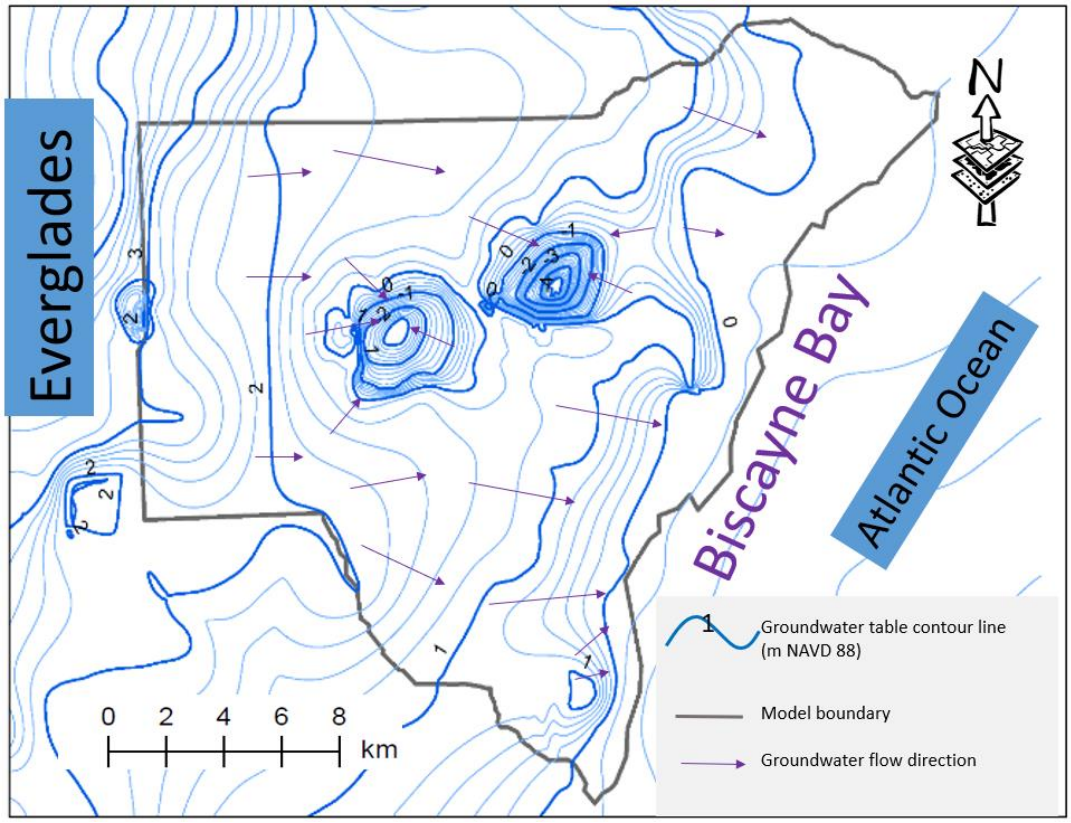

Figure 4-4. Dry season potentiometric surface of the BA modified from (Prinos and Dixon, 2016). The black line indicates the model area boundary.

4.4. Groundwater Modeling Protocol

Like other hydrological modeling, groundwater modeling will follow a standard modeling protocol from conceptual model to actual model development, calibration, validation to model verification (Figure 4-5).The key steep in the modeling process including the forward model that produces a groundwater level using the conceptual model of the study area that is integrated with hydraulic characteristics and source and sinks as input, is described in a number of groundwater modeling documents (Anderson et al., 2015). The forward model was subjected to statistical estimation (at the calibration and manual adjustment at the validation stage) of the hydraulic parameters (Figure 4-5) using observed groundwater level and sources and sinks.

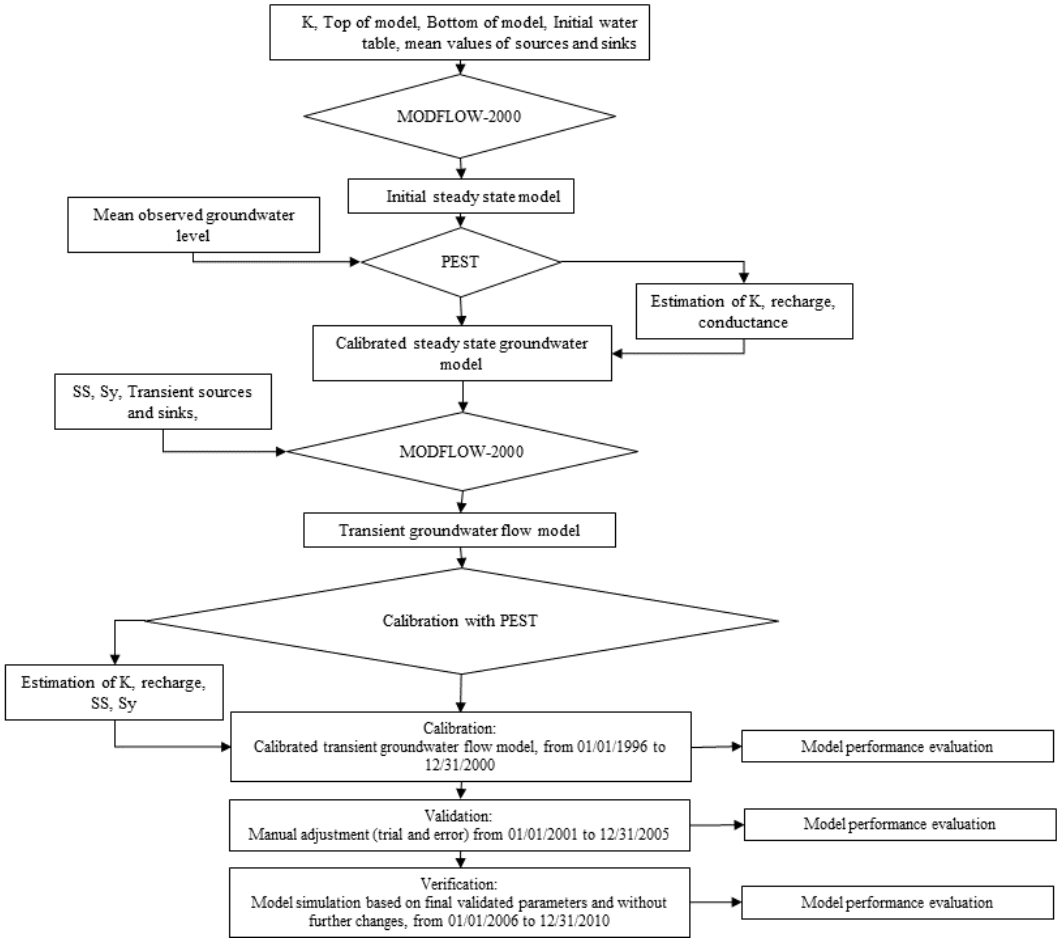

Figure 4- 5. Groundwater modeling procedure applied in this study.

The performance of the model was measured by comparing the simulated and observed groundwater head at the monitoring station (Anderson et al., 2015; Gupta et al., 2002). The description of the conceptual model, model setup and datasets used in this study are provided in detail under the sections below.

4.5. Conceptual model

The groundwater flow model of the BA in this study was developed based on the conceptual hydrological model indicated in the schematics below (Figure 4-6). It

is a wedge-shaped water table aquifer with a maximum thickness of up to >40 m near the Atlantic coast (East in Figure 4-6). It pinches out at the surface in the central Everglades area. In this study, the BA is represented as a single layer unconfined aquifer with the water table forming the top of the model and an impervious layer bounding the bottom. The general groundwater flow direction is from west to east. The groundwater flow regime in the aquifer is intercepted by canals, municipal water supply wells, and artificial lakes, which also have hydrological effects on the water balance of the aquifer. Therefore, estimation of the groundwater and surface water interaction and the effect of pumping are considered as part of the parameters in this groundwater flow-modeling protocol.

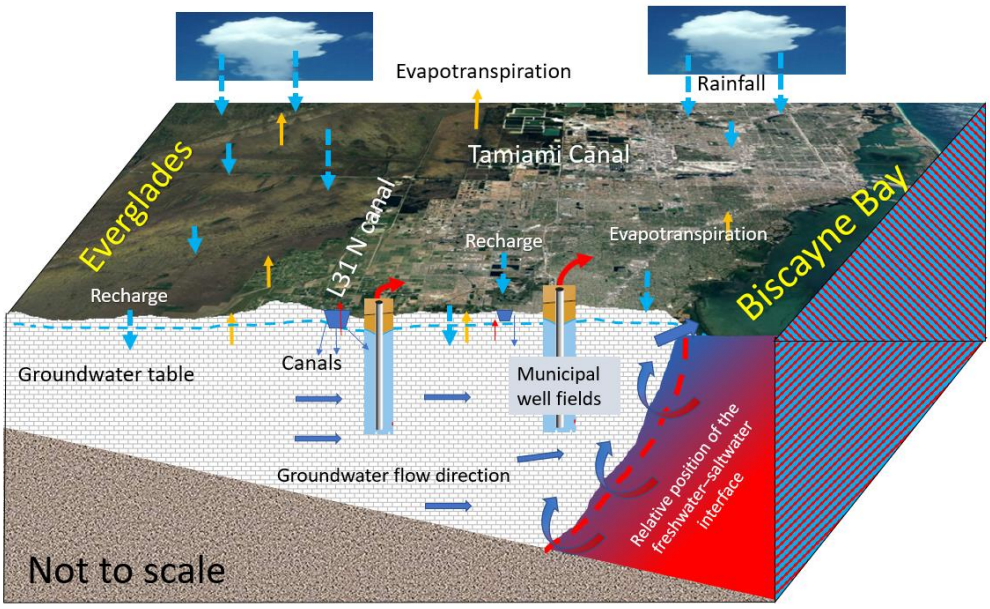

Figure 4- 6. Diagram indicating key hydrological features in the model domain. The study area is located east of the L31N canal and south of the Tamiami canal. The cross sectional of the BA (front view of the block diagram) represent a wage shaped aquifer with maximum thickness in the coastal region (figure not to scale). The underlining grey shad represents the improvises layer that separates the surficial aquifer from the reset of the subsurface.

Conceptually, the inflow components of the groundwater balance in the study area are rainfall, recharge, regional groundwater circulation, and leakage from canals. The outflow components of the groundwater balance are evapotranspiration, groundwater pumping, groundwater discharge through canals, and coastal groundwater discharge. The following sections describe the boundary conditions, initial conditions, governing equations of groundwater flow, and mathematical formulation for estimation of all model parameters.

4.6. Initial conditions and hydraulic properties

The BA has a dual-porosity system comprising matrix (primary porosity) and dissolution features (secondary porosity). The different hydrostratigraphic units forming the BA are characterized by a wide range of porosity (Fish and Stewart, 1991). The dissolution features dominate the porosity systems with an estimated porosity of 14 to 70% (Whitman and Yeboah-Forson, 2015). A tracer test in the BA estimated the effective porosity as 4 to 41% (Renken et al., 2008).

Using model calibration, several studies have suggested that the effective porosity of the aquifer is between 20 and 30% (Hughes and White 2014; Merritt et al., 1996; Langevin, 2003). The mean hydraulic conductivity is 9,000 m/d (Fish and Stewart, 1991; Wacker et al., 2014). The effective porosity value of an aquifer is required in particle-tracking simulations (Anderson et al., 2015). Besides porosity, the hydraulic characteristics of the BA have been examined by several studiesas shown in Table 4-1.

Table 4- 1. Summary of hydraulic characteristics of the BA (Surficial Aquifer). The estimation shows a wide range of parameter values that is because of the differences in methods and the spatial resolution used for the estimation.

S.No	Parameter	Value	Source
1	Transmissivity $\left(\frac{ft2}{d}\right)$	1.0 x 10^6 4.3 x 10^5 to 1.9 x 10^6 35,000	Fish and Stewart 1991. Hughes and White, 2014. Wacker et al., 2014.
2	Vertical Hydraulic Conductivity $\left(\frac{m}{day}\right)$	40 to 9,900 (mean of 8,200) 9,000 m/d	Wacker et al. 2014. Langevin 2003.
3	Horizontal Hydraulic Conductivity $\left(\frac{m}{day}\right)$	15 to 90	Langevin 2003.
4	Anisotropy $\left(\frac{Kv}{Kh}\right)$	1.18 to 2.83	Yeboah-Forson and Whitman, 2014.
5	Specific Yield	0.2 to 0.25 0.2 0.2 to 1.0	Hughes and White 2014. Merritt et al., 1996. Langevin 2003.
6	Storage Coefficient	1 x 10^{-5} 2 x 10^{-5}	Dausman and Lengvin 2005. Langevin 2003.
7	Total porosity Effective porosity	14 to 70% 20%	Yeboah-Forson and Whitman, 2014. Langevin 2003.

Groundwater flow modeling starts with the development of a steady-state model that is used as input for a transient state model (Anderson et al., 2015; Franke et al., 1987). The mean groundwater table contour map of the area during the dry season (Prinos and Dixon, 2016) was used as an initial condition for the groundwater head (Figure 4-4). The steady-state model was developed using mean values of the observed groundwater head, surface water stage in canals, pumping rate, and sea level condition, as suggested in different studies (Franke et al., 1987).

Aquifer data were collected from the USGS multiple-layer regional groundwater flow model for Miami-Dade County (Hughes and White, 2014). The USGS MODFLOW-NWT[1] model has three layers, but for this study, the hydraulic characteristics of the three layers were converted into a single layer (Figure 4-6) using weighted mean techniques (Equation 4-1), as suggested in different studies (Anderson et al., 2015; Hill and Tiedeman, 2007). The weighted mean of the single-layer hydraulic conductivity was calculated using the layer thickness data collected from the Lower East Coast Sub-regional (LECsR) MODFLOW Model of the SFWMD (Giddings et al., 2014). The layers' hydraulic conductivity, thickness, specific yield, specific storage, and rater map is given in Appendix 1. The single-layer horizontal hydraulic conductivity (Figure 4-7a) was estimated using:

[1]In this report, this data source is referred to as the USGS model. All the information in reference to the USGS model is freely available online at https://water.usgs.gov/GIS/metadata/usgswrd/XML/sir2014-5162_usgsdatarelease.xml. The USGS model data used in this study was accessed in August 2018.

$$K_h = \frac{\sum_{i=1}^{n} K_i b_i}{\sum_{i=1}^{n} b_i} \qquad i=1,2,3. \qquad (4\text{-}1)$$

where K_h is the weighted horizontal hydraulic conductivity of the single layer, K_i is the horizontal hydraulic conductivity of each layer (i=layer number 1, -2, and -3), and b_i is the individual layer's thickness.

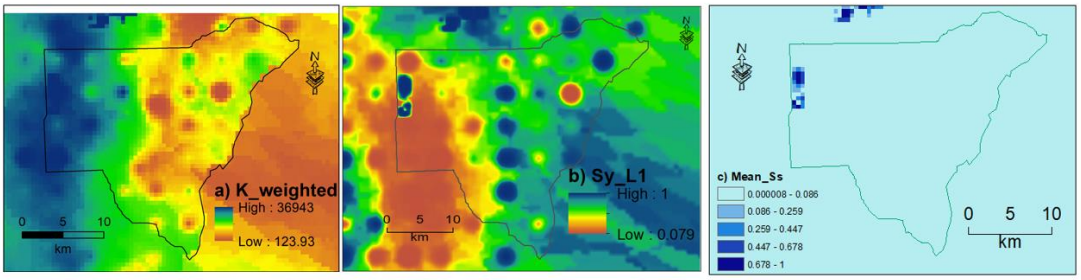

Figure 4- 7. A) Single-layer weighted mean hydraulic conductivity, B) Single-layer-specific yield (Sy), and C) Single-layer-specific storage (Ss) of the BA. Source: Miami-Dade County USGS groundwater flow model (Hughes and White, 2014).

4.6.1. Source and sinks

Recharge: Groundwater recharge is the volume of water that reaches the BA from various sources. The primary sources of recharge are diffused recharge from rainfall and localized recharge from canal leakage. Diffused recharge of 38 cm/year was estimated by model calibration (Langevin, 2003). In Miami-Dade County, the mean annual rainfall is 150 cm/year. Accordingly, the estimated effective rainfall recharge of 38 cm/year (Langevin, 2003) accounts for around 25% of the total annual rainfall in the locality. Therefore, in this study, the initial model was simulated using 25% of the areal precipitation in each recharge zone. In groundwater modeling, recharge can be estimated as effective rainfall, the volume of rainfall the makes to

groundwater recharge, or as the balance between rainfall, runoff and evapotranspiration. The latter two parameters are better used if the purpose of the model were to assess absolute groundwater balance. However, in this study a realistic recharge estimate was used as a frame of reference to assess how change in effective recharge affects the groundwater condition. The effective recharge is rather assumed as the net rainfall that reaches to the groundwater table. In this case, 25% of the rainfall is used as an initial recharge to start the model.

The recharge zones are delineated using the Thiessen polygons (Figure 4-8) of point rainfall measurement stations in the study area. Six rainfall measurement stations with limited missing data values were selected, so the model area is divided into six Thiessen polygons that each represent a recharge zone. Diffused recharge from the return flow of irrigation applications for crop production, recreational areas, and septic tanks are reported (Hughes and White, 2014). However, the model area in this study is prominently covered by urban infrastructure, so we have assumed that avoiding these terms will introduce minimal error.

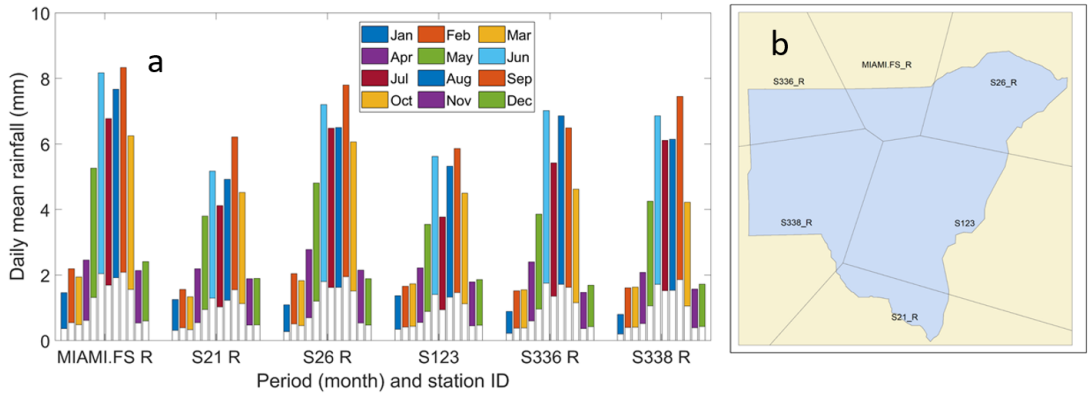

Figure 4- 8. a) Comparison of monthly rainfall and applied groundwater recharge. The white area under each bar represents 25% rainfall, the net rainfall that goes into the groundwater recharge. b) Recharge zone polygons represent the six rainfall measurement stations. The Thiessen polygons of the stations define the recharge zones in the groundwater model.

Groundwater pumping: Groundwater pumping is one of the hydrological stressors in the BA. In Miami-Dade County, the BA is pumped from 22 wellfields to produce 1.35 x10^6 to 1.68 x 10^6 m^3/d (Lohmann et al., 2012). There are four wellfields in the study area: Alexander Orr (AO) with 10 pumping wells; Snapper Creek (SC) with 4 pumping wells; Southwest (SW) with 16 pumping wells; and West (WW) with 4 pumping wells (Figure 4-9). The groundwater pumping volume in the study area does not change significantly over the study period. Figure 4-9 indicates the daily groundwater pumping volume of randomly selected individual wells.

Figure 4- 9. Groundwater pumping rate from randomly selected wells from the four wellfields within the model domain: AO10 for Alexander Orr well number 10; SC24 for Snapper Creek well number 24, SW20 for South West well number 20, and WW30 for West Wellfield well number 30. The location of the four wellfields is indicated in Figure 4-7.

The groundwater pumping data in the USGS model is shown in Figure 4-9. This pumping rate data are used to define the daily pumping rate in the MODFLOW Well Package. A detailed description of the groundwater pumping data is presented in the USGS model's documentation report (Hughes and White, 2014).

4.6.2. Boundary condition

Canal boundaries: Canals bound the entire model area (Figure 4-10). The Tamiami (C-4) and Black Creek (C-1) canals form the north and south boundaries, respectively. The L-31N canal is the west boundary, while the coastline along the Biscayne Bay bounds the east side of the model area.

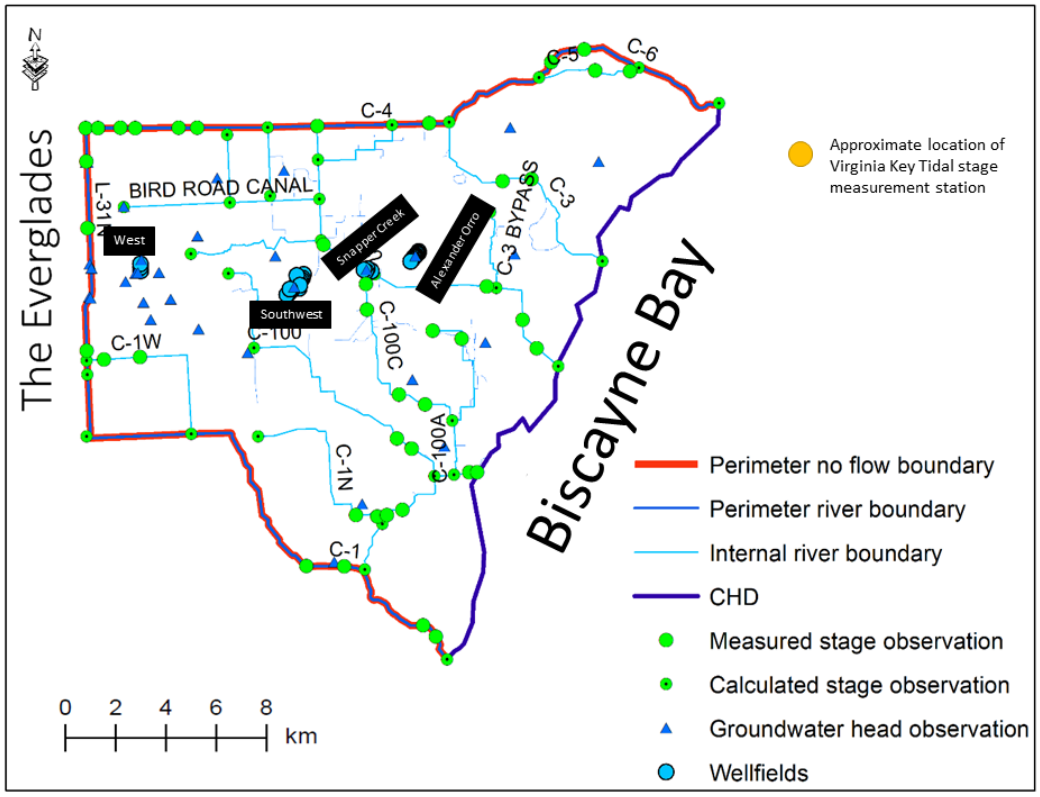

Figure 4- 10. The physical distribution of boundaries, four wellfields, and groundwater level monitoring wells within the model domain. The coastline is defined as an observed head that varies with time, which is referred to as a Time Variant Specified head (CHD) boundary in MODFLOW.

All canals are represented as river boundaries using the river model in MODFLOW 2000 (Harbaugh et al., 2000). In MODFLOW, rivers are conceptualized as head-dependent flow boundaries. For rivers, the observed surface water head is used as a required input at every river node (Brunner et al., 2010). There are 73 river nodes in the model, and for 46 of them, observed surface water level measurements are available. In river nodes where observational data are not available, the water stage was estimated using applicable geometric relations such as triangle similarities by right angle–hypotenuse-side or angle–angle–angle or slope-intercept approaches.

Both the observed and calculated surface water levels represent water stages at the respective river nodes in the model.

Coastal Boundary: Large water bodies that cannot be affected by the stress conditions within the model domain can best be defined as Specified Head Boundary Conditions (Anderson et al., 2015). Therefore, the coastal boundary is represented by the MODFLOW time-variant specified head (CHD) package. The CHD boundary is applied along the coastline cell. Based on data availability and proximity to the model domain's coastal boundary criteria, the tidal fluctuation record from Virginia Key (Figure 4-11) is selected to represent the sea level fluctuation along the coastline.

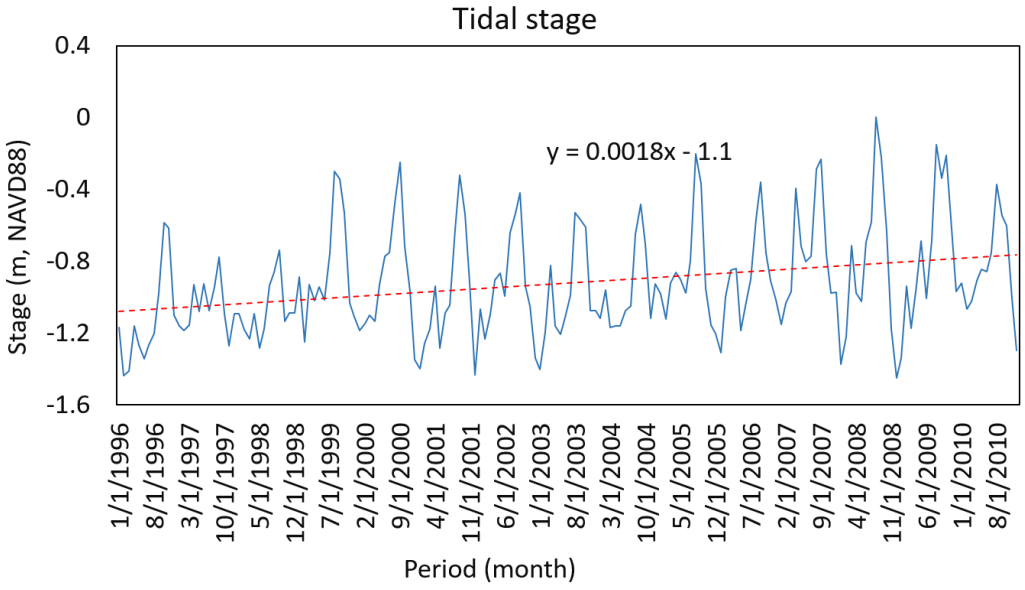

Figure 4- 11. Monthly average tidal stage measured at Virginia Key. The tidal stage is used as a time-variant specified head boundary condition.

4.6.3. Governing Equation

Groundwater flow models of the BA were developed using USGS MODFLOW 2000 (Harbaugh et al., 2000). The following is the governing equation applied in MODFLOW (Equation 4-2) when the principal axes of hydraulic conductivity are aligned with the Cartesian coordinate directions:

$$\frac{\partial}{\partial x}\left(K_{xx}\frac{\partial h}{\partial x}\right)+\frac{\partial}{\partial y}\left(K_{yy}\frac{\partial h}{\partial y}\right)+\frac{\partial}{\partial z}\left(K_{zz}\frac{\partial h}{\partial z}\right)\pm W=\mathbf{S_s}\frac{\partial h}{\partial t} \qquad (4\text{-}2)$$

where K_{xx}, K_{yy}, and K_{zz} are the medium hydraulic conductivity in the x, y, and z directions [L/T], respectively, h is the hydraulic head [L], W is the source and sink term given in volumetric flux per unit volume in a given time [T^{-1}], Ss is the specific storage of the porous material [L^{-1}], and t is time (T) (Anderson et al., 2015; Harbaugh et al., 2000; McDonald and Harbaugh, 1988; Wang and Anderson, 1982).

The specific storage of the porous material [L^{-1}] represents the volume of water discharge from a confined aquifer per unit surface area of aquifer per unit aquifer thickness per unit change in head. As the BA is unconfined, additional water can be drained from pore spaces due to gravity (water drained as a function of the aquifer yield). Therefore, groundwater flow in an unconfined aquifer is a function of both the specific storage (Ss) and the specific yield (Sy) terms given as total storativity, or simply storativity. The storativity (S) of an unconfined aquifer is given as (Equation 4-3):

$$S = Sy + Ss*b, \quad (4\text{-}3)$$

where b is the saturated aquifer thickness [L].

The model accounts for modification based on the Dupuit–Forchheimer assumptions for practical application of the governing equation (Equation 1) to simulate groundwater head in a 2D model of unconfined aquifer conditions. One of the assumptions is that groundwater flow is horizontal, so the equipotential surface is vertical, and the hydraulic gradient is equal to the slope of the free surface. The assumptions hold if the slope of the water table is small, which implies that the vertical flux is constant; hence, the partial derivative Kzz(dh/dz) =0. Another modification to the governing groundwater flow equation is the substitution of the Ss term with Sy/b. Therefore, a 2D groundwater flow in an unconfined aquifer can be simulated using the following equation:

$$\frac{\partial}{\partial \mathrm{x}}\left(\mathrm{K_{xx}} h \frac{\partial \mathrm{h}}{\partial \mathrm{x}}\right) + \frac{\partial}{\partial \mathrm{y}}\left(\mathrm{K_{yy}} h \frac{\partial \mathrm{h}}{\partial \mathrm{y}}\right) \pm \mathrm{W} = \mathrm{S}_y \frac{\partial \mathrm{h}}{\partial \mathrm{t}} \quad (4\text{-}4)$$

In this case, the K*h term represents the aquifer's vertically integrated parameter known as transmissivity. Further details on the application and derivation of groundwater flow are available in hydrogeology books (Anderson et al., 2015; Wang and Anderson, 1982).

Water exchange between the aquifer and different head-dependent conditions, such as rivers, lakes, and the ocean boundaries, is calculated as a function of the hydraulic head difference between the reservoirs (Equation 4-5). For hydraulically

connected systems (conditions), the groundwater surface-water interaction is calculated, thus forming a gaining river (Equation 4-5). A lower groundwater head condition leading to a hydraulically disconnected system is evaluated by considering that the river is a losing river system (Equation 4-6). In either case, the volume of water exchange is a function of the river bed conductance (Equation 4-7) (Harbaugh et al., 2000; McDonald and Harbaugh, 1988):

$$Q_{RIV}=C_{RIV}(H_{RIV}-h) \qquad H_{RIV}-h>0 \qquad (4\text{-}5)$$

$$Q_{RIV}=C_{RIV}(H_{RIV}-R_{BOT}) \qquad h\leq R_{BOT} \qquad (4\text{-}6)$$

$$C_{RIV} = \frac{K_r}{M} L W \qquad (4\text{-}7)$$

where C_{RIV} [L^2/T] is the canal bed conductance, and L [L] and W [L] are the length and width of the canal cross-section, respectively. M [L] is the thickness of sediment in the canal. K_r is the vertical hydraulic conductivity of the aquifer. Q_{RIV} [L^3/T] is the rate of leakage, and H_{RIV} [L], h [L], and R_{BOT} [L] are water head at the canal, groundwater, and elevation at the canal bottom, respectively. The term $\frac{K_r}{M}$ refers to the vertical leakage coefficient of the canals.

Oceanic water has a higher density than the fresh water in the aquifer. Consequently, to incorporate the effect of density, the equivalent freshwater head is calculated by (Hughes and White, 2014):

$$h_f = \frac{\rho_s}{\rho_f} h_{coast} - \frac{\rho_s - \rho_f}{\rho_s} z \qquad (4\text{-}8)$$

where h_f [L] is the freshwater head, h_{coast} [L] is the sea level [L], ρ_s = 1000 kg m^{-3} and ρ_f = 1025 kg m^{-3} are the densities of freshwater and seawater, respectively, and z [L] is the bathymetric elevation. The BASIC (BAS), Layer-Property Flow (LPF), WELL (WELL), RECHARGE (RCH), RIVER (RIV), and Time-Variant Specified Flux (CHD) packages of MODFLOW were used to simulate the groundwater flow process and its interaction with the different sources and sinks in the model domain.

The equivalent freshwater head is applied only on the coastal boundary model cells. There is not enough information found to address further changes in the effect of salinity across the boundary line and within the model domain.

4.6.4. Spatial and temporal discretization

A single-layer MODFLOW 2000 model was developed with the water table at the top of the model and a no-flow boundary at the bottom. The model covers 1114.7 km^2 and was designed in a projected coordinate system using UTM Zone 17N and the North American Horizontal Datum. The elevation is represented by meters above NAVD88 (m, NAVD88).

The model has grid dimensions of 100 m by 100 m with 49,928 active cells and 61,872 inactive cells (Figure 4-12). The canals in the model domain are represented by the river module of MODFLOW. Pumping wells are defined by the well model and denoted by yellow dots, while the coastal boundary is defined by CHD boundary condition. The purple dots along the coastline represent the CHD boundary condition.

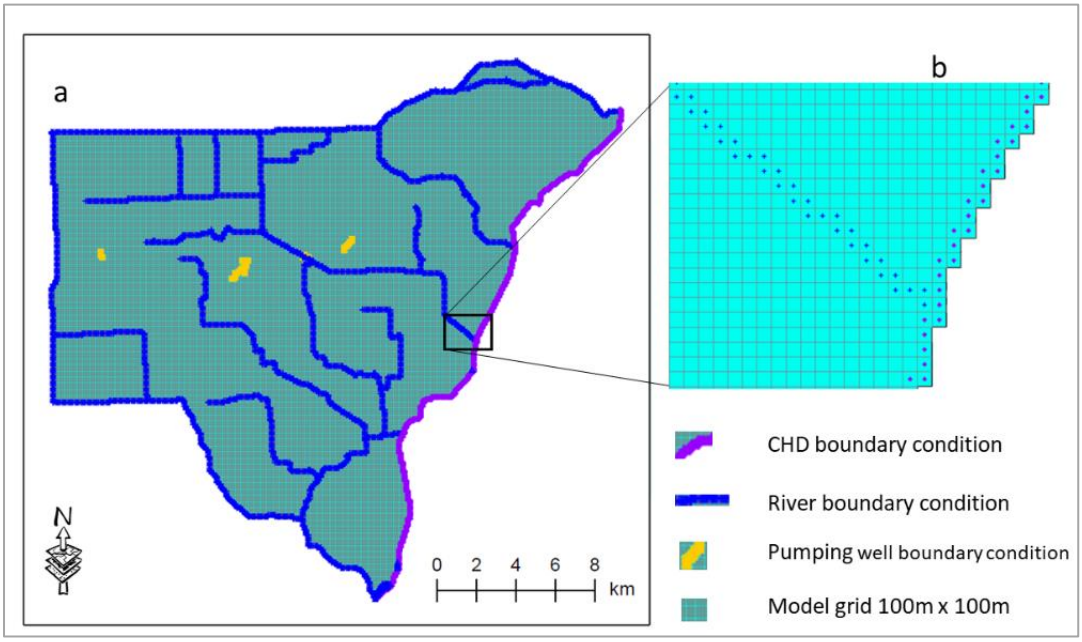

Figure 4- 12. a) Grid design and boundary conditions implemented in MODFLOW and b) a magnified version of a section in the model domain indicating that the boundary conditions form discrete points located at the center of the respective grids.

The transient model was simulated on a daily time scale using a MODLFOW time step of 10. The model was simulated using a time-step multiplier of 1.42. For stable simulation of nonlinear MODFLOW problems, a time step greater than 5, a time step multiplier of 1.1 to 1.5, and an optimum value of 1.42 are recommended (De Marsily et al., 2005; Hill and Tiedeman, 2007).

4.6.5. Model calibration, validation, and verification

Calibration: Groundwater model calibration is a statistical procedure (Doherty et al., 2010) with the goal of estimating the optimum aquifer hydraulic parameters. This is accomplished by using the observed groundwater head (h_o) and a predefined mode calibration objective function (Reilly and Harbaugh, 2004). In this study, spatially distributed groundwater-monitoring stations served as calibration

targets (Figure 4-13). The model was calibrated for the five years between 01/01/1996 and 12/31/2000 using the highly parameterized inversion technique with PEST (Doherty et al., 2010). PEST is a nonlinear parameter estimation procedure that processes an inverse MODFLOW using observed groundwater head as an input to solve for user-defined aquifer parameters (Anderson et al., 2015; Doherty et al., 2010).

The initially estimated diffused groundwater recharge, water leakage from canal (conductance) and aquifer horizontal hydraulic conductivity values were estimated for calibration of the steady state model. In addition, aquifer specific storage and specific yield values were used to calibrate the transient model.

Validation: The validation stage is considered as a check and balance to evaluate the acceptability of the estimated parameter values by comparing with the realism of geological information and literatures. At the same time the validating stage gives an additional layer of evaluating the model performance by running a simulation in a different time window. For the validation stage of the modeling protocol, the calibrated model was simulated by manually changing the recharge and hydraulic conductivity until better model performance was achieved. The overall model validation was considered for five years between 01/01/2001 and 12/31/2005).

Verification: In the model verification stage, the validated model was simulated for an extended period (without any change in the input parameters used in the validation stage). Model verification is intended to assess the model's ability to

simulate the groundwater table conditions in the observation well sites. The period of 01/01/2006 to 12/31/2010 was used for model verification. The verification stage is considered as a measure of assessing the models predicting ability by changing one or any combination of stress conditions, while maintain the hydraulic properties unchanged.

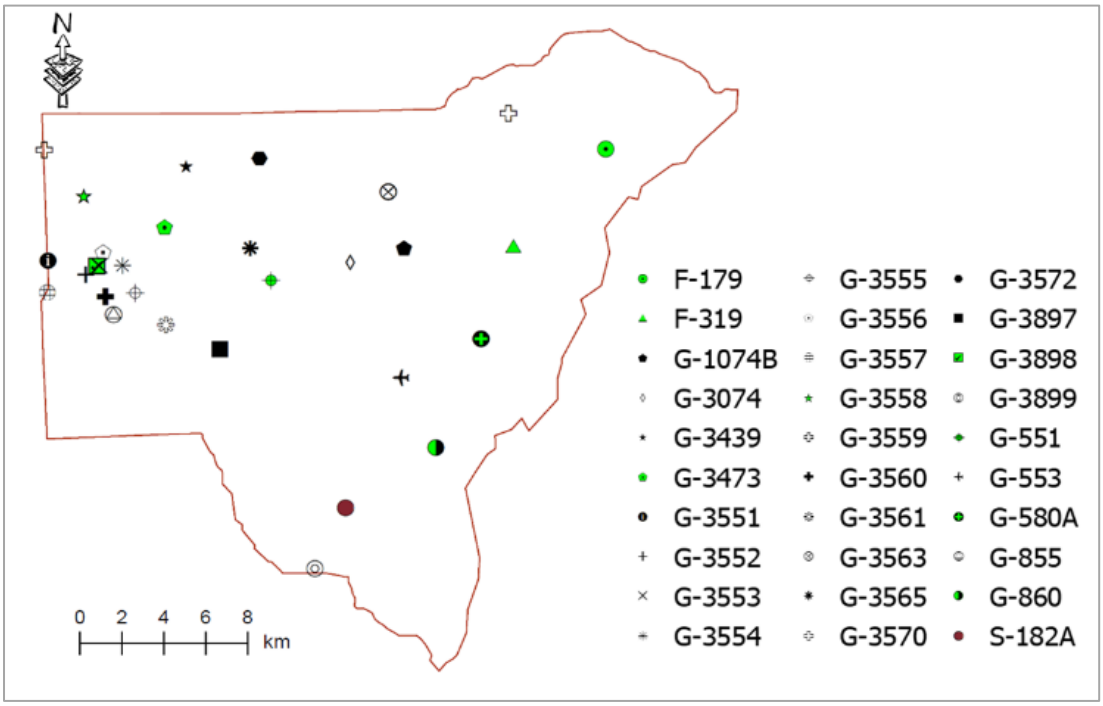

Figure 4- 13. Spatial distribution of calibration target groundwater table observation wells.

4.6.6. Model Performance Evaluation

The performance of the groundwater flow model was assessed using the objective functions described below (Equations 4-9 to 4-12).

Bias Ratio (BIAS): For an observed groundwater head h_o and simulated groundwater head h_s, the bias ratio or percent bias measures the relative tendency of

the model product compared to the observation (Gupta et al., 2002; Hoshin Vijai et al., 1999):

$$\text{PBIAS} = \sum_{j=1}^{v}\left[\left(\frac{\sum_{i=1}^{n_j}(h_s - h_o)}{\sum_{i=1}^{n_j} h_o}\right)\right] \quad (4\text{-}9)$$

PBIAS helps to determine whether the simulation tends to overestimate (PBIAS >0) or underestimate (PBIAS<0) the observation data. A PBIAS of zero denotes the best fit between the simulation and observation data.

Coefficient of Determination (R^2): R^2 measures how well the simulation replicates the observed groundwater head. It defines the degree of collinearity between the observed and simulated heads and is computed using the square of the covariance of the simulated groundwater head with the observed data. R^2 for a pair of the datasets is any of the non-diagonal components of the correlation matrix calculated by:

$$R^2(ho, hs) = \left(\frac{\sum_{i=1}^{n}(h_{oi} - \bar{h}_o)(h_{si} - \bar{h}_s)}{\sqrt{\left[\sum_{i=1}^{n}(h_{oi} - \bar{h}_o)^2 (h_{si} - \bar{h}_s)^2\right]}}\right)^2 \quad (4\text{-}10)$$

where $\bar{h}_o$ and $\bar{h}_s$ are the means of the observed and simulated data, respectively. The coefficient of determination ranges from 0 to 1.

Root mean square error (RMSE): RMSE measures the mean of the squared residual evaluated by:

$$\mathrm{RMSE} = \sum_{i=1}^{n} \frac{\left(\sqrt{\sum_{i=1}^{n}(h_{oi} - h_{si})^2}\right)}{n} \qquad (4\text{-}11)$$

Nash-Sutcliffe Efficiency Coefficient (NS): NS determines the relative magnitude of the residual variance compared to the variance of the observed data:

$$\mathrm{NS} = \sum_{i=1}^{n} \left(1 - \left[\frac{\sum_{i=1}^{n}(h_{oi} - h_{si})^2}{\sum_{i=1}^{n}(h_{oi} - \bar{h}_o)^2}\right]\right) \qquad (4\text{-}12)$$

NS ranges from –∞ to one and signifies how high the performance of the model is in mimicking the observed data in terms of magnitude and hydrography (Nash and Sutcliffe, 1970).

4.7. Results and Discussion

As part of the results and discussion, a description is presented for the steady and transient state model and the model performance result.

4.7.1. Steady state simulation and evaluation

The initial steady-state groundwater flow model was developed using the mean values of the observed sources and sink and the aquifer hydraulic properties. The initial steady-state groundwater flow model was used to develop a stable base case groundwater flow model after initial simulation followed by calibration. In general the initial simulation mimics the input water table distribution map (Prinos and Dixon, 2016). Given the model performance and water balance information the model is needed to be calibrated. The calibration of initial model has improved the

model performance evaluation (R^2) and it has changed the water balance components as indicted in the table below. The water balance was calculated in a cell by cell basis using ZONBUDGET.

Table 4- 2. Steady-state volumetric water balance based on the initial simulation and after calibration of the initial simulation. The water balance was calculated in a cell by cell basis using ZONBUDGET.

	Initial simulation	After Calibration
Source/ Sink	Volumetric Flow IN (m^3)	Volumetric Flow IN (m^3)
Constant head	0	0
Wells	0	0
River leakage	2,662,449	3,439,662
Recharge	194,077	217,515
Total IN	2856526	3,657,177
	Volumetric Flow OUT (m^3)	Volumetric Flow OUT (m^3)
Constant head	218,105	328,187
Wells	634,939	634,939
River leakage	2,003,523	2,694,052
Recharge	0	0
Total OUT	2,856,567	3,657,178
In-out	-41	0
Percent error	0	0

The base-case steady-state groundwater model of the BA indicates that the western boundary has higher head conditions close to 1.1 m above NAVD 88 (Figure 4-14). This model result agrees with the flow condition based on the observational water table map of the BA (Prinos and Dixon, 2016) and regional model results (Hughes and White, 2014; Lohmann et al., 2012). The high level of correlation of the simulated groundwater table conditions (R^2=0.9) with the observed data suggests that a steady-state model is a robust tool for evaluation of the response of the aquifer to changes in certain parameters. The model suggests that the groundwater head is higher near the canals. There is a steep water-table gradient near the wellfields and the coastal boundary. The coastal boundary of the model domain has a water table surface that is parallel to the specified head boundary condition.

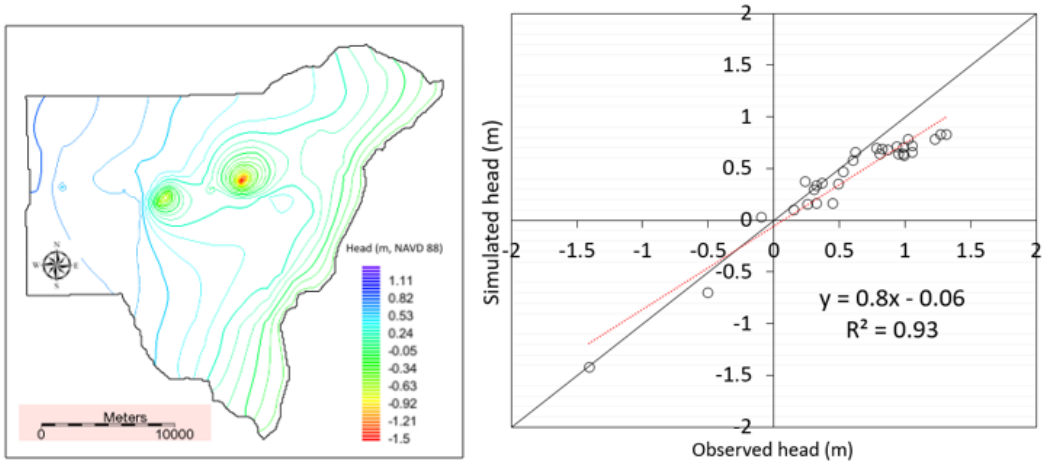

Figure 4- 14. Steady-state groundwater model results: a) steady-state groundwater head model with contour values representing groundwater head (m, NAVD88); and b) steady-state model performance evaluated using the observed groundwater head.

According to the model, diffused groundwater recharge and leakage from canals form the inflow component of the local water balance. Groundwater discharge

through rivers and the coastal boundary, as well as pumping through wells, accounts for the outflow components of the aquifer water balance (Table 4-2). This relationship is consistent with the established groundwater budget in the conceptual model of the study.

4.7.2. Transient state simulation and evaluation

The transient simulation follows steep by the steep process. First, the calibrated steady-state model is used as input to generate the initial transient groundwater model. The initial transient groundwater model was calibrated using zonal hydraulic conductivity, aquifer leakance, storage, specific yield, recharge as calibration parameters. In the validation stage, the recharge, hydraulic conductivity, and leakance were manually changed, and simulation was conducted in a different time window, as described in the main text of this annex. And finally, the verification stage the simulation is conducted without any change in all the hydraulic parameters achieved in the verification stage. The water balance of the different stages is indicated in the table below.

Table 4- 3. Volumetric water (m3) balance of the transient groundwater flow model.

Sources/Sinks	Initial		Calibration	
	Volumetric Flow IN (m^3)	Volumetric Flow OUT (m3)	Volumetric Flow IN (m^3)	Volumetric Flow OUT (m3)
Storage	93900.85	-3847.2895	14921.49	0
Constant head	0	-668398.66	0	-1025665
Wells	0	-646536.59	0	-646536.6
River Leakage	3034103	-1938393.7	1724467	-379875.2
Recharge	129172.1	0	312688.5	0
Total Source/Sink	3257176	-3257176.2	2052077	-2052077
Summary	In - Out	% difference	In - Out	% difference
Sources/Sinks	0.063	1.93E-06	-0.042	-2.03E-06
Total	0.063	1.93E-06	-0.042	-2.03E-06
	Validation		Verification	
	Volumetric Flow IN (m^3)	Volumetric Flow OUT (m^3)	Volumetric Flow IN (m^3)	Volumetric Flow OUT (m^3)
Storage	14625.835	0	46979.655	0
Constant head	0	-976336.1	0	-985002.6
Wells	0	-678031.2	0	-657237.2
River Leakage	1608797.4	-280220.5	1610590	-233489
Recharge	311164.51	0	218159.15	0
Total Source/Sink	1934587.8	-1934588	1875728.8	-1875729
Summary	In - Out	% difference	In - Out	% difference
Sources/Sinks	-0.035	-1.81E-06	-0.004	-2.09E-07
Total	-0.035	-1.81E-06	-0.004	-2.09E-07

The simulation results and observation data were compared in a series of hydrographs produced for the calibration (from 01/01/1996 to 12/31/2000), validation (from 01/01/2001 to 12/31/2005), and verification (from 01/01/2006 to 12/31/2010) stages (Figure 4-15). These hydrographs indicate that the simulation has successfully reproduced the observed groundwater head fluctuation in most of the observation stations. The pattern and seasonality of the groundwater head fluctuations are well established and in agreement with the records, but the model does not reflect the extremely high groundwater level conditions of some wells.

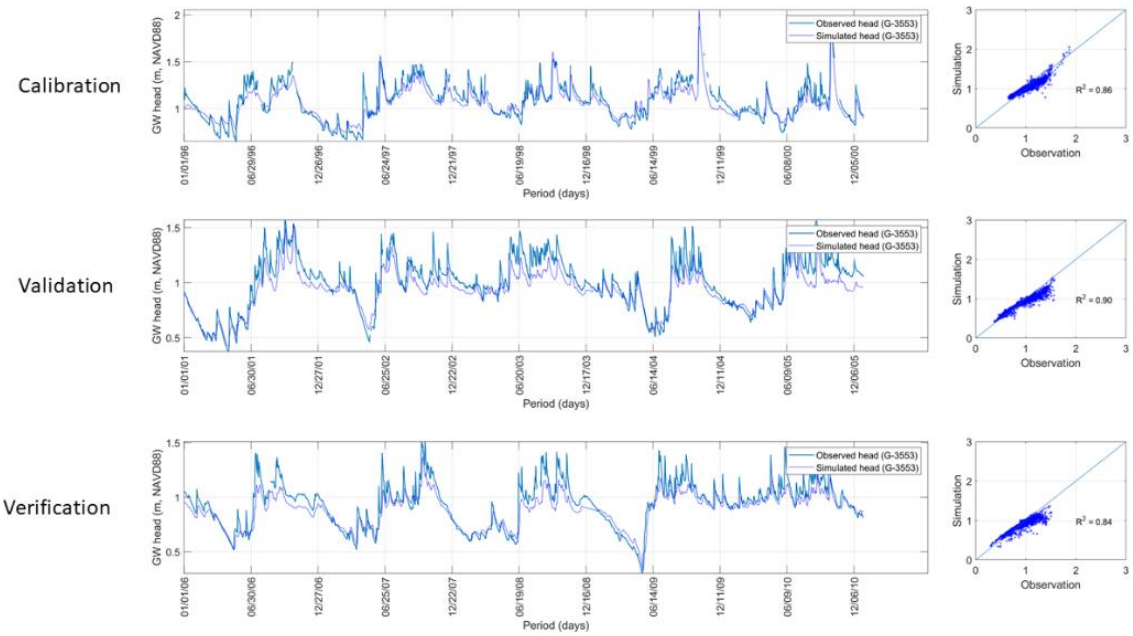

Figure 4- 15. Hydrographs of a randomly selected observation well showing comparisons between the simulated and observed transient groundwater head for model calibration, validation, and verification stages of the modeling process.

The model performance at each stage of the modeling process was evaluated using the bias ratio (BIAS), coefficient of determination (R^2), root mean square error (RMSE), and Nash-Sutcliffe Efficiency Coefficient (NS) values (Table 4-3). Given the

sample observations groundwater well data (G-3553), the model has a high level of performance simulating the groundwater level in the model domain (R^2=0.86 and 0.9) for the calibration and validation phases. At the verification stage, the model shows a performance (R^2=0.84) but slightly lower than the validation stage. This discrepancy of the model performance between the validation and verification stage is not significant and the model is deemed to be reliable for scenarios evaluation under the circumstance that the groundwater boundary and hydraulic parameters does not significantly change. For the same well, the corresponding NS values for calibration, validation and verification stages were 0.82, 0.76 and 0.74, respectively (Table 4-3). The NS values are high indicating the model's capability in replicating observed groundwater heads.

Table 4- 4. The evaluation results of the groundwater model at calibration, validation, and verification stages of the modeling protocol.

	Calibration				Validation				Verification			
Well	BIAS	R^2	RMSE	NS	BIAS	R^2	RMSE	NS	BIAS	R^2	RMSE	NS
F-179	-0.24	0.52	0.25	0.46	-1.03	0.62	0.23	0.72	-0.02	0.51	0.22	0.69
F-319	-0.40	0.47	0.16	-0.24	-0.48	0.42	0.16	-0.69	-0.41	0.47	0.15	-0.44
G-551	0.06	0.64	0.39	0.23	0.33	0.42	0.39	0.31	0.08	0.54	0.34	0.51
G-553	-0.15	0.76	0.15	0.52	-0.16	0.79	0.13	0.55	-0.14	0.74	0.12	0.55
G-580A	-0.12	0.55	0.13	0.42	-0.12	0.48	0.11	0.39	-0.10	0.58	0.10	0.51
G-855	0.01	0.82	0.10	0.75	-0.02	0.84	0.11	0.77	-0.01	0.80	0.10	0.76
G-860	0.07	0.71	0.09	0.67	0.14	0.86	0.06	0.72	0.12	0.75	0.07	0.63
G-1074B	0.24	0.71	0.52	0.43	0.31	0.84	0.57	0.57	0.32	0.77	0.56	0.49
G-3439	-0.02	0.85	0.09	0.85	0.03	0.92	0.07	0.90	0.07	0.79	0.10	0.67
G-3473	0.05	0.88	0.08	0.84	0.05	0.90	0.08	0.86	0.02	0.84	0.07	0.83
G-3551	-0.07	0.83	0.12	0.55	-0.09	0.93	0.15	0.63	-0.07	0.91	0.13	0.69
G-3552	-0.03	0.87	0.09	0.80	-0.06	0.92	0.11	0.77	-0.03	0.85	0.10	0.78
G-3553	-0.02	0.86	0.08	0.82	-0.07	0.90	0.12	0.76	-0.06	0.85	0.10	0.74
G-3554	-0.12	0.90	0.16	0.43	-0.15	0.92	0.18	0.35	-0.15	0.86	0.17	0.27
G-3555	0.02	0.86	0.09	0.82	-0.01	0.88	0.09	0.83	0.00	0.84	0.08	0.81
G-3556	-0.02	0.86	0.08	0.84	-0.05	0.92	0.09	0.84	-0.04	0.86	0.09	0.81
G-3557	-0.09	0.84	0.15	0.35	-0.13	0.90	0.19	0.38	-0.09	0.86	0.15	0.58
G-3558	0.12	0.61	0.19	-0.03	0.11	0.83	0.15	0.53	0.13	0.87	0.14	0.46
G-3559	-0.02	0.84	0.06	0.73	-0.02	0.95	0.05	0.93	-0.03	0.95	0.06	0.91
G-3560	-0.02	0.83	0.09	0.76	-0.05	0.88	0.11	0.76	-0.03	0.81	0.11	0.74
G-3561	0.05	0.76	0.10	0.70	0.02	0.85	0.08	0.83	0.02	0.83	0.07	0.81
G-3570	-0.31	0.58	0.30	0.05	-0.28	0.58	0.25	0.15	-0.22	0.30	0.20	0.02
G-3572	-0.07	0.77	0.10	0.61	-0.10	0.80	0.09	0.67	-0.02	0.70	0.09	0.82

Overall, the model performance has been improved at the validating stage than the calibration stage. In the validating stage, targeted local manual adjustments of recharge and river conductance are reasonably changed to improve the model performance. Overall, the model was able to simulate the groundwater table variabilities in the observation wells with maximum, minimum, average and median R^2 of 0.95, 0.3, 0.81, and 0.75 respectively. Some monitoring wells lack data records for parts of the modeling period; therefore, only 23 out of 30 monitoring wells are used to evaluate the model performance. High model performance is observed at wells located far from the canals and coastal boundary. The model has the highest performance in the simulation of the groundwater head fluctuation on the west side of the domain.

4.7.3. Limitations of the study

Groundwater modeling in the BA is complicated due to the controlled nature of the surface water flow system, aquifer heterogeneity, and the scale and reliability of observed data that affect the groundwater flow. This model is primarily for understanding the aquifer's response to various stress conditions. The study did not include surface water flow as part of the modeling procedure. It is assumed that the inflow and outflow (as surface flow) are balanced, and therefore, the net effect of surface water flow is limited.

Although equivalent freshwater head of the coastal boundary was calculated (to accommodate the effect of salinity of the freshwater head), the recalculated water level was applied only on the last grid cell of the model along the coastline. However,

practically the salinity distribution along the costal boundary is not linear. This change of salinity and its effect on the groundwater level in the costal boundary is not effectively captured by this model.

4.8. Conclusion and Recommendations

The developed groundwater flow model for the BA for the selected model domain, showed that both the steady state and transient simulations replicate the observed groundwater heads after calibration. It is also show that out of the 23 wells used for this study, wells located away from canals and coastal areas performed better than those located close to canals and coastal zones. This study has shown that the groundwater recharge in the BA is prominently derived from canal water leakage, which accounts for around 60% of the total groundwater recharge. About 43% of the groundwater recharge is contributed by diffused sources (mainly rainfall).

Under this study, several modeling attempts have been tested to include hydrological complexities while avoiding dry cells. However, as the BA is highly pervious, the exposure to dry cells will remain a modeling challenge. The modeling approach in this study, application of a single layer model using MODFLOW-2000 has indicted one possible way of developing a working model suitable to test a suite of hydrological stress conditions in the aquifer. This model can be a useful tool for analyzing the relative changes in groundwater table because of changes in hydrological stress conditions. However, this model cannot be used for absolute quantification of

hydrological water balance and aquifer parameter estimation. Given this, the effect of hydrological stress conditions shall be evaluated as a relative comparison.

Acknowledgment

Anteneh Z. Abiy has received the Florida International University Graduate School Dissertation Evidence Acquisition and Dissertation Year Fellowship awards that have helped for part of the research in this manuscript. This study is partly supported by the Everglades Foundation Scholarship, FIU for Everglades Fellowship awarded to Anteneh Abiy. The Southeast Environmental Research Institute (SERC), CREST-CAChE, and FCE-LTER of the Institute of Environment in FIU supported training and conference participation fees for Anteneh Z. Abiy.

References

Abiy, A.Z., Melesse, A.M., Abtew, W., Whitman, D., 2019. Rainfall trend and variability in Southeast Florida: Implications for freshwater availability in the Everglades. PLOS ONE 14, e0212008. https://doi.org/10.1371/journal.pone.0212008

Abtew, W., 2007. Evapotranspiration measurements and modeling for three wetland systems in South Florida. Journal of the American Water Resources Association. https://doi.org/10.1111/j.1752-1688.1996.tb04044.x

Abtew, W., Obeysekera, J., Irizzary-Ortiz, M., Lyons, D., Reardon, A., 2003. Evapotranspiration Estimation for South Florida. World Water and Environmental Resources Congress.

Abtew, W., Obeysekera, J., Shih, G., 1993. Spatial Analysis for Monthly Rainfall in South Florida1. JAWRA Journal of the American Water Resources Association 29, 179–188. https://doi.org/10.1111/j.1752-1688.1993.tb03199.x

Abtew, W., Trimble, P., 2010. El Niño-Southern Oscillation Link to South Florida Hydrology and Water Management Applications. Water Resources Management 24, 4255–4271. https://doi.org/10.1007/s11269-010-9656-2

Anderson, M.P., Woessner, W.W., Hunt, R.J., 2015. Applied groundwater modeling: simulation of flow and advective transport. Academic press.

Brakefield, L.K., Hughes, J.D., Langevin, C.D., Chartier, K., 2013. Estimation of capture zones and drawdown at the Northwest and West Well Fields, Miami-Dade County, Florida, using an unconstrained Monte Carlo analysis: recent (2004) and proposed conditions. US Geological Survey.

Brunner, P., Simmons, C.T., Cook, P.G., Therrien, R., 2010. Modeling surface water-groundwater interaction with MODFLOW: Some considerations. Ground Water. https://doi.org/10.1111/j.1745-6584.2009.00644.x

Causaras, C.R., 1985. Geology of the surficial aquifer system, Broward County, Florida; lithologic logs. US Geological Survey,.

Cunningham, K.J., Florea, L.J., 2009. The BA of southeastern Florida. Geography/Geology Faculty Publications 20.

Cunningham, K.J., Wacker, M.A., Robinson, E., Gefvert, C.J., Krupa, S.L., 2004. Hydrogeology and ground-water flow at Levee 31N, Miami-Dade County, Florida, July 2003 to May 2004: as part of the Comprehensive Everglades Restoration Plan.

De Marsily, Gh, Delay, · F, Gonçalv›s, · J, Renard, Ph, Teles, · V, Violette, · S, De Marsily, G, Gonçalv›s, J., Delay, F., Renard, P, Teles, V., 2005. Dealing with spatial heterogeneity Springer-Verlag 2005. Hydrogeology Journal. https://doi.org/10.1007/s10040-004-0432-3

Dessu, S.B., Price, R.M., Troxler, T.G., Kominoski, J.S., 2018. Effects of sea level rise and freshwater management on long-term water levels and water quality in the Florida Coastal Everglades. Journal of Environmental Management. https://doi.org/10.1016/j.jenvman.2018.01.025

Doherty, J.E., Hunt, R.J., Tonkin, M.J., 2010. Approaches to Highly Parameterized Inversion: A Guide to Using PEST for Model-Parameter and Predictive-Uncertainty Analysis. USGS: Scientific Investigations Report 2010-5211. https://doi.org/2010-5211

Fish, J.E., Stewart, M.T., 1991. Hydrogeology of the surficial aquifer system, Dade County, Florida.

Franke, O.L., Reilly, T.E., Bennett, G.D., 1987. Definition of boundary and initial conditions in the analysis of saturated ground-water flow systems: an introduction.

Freeze, R.A. and, Cherry, J.A., 1979. 1979, Groundwater. Englewood Cliffs, NJ: Prentice-Hall.

Giddings, J.B., Kuebler, L.L., Restrepo, J.I., Rodberg, K.A., Montoya, A.M., Radin, H.A., 2014. Lower east coast subregional (LECsR) MODFLOW model documentation.

Gupta, H.V., Sorooshian, S., Yapo, P.O., 2002. Status of Automatic Calibration for Hydrologic Models: Comparison with Multilevel Expert Calibration. Journal of Hydrologic Engineering. https://doi.org/10.1061/(asce)1084-0699(1999)4:2(135)

Haigh, I.D., Wahl, T., Rohling, E.J., Price, R.M., Pattiaratchi, C.B., Calafat, F.M., Dangendorf, S., 2014. Timescales for detecting a significant acceleration in sea level rise. Nature Communications 5, 3635.

Harbaugh, B.A.W., Banta, E.R., Hill, M.C., Mcdonald, M.G., 2000. MODFLOW-2000,The U.S Geological Survey Modular Ground-water Model – User Guide to Modularization Concepts and the Ground-water Flow Process, Open File Report 00-92. https://doi.org/10.3133/ofr200092

Harwell, M. a, Gentile, J.H., Bartuska, a, Harwell, C.C., Myers, V., Obeysekera, J., Ogden, J.C., Tosini, S.C., 2000. A science-based strategy for ecological restoration in South Florida. Urban Ecosystems 3, 201–222.

Hill, M.C., Tiedeman, C.R., 2007. Effective groundwater model calibration: With analysis of data, sensitivities, predictions, and uncertainty, John Wiley & Sons. https://doi.org/10.1111/j.1745-6584.2007.00398.x

Hoffmeister, J.E., Stockman, K.W., Multer, H.G., 1967. Miami limestone of Florida and its recent Bahamian counterpart. Bulletin of the Geological Society of America. https://doi.org/10.1130/0016-7606(1967)78[175:MLOFAI]2.0.CO;2

Hoshin Vijai, G., Sorooshian, S., Ogou, P.Y., 1999. Status of Automatic Calibration for Hydrologic Models: Comparison with Multilevel Expert Calibration. Journal of Hydrologic Engineering.

Hughes, J.D., White, J.T., 2014. Hydrologic conditions in urban Miami-Dade County, Florida, and the effect of groundwater pumpage and increased sea level on canal leakage and regional groundwater flow.

Langevin, C.D., 2003. Simulation of Submarine Ground Water Discharge to a Marine Estuary: Biscayne Bay, Florida. Ground Water. https://doi.org/10.1111/j.1745-6584.2003.tb02417.x

Lohmann, M.A., Swain, E.D., Wang, J.D., Dixon, J., 2012. Evaluation of effects of changes in canal management and precipitation patterns on salinity in Biscayne Bay, Florida, using an integrated surface-water/groundwater model. US Geol Surv Sci Invest Rep 5009, 94.

McDonald, M.G., Harbaugh, A.W., 1988. A modular three-dimensional finite-difference ground-water flow model. US Geological Survey Reston, VA.

Merritt, M.L., 1996. Simulation of the water-table altitude in the BA, southern Dade County, Florida, water years 1945-89. US Geological Survey Water Supply Paper.

Meyer, F.W., 1989. Hydrogeology, ground-water movement, and subsurface storage in the Floridan aquifer system in southern Florida.

Meyers, J.B., Swart, P.K., Meyers, J.L., 1993. Geochemical evidence for groundwater behavior in an unconfined aquifer, south Florida. Journal of Hydrology 148, 249–272.

Nash, J.E., Sutcliffe, J.V., 1970. River flow forecasting through conceptual models part I — A discussion of principles. Journal of Hydrology. https://doi.org/10.1016/0022-1694(70)90255-6

Niswonger, R.G., Panday, S., and Ibaraki, M., 2011. MODFLOW-NWT, a Newton formulation for MODFLOW-2005. US Geological Survey Techniques and Methods, 6(A37), p.44. http://pubs.usgs.gov/tm/tm6a37/pdf/tm6a37.pdf.

NOAA, 2015. Mean Sea level Trend, 8724580 Key West, Florida.

Obeysekera, J., Browder, J., Hornung, L., Harwell, M. a, 1999. The natural South Florida system I: Climate, geology, and hydrology. Urban Ecosystems 3, 223–244. https://doi.org/doi: 10.1023/A:1009552500448

Painter, S., Başağaoğlu, H., and Liu, A., 2008. Robust representation of dry cells in single-layer MODFLOW models. Groundwater, 46(6), pp.873-881.

Parker, G.G., Ferguson, G.E., Love, S.K., 1955. Water resources of southeastern Florida, with special reference to geology and ground water of the Miami area. USGPO,.

Prinos, S.T., 2005. Correlation analysis of a ground-water level monitoring network, Miami-Dade County, Florida.

Prinos, S.T., Dixon, J.F., 2016. Statistical analysis and mapping of water levels in the BA, water conservation areas, and Everglades National Park, Miami-Dade County, Florida, 2000–2009, Scientific Investigations Report. Reston, VA. https://doi.org/10.3133/sir20165005

Reese, R.S., Cunningham, K.J., 2000. Hydrogeology of the gray limestone aquifer in southern Florida. USGS,.

Renken, R.A., Cunningham, K.J., Shapiro, A.M., Harvey, R.W., Zygnerski, M.R., Metge, D.W., and Wacker, M.A., 2008, Pathogen and chemical transport in the karst lime-stone of the Biscayne aquifer 1. Revised conceptualization of groundwater flow: Water Resources Research, v. 44, W08429, http://dx.doi.org/10.1029/2007WR006058.

Renken, R.A., Dixon, J., Koehmstedt, J., Lietz, A.C., Ishman, S., Marella, R., Telis, P., Rogers, J., Memberg, S., 2005a. Impact of anthropogenic development on coastal ground-water hydrology in Southeastern Florida, 1900-2000, US Geological Survey Circular.

Renken, R.A., Dixon, J., Koehmstedt, J., Lietz, A.C., Ishman, S., Marella, R., Telis, P., Rogers, J., Memberg, S., 2005b. Impact of anthropogenic development on coastal ground-water hydrology in Southeastern Florida, 1900-2000. US Geological Survey Circular 1–87.

Saha, A.K., Moses, C.S., Price, R.M., Engel, V., Smith, T.J., Anderson, G., 2012. A Hydrological Budget (2002-2008) for a Large Subtropical Wetland Ecosystem Indicates Marine Groundwater Discharge Accompanies Diminished Freshwater Flow. Estuaries and Coasts. https://doi.org/10.1007/s12237-011-9454-y

Sandoval, E., Price, R.M., Whitman, D., Melesse, A.M., 2016. Long-term (11 years) study of water balance, flushing times and water chemistry of a coastal wetland undergoing restoration, Everglades, Florida, USA. Catena. https://doi.org/10.1016/j.catena.2016.05.007

Swain, E., 2012. Stochastic analyses to identify wellfield withdrawal effects on surface-water and groundwater in Miami-Dade County, Florida. Journal of Environmental Management. https://doi.org/10.1016/j.jenvman.2012.08.033

Wacker, M.A., Cunningham, K.J., Williams, J.H., 2014. Geologic and hydrogeologic frameworks of the BA in central Miami-Dade County, Florida. US Geological Survey Investigations Report 5138.

Wang, H.F., Anderson, M.P., 1982. Introduction to groundwater modeling: finite difference and finite element methods. Introduction to groundwater modeling: finite difference and finite element methods. https://doi.org/10.1029/eo063i037p00778-02

Whitman, D., Yeboah-Forson, A., 2015. Electrical resistivity and porosity structure of the upper BA in Miami-Dade County, Florida. Journal of Hydrology 531, 781–791. https://doi.org/10.1016/j.jhydrol.2015.10.049

Wilcox, W.M., Solo-Gabriele, H.M., Sternberg, L.O.R., 2004. Use of stable isotopes to quantify flows between the Everglades and urban areas in Miami-Dade County Florida. Journal of Hydrology 293, 1–19. https://doi.org/10.1016/j.jhydrol.2003.12.041

5. CHAPTER V: SIMULATION OF THE GROUNDWATER TABLE OF THE BISCAYNE AQUIFER UNDER INDVIDUAL AND COMBINED INDUCED MULTIPLE STRESS CONDITIONS

5.1. Abstract

The position of the water table and groundwater flow in the Biscayne Aquifer (BA) is driven predominantly by a hydraulic gradient generated by hydrological stress and water resource management practices in the area. The potential for long-term drought, enhanced groundwater pumping, and sea level rise can trigger changes in the position of the groundwater table in a way that compromises the quality and quantity of freshwater in the area. To date, the extent of the combined effect of stress conditions on the distribution of the groundwater table condition has not been evaluated in adequate detail. The objectives of this study are to assess the groundwater table response to changes of individual and combined stress conditions in the BA and also to evaluate how a hypothetical facilitated groundwater recharge can benefit freshwater availability while the aquifer is subject to various hydrologic stress conditions. A calibrated groundwater flow model is used to simulate the groundwater table condition under individual and combined stress conditions. Nine individual and three combined stress conditions (increased drought, increased groundwater pumping rate, and increased sea level) scenarios were implemented to simulate the groundwater table conditions. A hypothetical recharge zone is applied to examine the effect of accelerated recharge as a countermeasure to curb the adverse effects of the combined stress conditions. Results

showed high levels of regional groundwater decline during times of drought. The position of the groundwater table was highly sensitive to the reduction of leakage from canals. An increased pumping rate resulted in a localized effect within the vicinity of wellfields. Likewise, the impact of sea level rise was localized to the coastal region with a potential of flooding up to 5km inland. Maintaining the balance between rainfall conditions, canal water stage, and pumping pressure is essential for the water resources management in the BA. During sustained drought and high sea level rise conditions, direct-controlled recharge mechanisms can assist with freshwater sustainability. Simulation of the groundwater table conditions under combined stress conditions indicates that the groundwater table decreases along the most inland boundary while the coastal side increases. The application of induced recharge has indicated a potential option to counter the effect of high drought and groundwater pumping conditions. However, under higher sea level conditions, the application of induced recharge could produce coastal flooding with the groundwater table rise. Therefore, groundwater recharge as a management tool to counter the adverse effect of drought, groundwater pumping, and sea level rise is possible only if recharge is maintained at an optimum level. It is recommended that the feasibility and optimum level of induced groundwater recharge be evaluated by identifying and integrating various social and environmental elements.

Keywords: Modelling, scenarios, drought, groundwater pumping, MODFLOW, PEST.

5.2. Introduction

Groundwater in coastal aquifers is subject to many natural and anthropogenic stress conditions that can potentially compromise the sustainability of freshwater-dependent ecosystems and domestic water supply. Stress conditions including sea level rise, groundwater pumping, and drought have been outlined as the primary drivers of change resulting in adverse effects in a hydrological regime. Sea level rise leading to saltwater intrusion and flooding has been reported in a number of studies (Blanco et al., 2013; Chang et al., 2011; Sefelnasr and Sherif, 2014; Werner et al., 2013; Werner and Simmons, 2009). Groundwater pumping has been associated with groundwater overdraft in various aquifers (Abd-Elhamid and Javadi, 2011). Likewise, the effect of drought is perceived through increased evaporation and limited groundwater recharge, leading to groundwater table decline (Arumí et al., 2013; Peters et al., 2005). Although groundwater table fluctuation is a natural process, the level of water table decline can be contributable to one or multiple combinations of stress conditions.

Maintaining a higher groundwater table in the Biscayne Aquifer (BA) is the critical aspect of sustaining freshwater resources in Southeast Florida. The greater Everglades ecosystem and water supply for domestic and irrigation water use rely predominantly on higher groundwater head conditions in the BA. However, located on a highly porous limestone terrain and flat topography, the groundwater table in the aquifer is highly controlled by water engineering operations and hydrological stress conditions. Drought, sea level rise, and groundwater pumping are the key hydrological stress

conditions that affect groundwater table elevation in the BA (Hughes and White, 2014). In the BA, drought triggers limited aquifer recharge, leading to groundwater table decline (Abtew et al., 2007; Sullivan et al., 2014). Meanwhile, higher stands of sea level lead to the increased encroachment of saltwater into the aquifer, pushing the overlying fresh groundwater table upward in the coastal regions and, thus, decreasing the hydraulic gradient to the coast (Renken et al., 2005; Werner et al., 2013).

The natural flow regime in the Everglades as well as the BA is highly controlled and adversely affected by the water resources drainage practices implemented for land acquisition for urban development and agricultural expansion. These development practices have changed the overall hydrologic regime, rendering the Everglades ecosystem highly susceptible to hydrological stress conditions such as drought and groundwater pumping. As a result, the Comprehensive Everglades Restoration Plan (CERP) is launched to restore the Everglades, as much as possible, to its predevelopment stage. As part of this effort, maintaining the balance between public water supply and Everglades restoration is the key component of the freshwater CERP. The CERP (USACE,1999) attempts to strike a balance between restoring water levels and flows in the remaining natural portion of the Everglades and preventing flooding in the urban/agricultural areas to the east (Price et al., 2019). According to CERP, water storage facilities are being constructed in different parts of the Everglades wetland system. Despite these efforts, it is predicted that additional water must be made available for urban and agricultural uses (Gonzalez, 2005). The public water supply system in the BA greatly relies on recharge from the Everglades wetland. In the face of the growing urban

water demand and the incidence of drought, the urban water supply system will be increasingly dependent on groundwater recharge that comes from the Everglades and Lake Okeechobee. However, recently, the construction of the seepage wall, the western boundary (Figure 5-1c), is expected to compartmentalize the subsurface flow and effectively reduce the regional groundwater circulation (Wilcox et al., 2004). Flow compartmentalization using the seepage wall can also reduce the potential for flooding in the urban section of the area. In either case, the seepage wall is aimed at enabling more water flow into Everglades National Park, by which the potential for groundwater recharge from the Everglades into the water supply well fields can be greatly compromised.

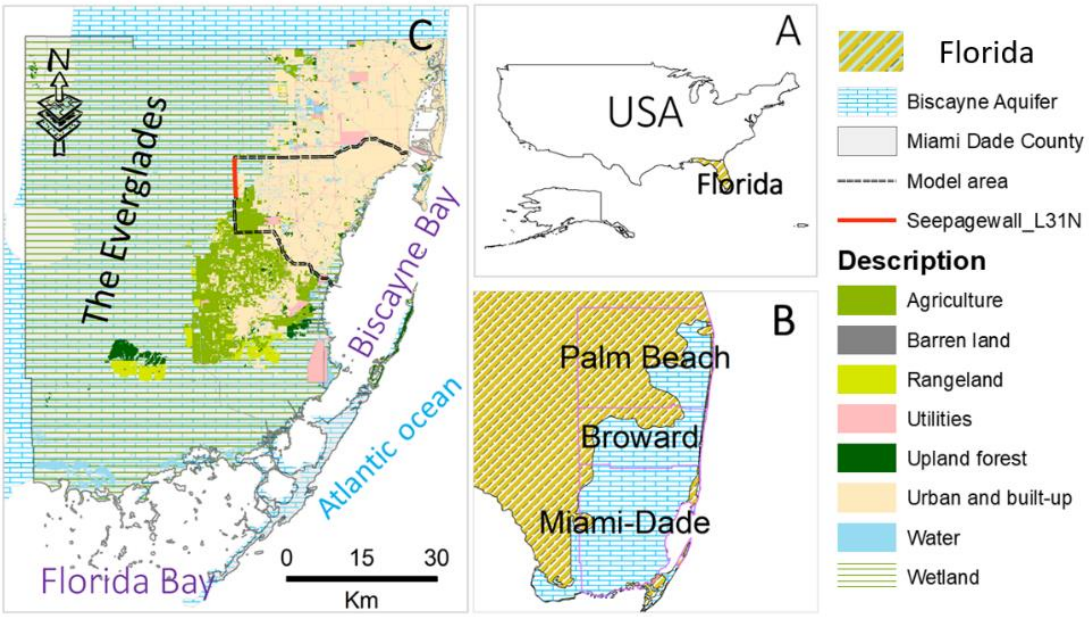

Figure 5- 1. Location map of the study area. A) location of the Florida Peninsula, B) the three counties in Southeast Florida that depend on groundwater supply from the BA, and the spatial coverage of the underlining prominently limestone BA, and C) land cover in Miami-Dade County and the outline of the model domain in this study.

Enabling a self-sufficient and resilient urban water supply system can be an alternative to decrease the Biscayne Aquifer's dependence on Everglades water, thereby promoting a successful CERP. Given the potential incidence of drought and already higher groundwater demand, the provision of an independent groundwater recharge system to the urban side of the BA can be an alternative solution to effectively decrease the dependence of the urban water supply system by maintaining a continuous source of recharge and a high water level. However, previous studies have not evaluated the combined effects of drought and groundwater pumping on the urban side of the BA devoid of recharge from the Everglades. In addition, the potential contribution of a recharge zone to providing a continuous recharge under a combined drought and high groundwater pumping condition is not assessed. Several studies have documented the importance of maintaining a high-water level in the BA (Merritt, 1996; Langevin and Dausman, 2005; Lohmann et al., 2012; Langevin, 2003; Renken et al., 2005). Lowering the canal water level and drought conditions were reported to decrease the groundwater level in the BA (Lohmann et al., 2012). By changing the groundwater pumping rate, canal water level, and sea level, USGS groundwater modeling work determined that high-stress conditions are responsible for an accelerated saltwater intrusion in the aquifer (Hughes and White, 2014). Besides the evaluation of how the aquifer responds to changes in these stress conditions, the next step in that initial modeling effort would be to determine the spatial sensitivity of the groundwater table under combined stress conditions and to evaluate the potential contribution of regional groundwater recharge as a solution to maintain a sustainable freshwater supply. For practical application, it is

important to apply the combined hydrological stress conditions to the simulation of various hypothetical scenarios. Provision of a self-sufficient freshwater supply system independent of recharge from the Everglades is the preliminary theme of this research. Hence, the evaluation of how a hypothetical groundwater recharge zone contributed to the underlying groundwater recharge challenges in the aquifer will offer an alternative solution to the successful implementation of CERP. Enabling the urban water supply system can be an alternative and key contribution to the success of the CERP. Therefore, the objectives of this study are to: 1) evaluate the impact of individual and combined stress conditions on the regional groundwater table dynamics in the BA; 2) assess the potential contribution of hypothetical groundwater recharge as a countermeasure to maintain a higher groundwater table condition, and 3) describe the implications for freshwater management options in the area.

5.3. Methodology

5.4. Groundwater modeling and data use

The groundwater modeling procedure and data used were described in the model documentation (Chapter 4).

5.5. Scenarios and scenario analysis

5.5.1. Individual scenarios

Scenarios were used to test and evaluate a set of hypothetical stress conditions that have practical importance and to understand the aquifer's response to changes in

potential stress conditions. Theoretically, a decreasing recharge and increasing groundwater pumping would cause a decline in groundwater head. Sea level rise can cause a relative increase in the hydraulic gradient on the ocean side, leading to saltwater intrusion. However, the magnitude and timing of these expected changes vary according to the nature of the aquifer and the overall geometry of the hydrologic system.

Accordingly, selected scenarios are proposed to reflect the effects of changing diffused recharge, surface water stage in canals, pumping rate, and sea level. The steady-state model is computationally manageable in that it is used to evaluate 38-hypothetical scenarios. The groundwater head in monitoring wells was compared to the scenario results to assess the effect of the changes. After analyzing the steady-state scenarios, the number of scenarios for transient simulation was decreased. The diffused recharge and surface water stage in canal conditions are identified to represent drought conditions. Therefore, the transient model scenarios analyze the effect of drought, increased pumping, and sea level rise conditions.

The impact of drought is evaluated by decreasing the diffused recharge and water level in canals. Both are decreased using:

$$h_{st} = h_{0t}(1 - p) \qquad (5\text{-}1)$$

where h_{0t} is the observed water level (initial recharge rate in case of recharge calculation) for a given scenario at a given time t, h_{st} is the calculated water level (initial recharge rate

in case of recharge calculation) for a given scenario at a given time t, and p is a hypothetical rate of decrease for the water level or recharge rate for different scenarios.

The recharge rate and water level in canals are linearly decreased using equation 5-1 by changing the p value of 0.05, 0.15, and 0.25 for scenarios 1 to 3, respectively (Table 5-1). In cases where a water level of zero is encountered, the scenario values are simply replaced by 0.05, 0.15, and 0.25 for scenarios 1 to 3, respectively. Scenarios of increased groundwater pumping were simulated using p values of -0.05, -0.15, and -0.25 for scenarios 4 to 6, respectively.

Table 5- 1. Summary of the individual scenarios used to simulate groundwater table under varied stress conditions.

Scenarios	Canal water level	Diffused recharge	Groundwater Pumping	Sea level rise
Senario-1	Decreased by 5%	Decreased by 5%		
Senario-2	Decreased by 15%	Decreased by 15%		
Senario-3	Deceased by 25%	Deceased by 25%		
Senario-4			Increased by 5%	
Senario-5			Increased by 15%	
Senario-6			Increased by 25%	
Senario-7				Increased by 0.1 cm/month
Senario-8				Increased by 0.2 cm/ month
Senario-9				Increased by 0.3 cm/month

A linear transformation analytical model that iteratively builds upon the observed tidal fluctuation record (Equation 5-2) was applied to generate the tidal stage for hypothetical scenarios of rising sea levels (scenarios 7 to 9). The assumption for this process is that the observed tidal fluctuation pattern will be replicated.

$$Sl_{ti} = Slo_{ti} + \sum_{i=1}^{n} r * i \qquad (5\text{-}2)$$

Sl_{ti} is the hypothetical scenario tidal stage corresponding to the observed tidal stage, Slo_{ti}, while r is the linear rate of the hypothetical sea level rise, and i is the index of sequential time series data.

From Equation 5-2, the sea level rise rate term (i) is critical to define the scenarios. In this study, historical rates of sea level rise were defined according to the observed sea level changes of 13 cm evaluated from 2001 to 2015 (Dessu et al., 2018) and 7.62 cm between 1992 and 2015 (NOAA, 2015). The observed data indicate that the sea level rises by 0.077 to 0.028 cm/month. The observed tidal fluctuation used in this study has a slope of 0.0018 m/month (Figure 4-11 in Chapter 4). However, the sea level rise is accelerating exponentially (Haigh et al., 2014). Therefore, to reflect potential future conditions, the hypothetical sea level rise rate (i) is intentionally defined to be higher than the observed rate. These hypothetical rates of sea level rise (i) represent future conditions of 0.10 cm/month (scenario 7), 0.20 cm/month (scenario 8), and 0.30 cm/month (scenario 9) (Table 5-1).

Overall, a total of nine transit model scenarios were designated (Figure 5-2). Scenarios 1 to 3 refer to the drought conditions represented by decreased diffused recharge (Figure 5-2a) and decreased water level in canals (Figure 5-2b). Scenarios 4 to 6 are the simulations to assess the effect of increased groundwater pumping (Figure 5-2c). Likewise, the scenarios 6 to 9 are simulated by changing the sea level according to the suggested sea level rise rate in table 5-1 (Figure 5-2d).

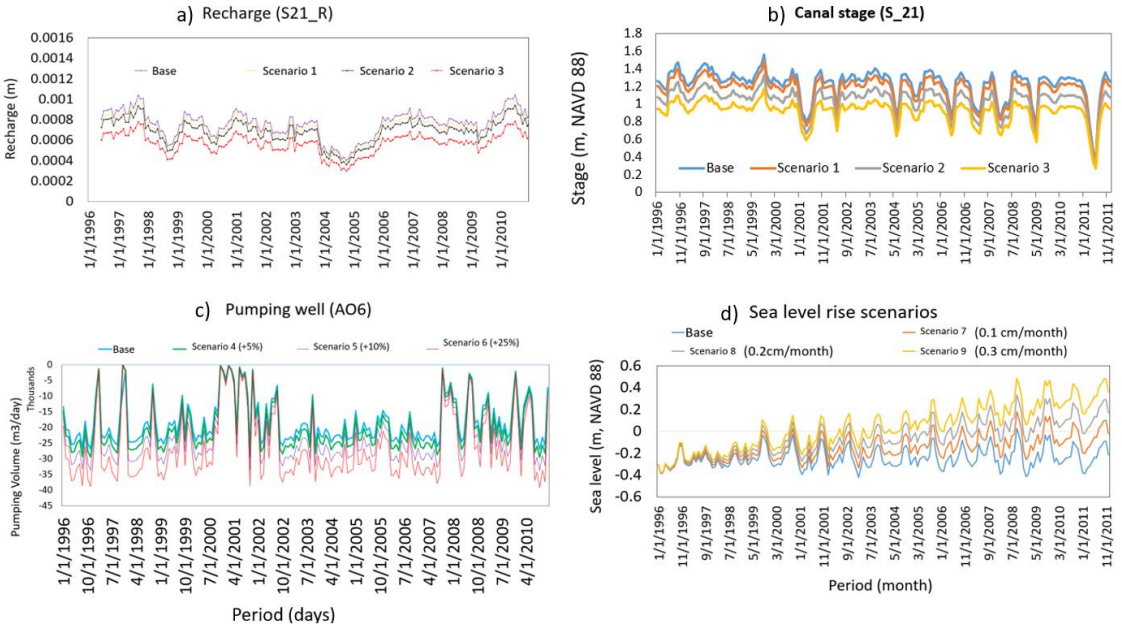

Figure 5- 2. Applied hypothetical scenarios. Three scenarios from each of the stress conditions were created based on the base-case situation.

For further analysis, evaluation, and comparison of the groundwater head response to different scenarios, the simulated groundwater head in each scenario was sampled at 100-m intervals starting from the coastline (0 m) and extending to the western side of the model (25.2 km). The assigned groundwater head monitoring stations are

located along the shoreline up to the Everglades boundary, passing perpendicular to the potentiometric surface.

5.5.2. Combined Scenarios

The scenarios are intended to evaluate the groundwater table in response to multiple stresses applied to the base case model. Three combined stress and three management conditions—a total of six scenarios—are simulated. Unlike the individual stress condition scenarios, the combined stress condition scenarios refer to the representation of drought, groundwater pumping, and sea level rise were applied to the based case model altogether (Table 5-2). The combined stress condition scenarios, named as lower, intermediate, and severe, were simulated to represent the effect of varied combined stress conditions by concurrently changing drought, groundwater pumping, and sea level rise, calculated by changing rate of decrease as given in equation 5-2, above. The respective combined stress conditions scenarios rate of change is indicated in the table below.

Table 5- 2. Induced stress conditions applied to simulate the effect of combined stress conditions on the groundwater table dynamics. Drought represents a decreasing recharge from diffused recharge and surface water level in canals.

Combined Scenario	Stress conditions		
	Drought	Pumping	Sea-level rise*
Lower	increase by 5%	increase by 5%	Increase by 0.10 cm/month
Intermediate	increase by 10%	increase by 5%	Increase by 0.25 cm/month
Severe	increase by 25%	increase by 5%	Increase by 0. 30cm/month

*The model uses the monthly sea level rise rate to transform observed sea level data. As part of the combined stress condition scenarios, the base case sea level data was recalculated based on p values of 0.1 cm/month, 0.2 cm/month, and 0.3 cm/month for the lower-, intermediate-, and severe-level scenarios, respectively.

5.5.3. Recharge scenario

As a representation of groundwater management, the effect of induced recharge was simulated by delineating a recharge zone in the western margin of the model domain (Figure 5-3). The recharge zone was selected after a qualitative GIS-based evaluation of the model domain based on the land use land cover (availability of open area), hydrological criteria (headwater zone), and topography (flatness) of the area. Accordingly, an existing open rock mining pit area is considered as a potential area for designating a recharge zone. The selected recharge zone is in the eastern boundary of the model domain and, therefore, can be assumed to be a reliable continuous source of groundwater recharge for downstream wellfields.

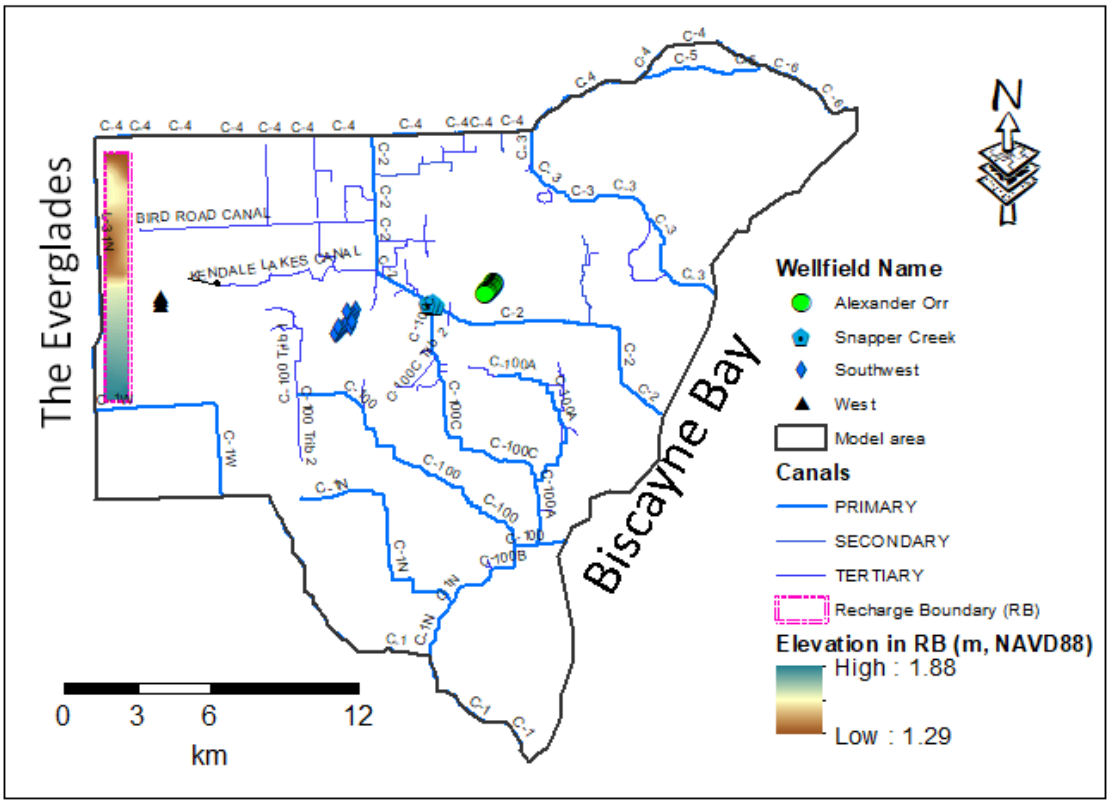

Figure 5- 3. Hypothetical recharge zone and elevation distribution across the selected area applied for the simulation of the effect of induced recharge on the groundwater table while the aquifer is subjected to combined stress conditions.

The topographic elevation in the selected recharge zone ranges from 1.88 to 1.29 (m NAVD 88), with an average elevation of 1.5 m NAVD. This hypothetical recharge zone is assigned a constant water level of 0.5 m above the mean land surface. This water level is applied to the three combined stress condition scenarios for the entire model simulation period.

5.6. Results and Discussion

5.6.1. Individual stress condition scenarios on steady-state model

Steady-state groundwater flow model scenarios of the BA were developed to evaluate the effect of time-averaged stress conditions on the groundwater head and to compare the level of change attributed to each of the stress conditions. A total of 38 steady state scenarios were simulated by applying hypothetical changes by decreasing the diffused recharge rate, decreasing the surface water stage in rivers, increasing the pumping rate, and inducing high sea level conditions.

In general, steady-state models are valuable tools to assess the sensitivity of a given model to various stress conditions in changes in hydraulic parameters (Anderson et al., 2015). In this study, the sensitivity of the model was assessed by iteratively changing the stress conditions in the steady-state model. This is considered as an important input to specify the quantity and scale of change of the stress conditions to the simulation of the transient model.

The long-term mean of each monitoring station provides the baseline groundwater head, which is contrasted with the head simulated by the specified scenarios. The difference between the base-case water level and the scenario-based simulation results are used to assess the aquifer response to changes in stress.

Decreasing the diffused recharge (Figure 5-4a) did not result in a noticeable change in the position of the groundwater level across most of the model domain. The

differences between water levels in the base case and each of the decreasing-recharge scenario simulations showed that the groundwater table is highly elastic to changes in diffuse recharge. Nevertheless, in relative terms, the scenarios of decreased diffused recharge introduced a decreasing change in water level near wellfields areas, such as G-1074B and G-3563.

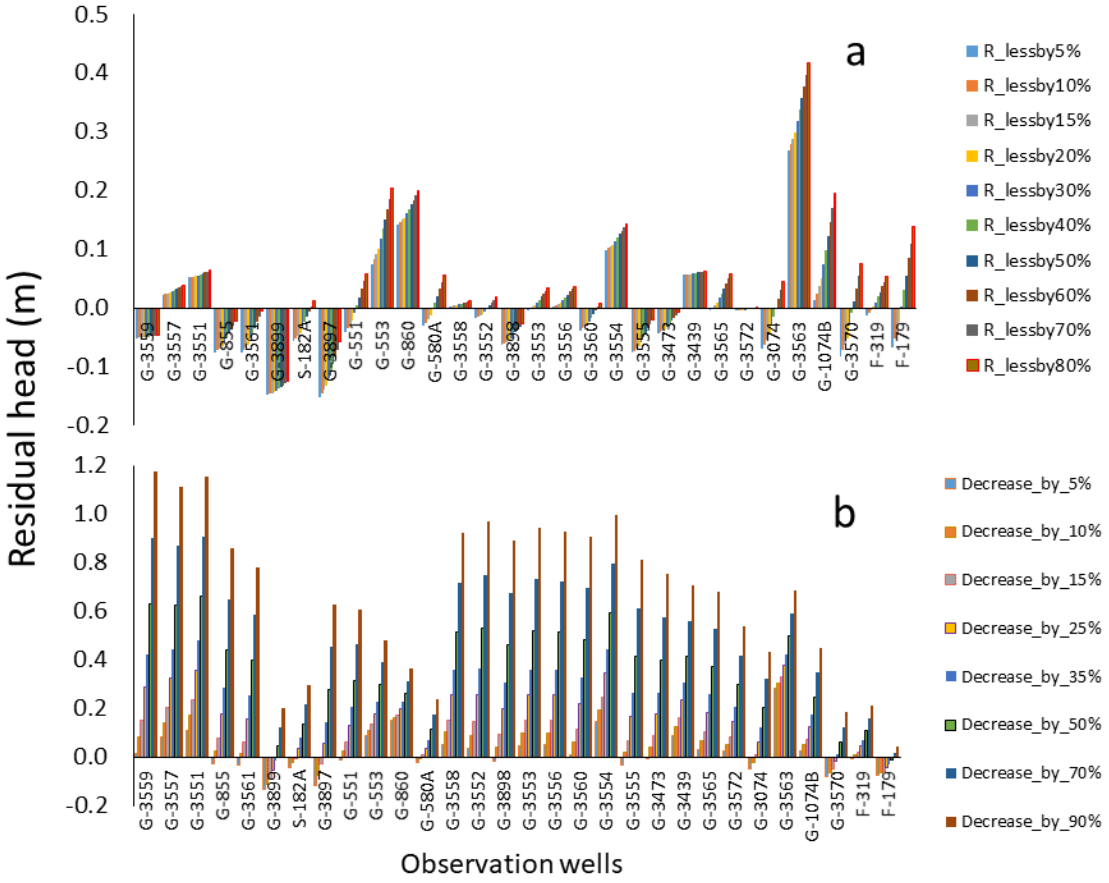

Figure 5- 4. Differences in water level between the base-case model and each of the scenario-based simulations when a) decreasing diffused recharge and b) decreasing surface water stage in canals. A positive residual water level indicates that the simulated groundwater head under the scenarios has caused the groundwater level to decline.

Decreasing the water level in canals triggered a dramatic decline of the groundwater head over almost the entire model domain (Figure 5-4b). The change in the

water level attributed to the change in canal water level varies spatially. The lowest change in water level condition is indicated at monitoring wells closer to canals and the coastal region. However, the decline in groundwater head attributed to the decreasing water level in canals is high in the inland area far away from water bodies.

An increased pumping rate relative to the current pumping rates at each wellfield is expected to produce a decline in the groundwater head. However, the groundwater head in areas closer to pumping wells shows a decline in response to increased pumping rates. In contrast, the groundwater head in the rest of the model domain did not show a visible response to changes in groundwater pumping (Figure 5-5a). The minimal response in the groundwater table away from pumping wells is expected for unconfined aquifers of high specific yield (Freeze and Cherry, 1979). In the case of rising sea level (Figure 5-5b), the groundwater head closer to the coastal region had the highest response. Nevertheless, this change is relatively small compared to the variability indicated by other stress conditions.

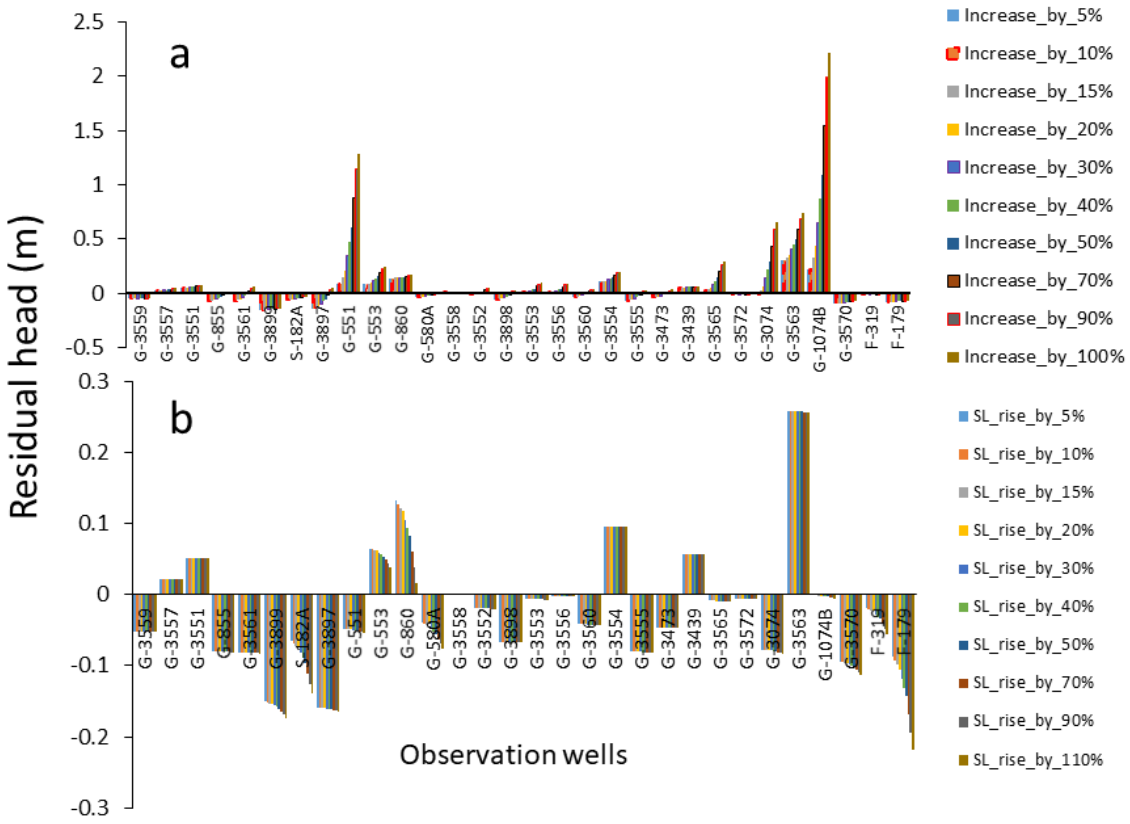

Figure 5- 5. Residuals of groundwater head simulations in response to a) increased pumping rate and b) increased sea level. The residuals are calculated as the difference in groundwater head between the base-case and scenario simulations. A negative residual indicates that the simulated groundwater head is higher than the base case.

The analysis of the steady-state scenarios indicates that the aquifer has the highest response to a decreased surface water level in canals across the entire model domain. Decreasing the diffused recharge has the same effect in terms of spatial coverage, but the magnitude of the residual standard deviation attributed to decreasing the diffused recharge is less by an order of magnitude. The change in groundwater head in response to an increased pumping rate and high sea level rise is restricted to wellfields and coastal regions, respectively. Proximity to canals and wellfields influences the aquifer's response

to changes in the surface water stage and pumping rate. Based on these results, the temporal evolution of the groundwater head due to hydrological drought can be better simulated by applying selected individual and the combined stress conditions that limit groundwater recharge (decreasing diffused recharge and surface water stage along canals).

Based on the steady-state individual stress condition scenarios assessment, it is decided to decrease the number of transient model scenarios. Also, the effect of diffuse recharge and declined in canal water level are considered to be representative of drought conditions. Whereas, change in groundwater pumping rate and sea-level rise are treated as standalone stress conditions. Hence, the transient individual model scenarios simulation is assessed by drought, groundwater pumping, and sea-level rise condition scenarios. Overall, nine individual stress conditions were selected for further investigation using the transient groundwater flow model (Tables 5-1 and 5-2). The details of these individual stress condition scenarios are given in the section below.

5.6.2. Individual stress condition scenarios on transient model

Transient scenarios were simulated to evaluate the evolution of groundwater head attributed to the cumulative effect of the applied hypothetical stress conditions over time. The sequential time series of the simulated groundwater head fluctuation along the east-west traverse line was arranged as a distance-time matrix that was further processed to develop interpolated charts. The base case interpolated chart (Figure 5-6) is characterized by the presence of a groundwater head mound approximately 4 to 6 km inland from the

coastline. The selected traverse line passes through one of the wellfields, and a cone of depression is situated at 8 to 11 km from the shoreline. Furthermore, high variability of the groundwater head occurs in the western boundary of the model area. The horizontal axis of the plots from Figures 5-6 through 5-9 indicates the spatial variation of the groundwater head with distance from the coastline sampled at 100-m intervals. The vertical axis is shown in units of time, indicating groundwater level fluctuation. The groundwater head is reported in meters in reference to NAVD 88.

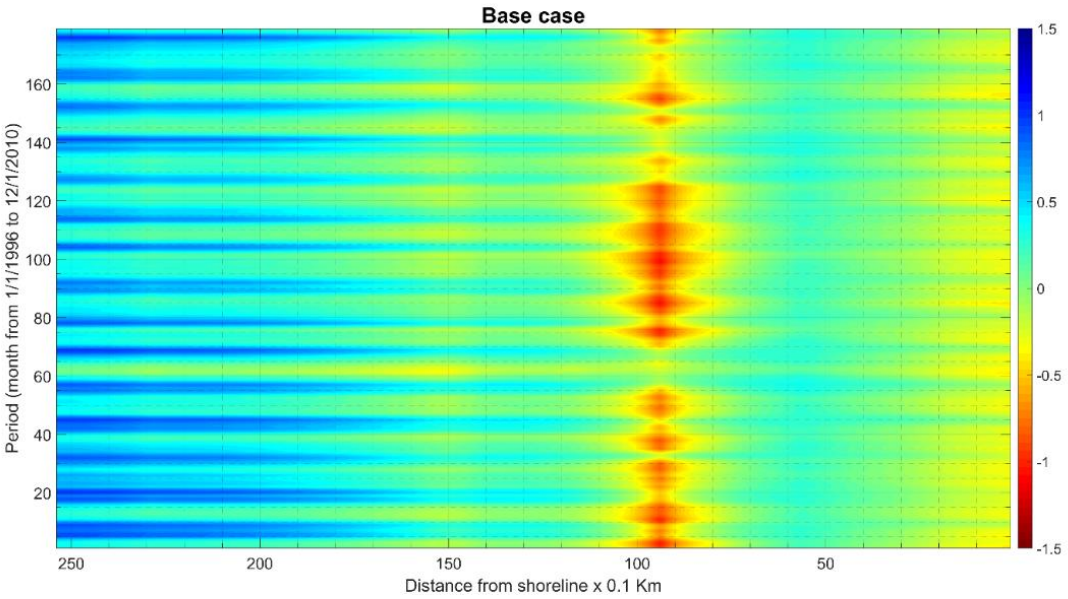

Figure 5- 6. Base-case sequential time-series of groundwater head along the east-west transect traversing from the coastline (0 m) to the Everglades boundary (25.1 km) of the model. The position of the water table is given in meters in reference to NAVD 88.

Decreasing the diffused recharge and surface water level in canals by 5% (scenario 1), 10% (scenario 2), and 25% (scenario 3) during the simulation period resulted in reductions in the groundwater head throughout the model domain in increasing order (Figure 5-7). The greatest decline in groundwater head is indicated in the

western boundary of the model. The coastal area up to 5 km inland does not display any remarkable changes in groundwater head due to drought conditions.

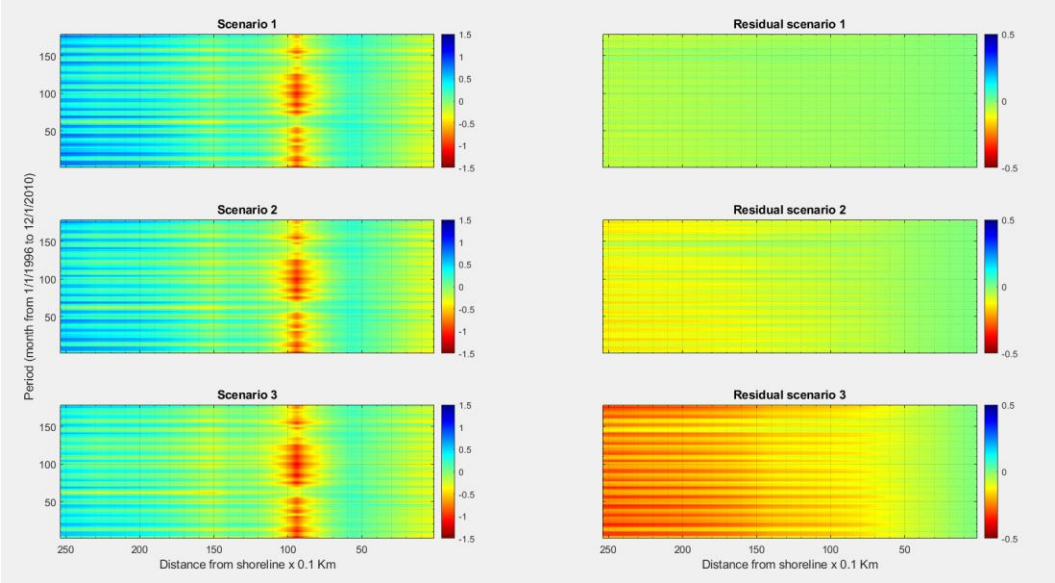

Figure 5- 7. Time series of groundwater table conditions due to drought scenarios along the east-west transect from the coastline (0 m) to the Everglades (25.1 km) boundary of the model. The residual plots refer to the difference between the water level in the base-case model and the water level in different scenarios.

The decline of the water table in the western boundary because of drought conditions can be associated with an increase in water loss from the aquifer storage (Table 5-3). It is evident that such change in water level increases the dependence of the groundwater system from canal water recharge coming from the Everglades area.

Increasing the groundwater pumping rates by 5% (scenario 4), 10% (scenario 5), and 25% (scenario 6) had localized effects closer to the wellfield areas (Figure 5-8). The residual water level of each scenario indicates a progressive decline of groundwater head and the expansion of the capture zone because of the increased pumping rate. Spatially,

the highest level of induced pumping rate indicates a minimal effect on the west side of the regional groundwater system and has little to no impact on the groundwater head in the coastal boundary. The volumetric water balance for induced pumping-rate scenarios indicates that higher pumping rates promote an increase in river leakage and aquifer storage demand (Table 5-3).

Table 5- 3. Volumetric water balance generated from different scenarios. The volumetric water balance is given in million cubic meters (MCM) and is used for relative referencing and interpretations. The water balance was calculated in a cell by cell basis using ZONBUDGET.

	Scenario-1		**Scenario-2**		**Scenario-3**	
Sources/Sinks	Flow In (MCM)	Flow Out (MCM)	Flow In (MCM)	Flow Out (MCM)	Flow In (MCM)	Flow Out (MCM)
Storage	0.049	0.000	0.053	0.000	0.061	0.000
Constant head	0.000	-0.959	0.000	-0.933	0.000	-0.861
Wells	0.000	-0.657	0.000	-0.657	0.000	-0.657
River leakage	1.592	-0.232	1.560	-0.219	1.518	-0.223
Recharge	0.207	0.000	0.196	0.000	0.164	0.000
Total source/sink	1.849	-1.849	1.809	-1.809	1.742	-1.742
Sources/Sinks	**Scenario-4**		**Scenario-5**		**Scenario-6**	
Storage	0.048	0.000	0.049	0.000	0.051	0.000
Constant head	0.000	-0.983	0.000	-0.982	0.000	-0.979
Wells	0.000	-0.690	0.000	-0.723	0.000	-0.784
River leakage	1.639	-0.232	1.668	-0.231	1.721	-0.228
Recharge	0.218	0.000	0.218	0.000	0.218	0.000
Total source/sink	1.906	-1.906	1.936	-1.936	1.990	-1.990
Sources/Sinks	**Scenario-7**		**Scenario-8**		**Scenario-9**	
Storage	0.046	0.000	0.045	0.000	0.042	0.000
Constant head	0.000	-0.950	0.000	-0.849	0.000	-0.707
Wells	0.000	-0.657	0.000	-0.657	0.000	-0.657
River leakage	1.583	-0.240	1.504	-0.260	1.395	-0.292
Recharge	0.218	0.000	0.218	0.000	0.218	0.000
Total source/sink	1.847	-1.847	1.767	-1.767	1.656	-1.656

The water level chart simulated under different pumping rate shows that increased pumping in the aquifer is associated with a decrease in the groundwater water level and expansion of the capture zone (Figure 5-8). The expansion of the capture zone promotes recharge from the canals. Therefore, the overall groundwater recharge from canal water is higher when pumping rates are higher.

The coastal water recharge through the constant head boundary suggests a small decrease when the pumping rate is increased. Although these scenarios were simulated while holding other variables constant, decreasing the surface water in canals better compensates for the enhanced pumping rates. Therefore, the overall change in the groundwater head dynamics is restricted to the vicinity of the wellfields.

Although the base-case pumping rate was not modified in these scenarios, groundwater pumping scenarios indicate a potential effect on the expansion of the wellfields' capture zone with pumping rate. Because of increased pumping rate the drawdown at well field areas could reach as high as 0.5 meters of water level as compared to the base case water level. The decreased coastal water exchange represents the net interchange between the model domain and the coastal boundary (ocean water). Although coastal groundwater exchange was not calibrated separately, a decreased loss from the system is attributed to limited groundwater discharge or increased inflow from the ocean. Therefore, drought conditions in the study area result in increased water demand for storage, decreased water outflow to the coastal region, and increased water influx through the coastal boundary.

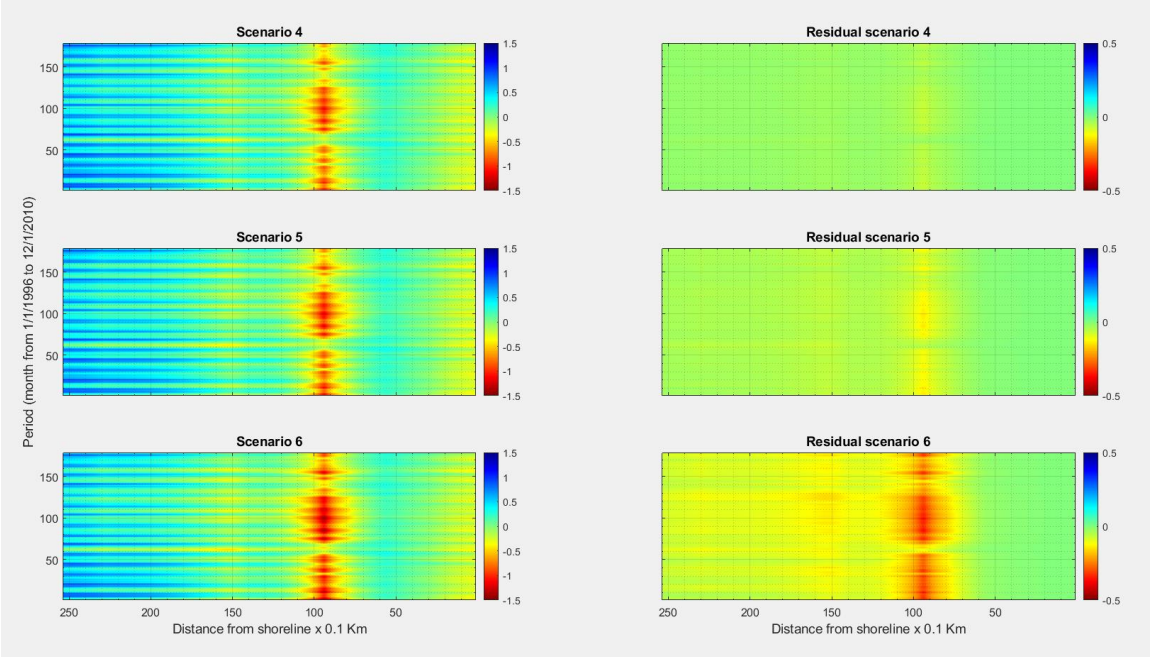

Figure 5- 8. Temporal variation of groundwater head attributed to induced higher groundwater pumping rates from the base-case model. The sequential time series data are collected along the selected traverse line.

Sea level rise scenarios developed by converting the observed tidal fluctuation record using 0.10 cm/month (scenario 7), 0.20 cm/month (scenario 8), and 0.30 cm/month (scenario 9) indicate that the effect of sea level rise on the regional groundwater head increases with time (Figure 5-9). Although the sea level rise is a continuous stress condition with influence that builds over time, its effect occurs within a distance of less than 5 km from the coastline. There is a progressive decline in the volume of coastal water exchange with increased sea level scenarios (Table 5-3), which implies a significant addition of water into the system from the constant head boundary. As shown by the residual water table charts of the transient model below, the gradual groundwater flow in the coastal boundary builds up over time and eventually leads to the water table rising above the surface.

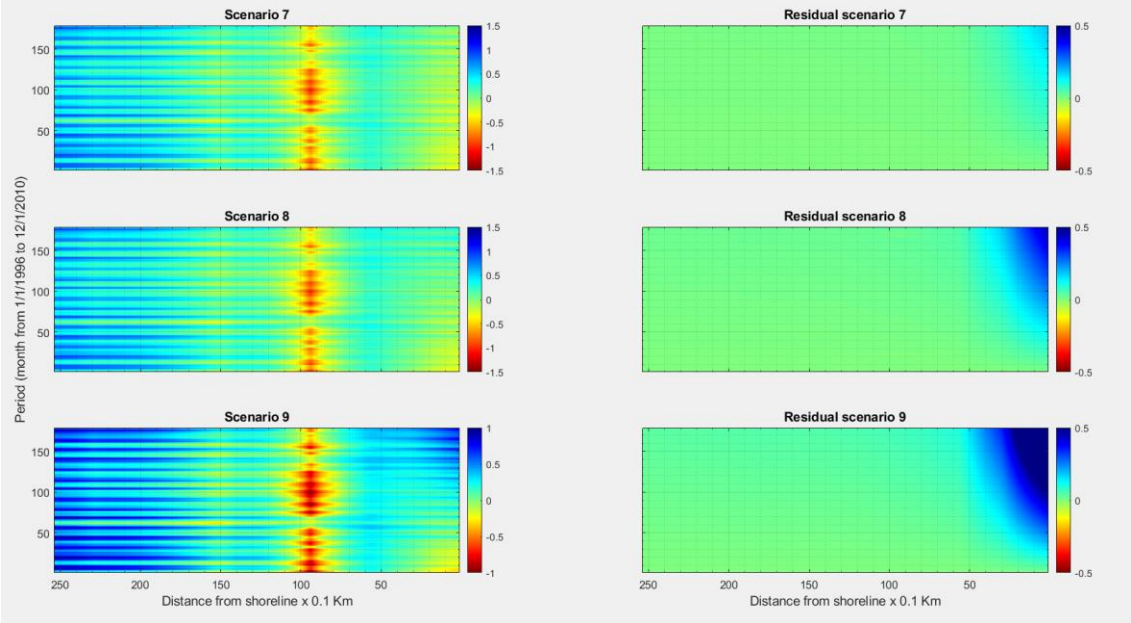

Figure 5- 9. Groundwater head fluctuations attributed to sea level rise scenarios compared to the base-case model. The sequential time series data were collected along the selected traverse line. Water level changes are measured in units of meters.

5.6.3. Combined stress condition and recharge zone scenarios

The application of the combined stress conditions has indicated an overall groundwater level decline in the inland side of the model domain. Although the effects of drought and groundwater pumping increased, the coastal side has responded in the form of an increasing groundwater table with an increasing sea level rise rate (Figure 5-10). In the coastal region, the water table condition has increased from -0.2m in the base case to about 0.6 m in the severe case scenario (Figure 5-10c). Overall, the groundwater table decline inland, coupled with the coastal boundary increases, can cause a change or decrease in the hydraulic gradient between freshwater and seawater.

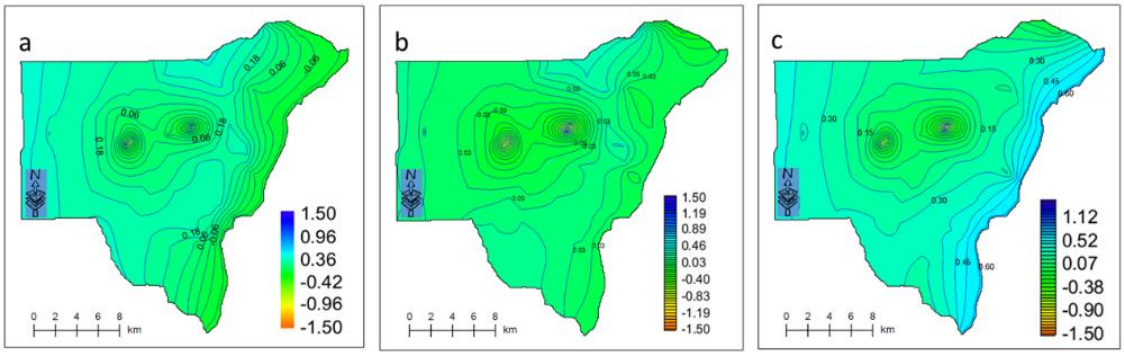

Figure 5- 10. Map view of the groundwater table under a) lower-level stress b) intermediate-level stress, and c) severe-level stress conditions. Elevation unit in meters (NAVD 88).

Although the combined stress conditions promoted the water table decline, the application of recharge has caused an increase in the groundwater level in the dominant part of the model domain. Likewise, the groundwater table in the coastal front has increased further; in the combined severe stress conditions scenario, the groundwater table rose to 0.77 m, attributed to the recharge effect (Figure 5-11).

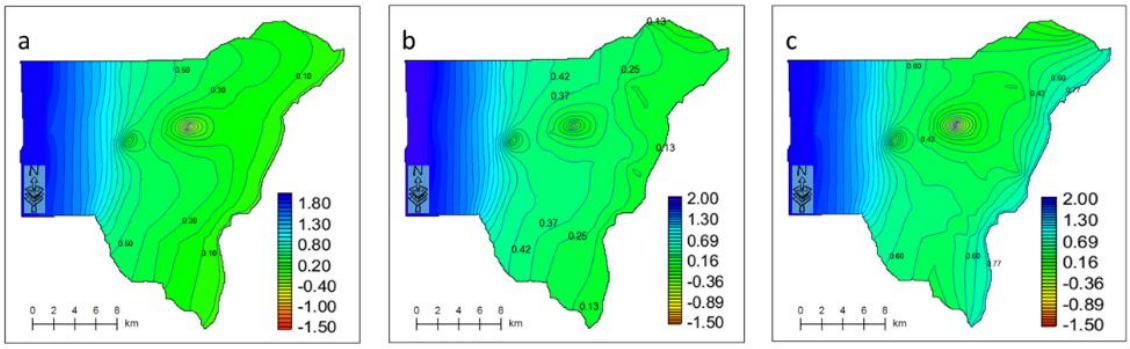

Figure 5- 11. Map view of the groundwater table with groundwater recharge in the western margin under a) lower-level stress b) intermediate-level stress, and c) severe-level stress conditions. Elevation unit in meters (NAVD 88).

5.6.4. Implications for freshwater management in the BA

As observed in the individual and combined stress condition scenarios, drought and an enhanced groundwater pumping rate cause a decrease in groundwater table conditions in the inland model domain. The simplified illustration of the different modeling scenarios indicates that drought conditions decrease groundwater recharge from rainfall and canal water seepage, causing the regional water table to decline. However, the groundwater table in the coastal boundary is not affected by drought (Figure 5-12b). Since the early 1990s, Southeast Florida has been receiving more rainfall than the long-term average (Abiy et al., 2019). The long-term average rainfall was estimated at around 1,507 mm per year, and since 1990, the mean annual rainfall has been 1,685 mm/year. This accounts for an over 11% increase in rainfall. Rainfall variability analyses, drought modeling, and drought frequency analysis results all imply that Southeast Florida may be heading toward a long-term drought phase. As a result, the inland side of the model domain is likely to be challenged by declining recharge, causing groundwater table decline.

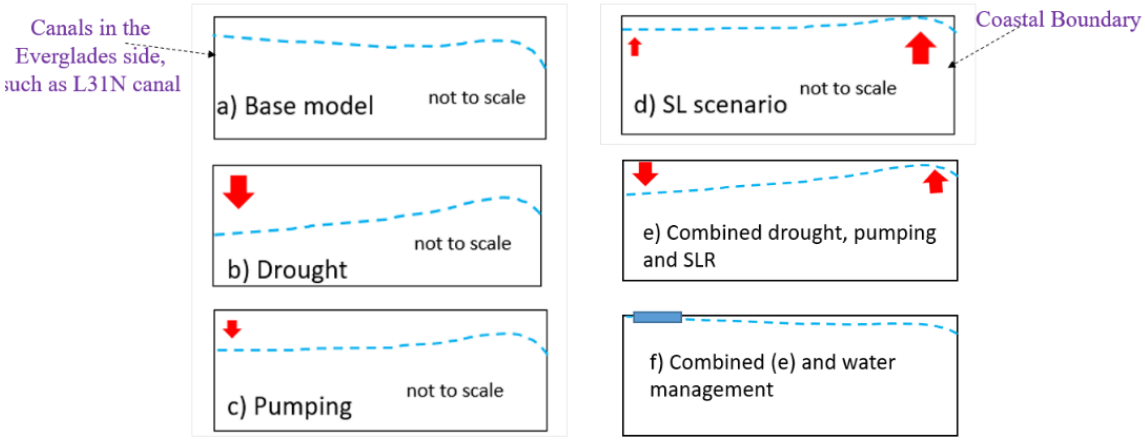

Figure 5- 12. Illustration of the groundwater table conditions in the base case model (a), induced scenarios of drought (b), increased groundwater pumping (c), sea level rise (d), combined drought, groundwater pumping and sea level rise (e), and addition of recharge zone under combined stress conditions (f). The red arrows illustrate the direction of the groundwater table under the given scenarios.

A high level of groundwater pumping has only a limited effect on the position of the groundwater table. In relative terms, the groundwater pumping affects water table conditions in the vicinity of the well field areas. The effect of groundwater pumping is more pronounced in the water level on the Everglades side than in the coastal region (Figure 5-12c).

Sea level rise causes higher groundwater table conditions in the coastal margin. On the other hand, given the prominence of tidal fluctuation and enhanced sea level rise, the coastal boundary is growing at an exponential rate (Haigh et al., 2014)—and, hence, the groundwater table in the coastal boundary will remain high (Figure 5-12d). Sea level rise conditions promote enhanced inland ingression of the salty oceanic water into the freshwater aquifer, allowing for saltwater intrusion and causing a higher groundwater table condition that is much closer to the topographic surface. At higher sea level rise

conditions, the coastal region, which is up to 5 km inland from the coastline, will be flooded because of the groundwater table rising above the land surface.

Overall, in the face of drought and increasing groundwater pumping, and the fact that the groundwater table level in the coastal boundary increases while the western side decreases, the implication is that the potential decline of the hydraulic gradient could lower or even divert the flow regime from east to west. The eastern boundary is oceanic saline water; therefore, the diminishment or reversal of the groundwater flow regime can trigger saltwater intrusion.

In realistic terms, the anticipated hydrological stress condition can coexist. Therefore, the realistic future groundwater conditions are illustrated under the combined drought, pumping, and sea level rise conditions (Figure 5-12 e). Combined stress conditions promote a reversal of the direction of the groundwater flow regime from the previous west-to-east direction to the east-to-west direction. High levels of sea level rise can potentially aggravate both coastal flooding and saltwater intrusion.

The effect of induced groundwater recharge under combined stress conditions (Figure 5-12f) from the western margin can be an appropriate solution to mitigate the underlying problems of groundwater table decline and saltwater intrusion while maintaining a successful Everglades restoration as outlined by CERP. Assuming the full emplacement of a subsurface flow barrier in the western margin of the model boundary, it is essential to assign the location of the induced recharge somewhere in the western margin, as it is necessary to maintain a higher groundwater table in the entire modeling

domain. Having a high groundwater table at the west of the model margin maintains the required hydraulic gradient irrespective of the potential effects caused by sea level rise. However, with induced recharge, the groundwater table in the coastal margin can rise above the required limit and cause flooding. As part of this study, the combination of induced recharge and higher-level sea level rise scenarios has suggested the potential of flooding inland up to 5 km from the coastline.

5.7. Conclusion and recommendations

Groundwater flow and its response to hypothetical stress conditions are simulated using a single-layer MODFLOW 2000 numerical model. Evaluation of specific stress conditions (drought, increased groundwater pumping, and different rates of sea level rise) indicated that the groundwater table in the BA is highly susceptible to changes in surface water level in canals. Increased groundwater-pumping and sea level -rise scenarios showed a local effect on the groundwater table conditions. Analysis of the individual scenario simulations indicates that the Everglades have the highest response to change in the stress conditions. Understanding the groundwater table response to different scales of combined stress conditions shows that canal water management, drought, and urban intensification lead to a decline in diffused recharge. The combined stress conditions are indicated in a multiplicative effect that can cause accelerated saltwater intrusion and flooding in the coastal area.

In the BA, discharge of up to 20% of annually intruded seawater was reported (Kohout, 1960). Given the presence of a mixing zone, the increased freshwater table is

associated with dilution in the mixing zone (Cooper, 1959; Kohout, 1964). Therefore, induced recharge can be a critical saltwater intrusion management issue in the area. Present saltwater intrusion management practices in this area involve increasing the groundwater table by allowing an increase in the surface water table near the coastal boundary. However, the saltwater intrusion process in the aquifer has affected both the regional flow dynamics as well as factors that influence the groundwater table dynamics.

The application of an induced hypothetical recharge to each of the combined stress condition scenarios indicates that the effect of increased drought and groundwater pumping can be effectively mitigated. The high level of reliance on groundwater for the water supply in Southeast Florida and more effective resource management should be designed based on information about the potential threat to water quality posed by changes in any combination of the underlining stress conditions in the area. For this, implementing a continuous groundwater recharge mechanism along the western boundary can make a greater contribution. In this case, it is important to note that the primary canal is the water divide for the locality and, hence, is a governing factor in the selection of the boundary at this location. As a result, this study is unable to evaluate the effect of the flow barrier structure on the groundwater flow system. However, the consideration of the LN31 canal as a water divide—and, hence, the eastern boundary for this model—provides a unique opportunity to assess what would happen to the urban water supply system if the flow obstruction structure were fully constructed.

Acknowledgment

Anteneh Z. Abiy has received the Florida International University Graduate School Dissertation Evidence Acquisition and Dissertation Year Fellowship awards that have helped for part of the research in this manuscript. This study is partly supported by the Everglades Foundation Scholarship, FIU for Everglades Fellowship awarded to Anteneh Z. Abiy. The South East Environmental Research Institute (SERC), CREST-CAChE, and FC-LTER of the Institute of Environment in FIU supported training and conference participation fees for Anteneh Z. Abiy.

References

Abiy, A.Z., Melesse, A.M., Abtew, W. and Whitman, D., 2019. Rainfall trend and variability in Southeast Florida: Implications for freshwater availability in the Everglades. PloS one, 14(2).

Abd-Elhamid, H.F., Javadi, A.A., 2011. Impact of sea-level rise and over- groundwater pumping on seawater intrusion in coastal aquifers. J. Water Clim. Chang. https://doi.org/10.2166/wcc.2011.053

Abtew, W., Pathak, C., Huebner, R.S., Ciuca, V., 2007. Chapter 2: Hydrology of the South Florida environment. South Florida Environ. Rep. 1, 2.1-2.72.

Anderson, M.P., Woessner, W.W., Hunt, R.J., 2015. Applied groundwater modeling: simulation of flow and advective transport. Academic press.

Arumí, J.L., Rivera, D., Holzapfel, E., Muñoz, E., 2013. Effect of drought on groundwater in a Chilean irrigated valley. Proc. Inst. Civ. Eng. Water Manag. https://doi.org/10.1680/wama.12.00064

Blanco, R.I., Melodie Naja, G., Rivero, R.G., Price, R.M., 2013. Spatial and temporal changes in groundwater salinity in South Florida. Appl. Geochemistry 38, 48–58. https://doi.org/10.1016/j.apgeochem.2013.08.008

Chang, S.W., Clement, T.P., Simpson, M.J., Lee, K.K., 2011. Does sea-level rise have an impact on saltwater intrusion? Adv. Water Resour. https://doi.org/10.1016/j.advwatres.2011.06.006

Cooper, H.H., 1959. A hypothesis concerning the dynamic balance of fresh water and salt water in a coastal aquifer. J. Geophys. Res. https://doi.org/10.1029/jz064i004p00461

Dessu, S.B., Price, R.M., Troxler, T.G., Kominoski, J.S., 2018. Effects of sea-level rise and freshwater management on long-term water levels and water quality in the Florida Coastal Everglades. J. Environ. Manage. https://doi.org/10.1016/j.jenvman.2018.01.025

Doherty, J.E., Hunt, R.J., 2010. Approaches to highly parameterized inversion: a guide to using PEST for groundwater-model calibration. U. S. Geol. Surv. Sci. Investig. Rep. 2010-5169. https://doi.org/2010-5211

Fish, J.E., Stewart, M.T., 1991. Hydrogeology of the surficial aquifer system, Dade County, Florida.

Giddings, J.B., Kuebler, L.L., Restrepo, J.I., Rodberg, K.A., Montoya, A.M., Radin, H.A., 2014. Lower east coast subregional (LECsR) MODFLOW model documentation.

Gonzalez, G.A., 2005. The comprehensive everglades restoration plan: Environmental or economic sustainability?. Polity, 37(4), pp.466-490.

Gupta, H.V., Sorooshian, S., Yapo, P.O., 2002. Status of Automatic Calibration for Hydrologic Models: Comparison with Multilevel Expert Calibration. J. Hydrol. Eng. https://doi.org/10.1061/(asce)1084-0699(1999)4:2(135)

Haigh, I.D., Wahl, T., Rohling, E.J., Price, R.M., Pattiaratchi, C.B., Calafat, F.M., Dangendorf, S., 2014. Timescales for detecting a significant acceleration in sea-level rise. Nat. Commun. 5, 3635.

Harbaugh, B.A.W., Banta, E.R., Hill, M.C., Mcdonald, M.G., 2000. MODFLOW-2000,The U.S Geological Survey Modular Ground-water Model – User Guide to Modularization Concepts and the Ground-water Flow Process, Open File Report 00-92. https://doi.org/10.3133/ofr200092

Hill, M.C., Tiedeman, C.R., 2007. Effective groundwater model calibration: With analysis of data, sensitivities, predictions, and uncertainty, John Wiley & Sons. https://doi.org/10.1111/j.1745-6584.2007.00398.x

Hughes, J.D., White, J.T., 2014. Hydrologic conditions in urban Miami-Dade County, Florida, and the effect of groundwater pumpage and increased sea-level on canal leakage and regional groundwater flow.

Kohout, F.A., 1964. The flow of fresh water and salt water in the BA of the Miami area, Florida. 161G-C 12–32.

Kohout, F.A., 1960. Cyclic flow of salt water in the BA of southeastern Florida. J. Geophys. Res. 65, 2133–2141. https://doi.org/10.1029/JZ065i007p02133

Langevin, C.D., 2003. Simulation of Submarine Ground Water Discharge to a Marine Estuary: Biscayne Bay, Florida. Ground Water. https://doi.org/10.1111/j.1745-6584.2003.tb02417.x

Langevin, C.D., Dausman, A.M., 2005. Numerical simulation of saltwater intrusion in response to sea-level rise, in: World Water Congress 2005: Impacts of Global Climate Change - Proceedings of the 2005 World Water and Environmental Resources Congress. https://doi.org/10.1061/40792(173)376

Lohmann, M.A., Swain, E.D., Wang, J.D., Dixon, J., 2012. Evaluation of effects of changes in canal management and precipitation patterns on salinity in Biscayne Bay, Florida, using an integrated surface-water/groundwater model. US Geol Surv Sci Invest Rep 5009, 94.

McDonald, M.G., Harbaugh, A.W., 1988. A modular three-dimensional finite-difference ground-water flow model. US Geological Survey Reston, VA.

Merritt, M.L., 1996. Simulation of the water-table altitude in the BA, southern Dade County, Florida, water years 1945-89. US Geol. Surv. Water Supply Pap.

Peters, E., Van Lanen, H.A.J., Torfs, P.J.J.F., Bier, G., 2005. Drought in groundwater - Drought distribution and performance indicators. J. Hydrol. https://doi.org/10.1016/j.jhydrol.2004.09.014

Price, R. and Schwartz, K. with Anderson, B. Boucek, R. Briceño,H. Cook, M. Fitz, C. Heithaus, M. Onsted, J. Rehage. J. 2019. Chapter 3: Water, Sustainability, and Survival in The Coastal Everglades: The Dynamics of Social-Ecological Transformation in the South Florida Landscape: 34-70. in Childers, D. L., Gaiser, E. and Ogden, L. (Eds). The coastal Everglades: the dynamics of social-ecological transformation in the South Florida landscape. Oxford University Press, NY.

Prinos, S.T., Dixon, J.F., 2016. Statistical analysis and mapping of water levels in the BA, water conservation areas, and Everglades National Park, Miami-Dade County, Florida, 2000–2009, Scientific Investigations Report. Reston, VA. https://doi.org/10.3133/sir20165005

Renken, R.A., Dixon, J., Koehmstedt, J., Lietz, A.C., Ishman, S., Marella, R., Telis, P., Rogers, J., Memberg, S., 2005. Impact of anthropogenic development on coastal ground-water hydrology in Southeastern Florida, 1900-2000, US Geological Survey Circular.

Sefelnasr, A., Sherif, M., 2014. Impacts of Seawater Rise on Seawater Intrusion in the Nile Delta Aquifer, Egypt. Groundwater 52. https://doi.org/10.1111/gwat.12058

Sullivan, P.L., Price, R.M., Miralles-Wilhelm, F., Ross, M.S., Scinto, L.J., Dreschel, T.W., Sklar, F.H., Cline, E., 2014. The role of recharge and evapotranspiration as hydraulic drivers of ion concentrations in shallow groundwater on Everglades tree islands, Florida (USA). Hydrol. Process. https://doi.org/10.1002/hyp.9575

Toth, J., 1963. A theoretical analysis of groundwater flow in small drainage basins. Journal of geophysical research, 68(16), pp.4795-4812.

U.S. ARMY CORPS OF ENGINEERS. 1999. Central and South Florida Project comprehensive review study. Final Integrated Feasibility Report and Programmatic Environmental Impact Statement, vols. 1–10. U.S. Army Corps of Engineers, Jacksonville District, Jacksonville, Florida, USA.

Wang, H.F., Anderson, M.P., 1982. Introduction to groundwater modeling: finite difference and finite element methods. Introd. to Groundw. Model. finite Differ. finite Elem. methods. https://doi.org/10.1029/eo063i037p00778-02

Werner, A.D., Bakker, M., Post, V.E.A., Vandenbohede, A., Lu, C., Ataie-Ashtiani, B., Simmons, C.T., Barry, D.A., 2013. Seawater intrusion processes, investigation and management: Recent advances and future challenges. Adv. Water Resour. 51, 3–26. https://doi.org/10.1016/j.advwatres.2012.03.004

Werner, A.D., Simmons, C.T., 2009. Impact of sea-level rise on sea water intrusion in coastal aquifers. Ground Water. https://doi.org/10.1111/j.1745-6584.2008.00535.x

6. CHAPTER V: CONCLUSIONS AND RECOMMENDATIONS

The balance between hydrological stress conditions and aggressive implementation of integrated water resources management practices determines the long-term freshwater availability in South Florida. In this study, the critical hydrological stress conditions for freshwater availability in the area are identified, and the position of the groundwater table is defined as the critical indicator that controls the volume of groundwater use and freshwater availability to maintain a healthy ecosystem in the Everglades. Factors that determine the position of the groundwater table in the BA are small-scale drought, enhanced groundwater pumping, and sea-level rise. The influence of the individual and combined stress conditions on the position of the groundwater table is assessed using a groundwater flow model. The study also recommends potential integrated water resource management options in South Florida.

6.1. Conclusions

Rainfall variability leading to meteorological drought influences the sustainability of freshwater and freshwater dependent ecosystems in South Florida. Also, the current high level of groundwater pumping and sea-level rise are the prominent hydrological stress conditions that influence the position of the groundwater table in the BA. Analysis of 110 years of monthly rainfall data in South Florida has shown that the rainfall variability in the area could be described by the systematic oscillation of rainfall above and below the long-term normal. The long-term rainfall average from 1906 to 2016 was 1506.8 mm. The rainfall variability ranges from seasonal to multi-decadal fluctuations.

The frequency analysis confirmed that drought in the area could sustain from seasonal variability to 3 to 5, 8 to 10, and 10 to 20 years range. For the time between 1906 and 2016, there were abrupt changes in the mean rainfall in 1970 and 1990. These sudden changes define three statistically significant rainfall regimes: average rainfall pre-1970 (1481 mm), between 1970 and 1990 (1368 mm), and post 1990 (1686 mm). Post-1990, the area received 16% higher rainfall than the long-term normal of 1506.8 mm/year.

Monthly rainfall trend analysis justified the presence of a higher rainfall regime after the early 1990s. This higher rainfall is attributed to increased rainfall in August. However, the rainfall in May and October is decreasing. As such, the increased rainfall in August has caused the previously bi-modal rainfall regime to shift into a unimodal rainfall regime. The decreasing rainfall in May and October is also shortening the wet season. More rainfall within a shorter wet season is associated with higher rainfall intensity. High rainfall intensity has the propensity to facilitate runoff loss. Therefore, although South Florida has been receiving more rainfall since the early 1990s, this higher rainfall has led to high runoff loss, but a limited contribution to freshwater storage.

In South Florida, seasonal rainfall variability, incidences of dry spells, and short-term drought ranging from 2–3 years are associated with ENSO fluctuations. In contrast, long-term rainfall variability is significantly controlled by AMO fluctuations. AMO fluctuation has a direct proportionality to rainfall, so that the positive AMO is associated with high rainfall and vice versa. The extant long-held wetness beginning in the early 1990s is associated with the positive phase of AMO. The association between rainfall

variability in South Florida and PDO is not statistically significant. However, given the emergence of a negative phase of AMO, it is highly likely that the current higher rainfall regime in South Florida will decline towards the average and eventually drop below the average. Rainfall is the primary freshwater input to the local hydrology and recharges to the BA, and therefore, lower rainfall conditions affect the groundwater table in the aquifer.

Adversely influencing the water level in canals and diffused groundwater recharge, drought has a regional effect on the position of the groundwater table conditions in the BA. Unlike the inland groundwater table, the coastal boundary has a lower response to drought conditions. A decline of the inland groundwater table while the coastal boundary groundwater table remains unchanged imposes a reduction in the hydraulic gradient between the freshwater and coastal boundary. This change in the hydraulic gradient influences the regional groundwater circulation from the Everglades to the coastal boundary. At a higher drought scenario, the declined groundwater table suggests that there is potential to reverse the hydraulic gradient in a manner to facilitate accelerated inland ingression of the salty oceanic water into the aquifer.

The effect of groundwater pumping is centralized on well-field regions. High levels of pumping pressure scenarios indicate a potential expansion of the radius of influence, although the change in the depth-to-the-groundwater table is not noticeable. As the radius of influence expands the well-field capture zone, the primary challenge (because of increased groundwater pumping in the aquifer) might be to deal with

wellhead contamination. However, wellhead contamination is beyond the scope of this study and, thus, was not assessed in detail.

Sea-level rise has multiple effects on freshwater in the BA. This study has indicated that the groundwater table will rise with sea-level, leading to flooding of up to 5 km inland. This analysis does not include the potential of inland inundation by ocean water. Given the possibility of inundation with sea-level rise, the inland extent of coastal flooding could be much more than 5 km from the coastline.

The groundwater table simulated under combined stress conditions agreed with the simulations under individual stress conditions, highlighting the potential of the reversal of the current west to east flow regime to an east to west flow. Therefore, drought and pumping pressure conditions are associated with an overall decline of the inland groundwater table. Besides drought, urbanization and urban intensification contribute to increases in surface imperviousness. In sustaining freshwater availability in South Florida, several integrated water resources management options have been identified.

6.2. Recommendations

The successful implementation of the comprehensive Everglades restoration plan and sustaining the freshwater availability in South Florida requires an integrated water resource management approach. Enabling groundwater recharge demand for public water supply should be considered as a key milestone to a successful implementation of ongoing restoration activities in the Everglades. In addressing water resource

requirements in the Everglades and public water supply in the region, potential integrated water resource management strategies are outlined below.

Recharge management – a primary integrated water resources management practice – can contribute to sustaining freshwater availability in an area. The design of an induced recharge zone and canal water management actions are recommended as part of recharge management practices. According to the model simulation scenario under combined stress and artificial recharge zone in the western boundary conditions, recharge in the western boundary offers a promising option to maintain an adequate groundwater head in the entire model domain. The recharge zone in the western boundary can maintain a reliable source of recharge to self-sustain the water supply-demand, as well as to serve as a counter major to the adverse effects from sea-level rise. However, the volume of recharge must be controlled at an optimum level, unless otherwise, the higher volume of recharge can cause flooding in different parts of the urban section. Managing the surface water stage in canals provides an alternative recharge management practice. However, canal recharge options are required to establish an appropriate flow regulation rule. These, being part of the management options, are recommended to conduct a detailed feasibility study at various social, environmental, and economic criteria.

As part of the strategy to enabling the urban water supply system devoid of the recharge from the Everglades, as well as, given the high rainfall potential in the region, enhanced rainwater harvesting must be considered as an integral part of the future freshwater management strategy in the area. Roof catchments for rainwater harvesting at

household and institution scales are potential resources that can cover water demand for irrigation applications in lawns and backyards. The understanding developed in this study are essential inputs to freshwater management strategies; it offers the opportunity to further analyze or revise the operation rules governing canal water flow and recharge optimization.

APPENDIX: MODEL INPUT OUTPUT INFORMATION

I. Aquifer hydraulic properties

Aquifer thickness information gathered from the Lower East Coast Subregional (LECsR) MODFLOW Model of the SFWMD (Giddings et al., 2014). The thickness of the first layer was calculated by subtracting the bottom of the layer one (b) from the topographic elevation map (a), likewise the difference between the bottom of layer one (b) and bottom of layer two (c) calculates the thickness of the second layer, and finally, the difference between the bottom of layer two(c) and bottom of layer three (d) was used to calculate the thickness of the third layer. All the calculations were made in the ArcGIS raster calculator platform.

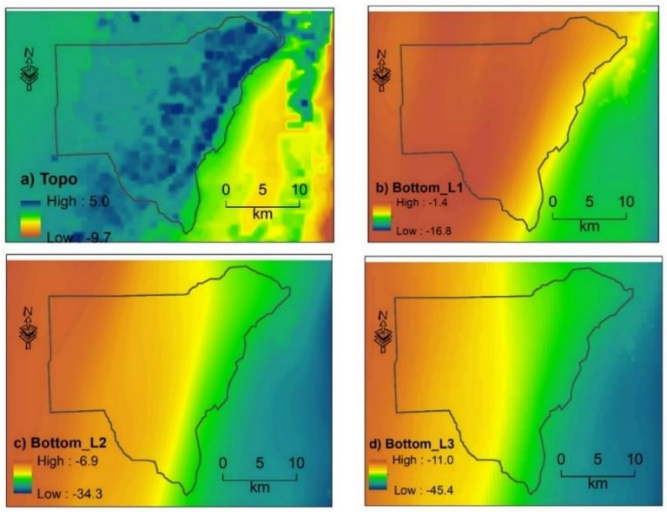

A single layer weight hydraulic conductivity was developed by calculating the geometric mean of the three layers of hydraulic conductivity given in the USGS

MODFLOW-NWT model (Hughes and White, 2014). The individual layer hydraulic conductivity was weighted by the respective layer thickness.

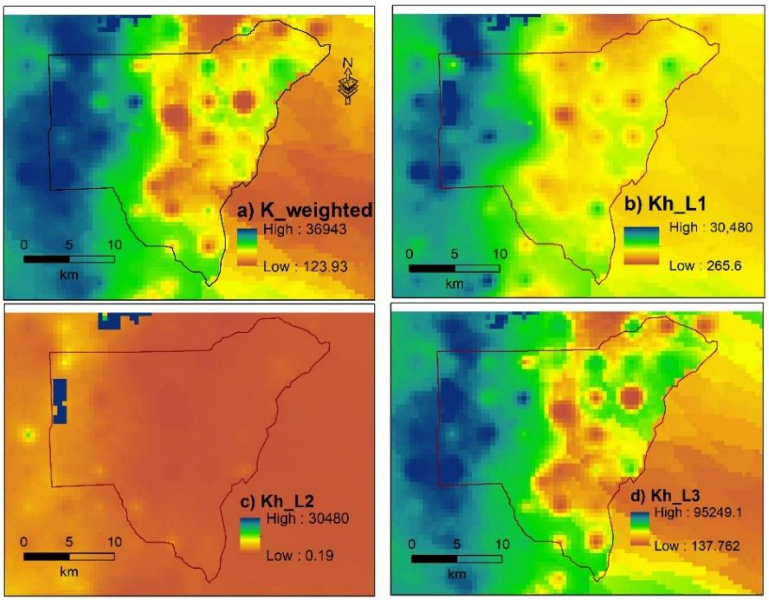

Mean specific storage layer was calculated as an arithmetic mean of the three layers specific storage data given in the USGS MODFLOW-NWT model (Hughes and White, 2014).

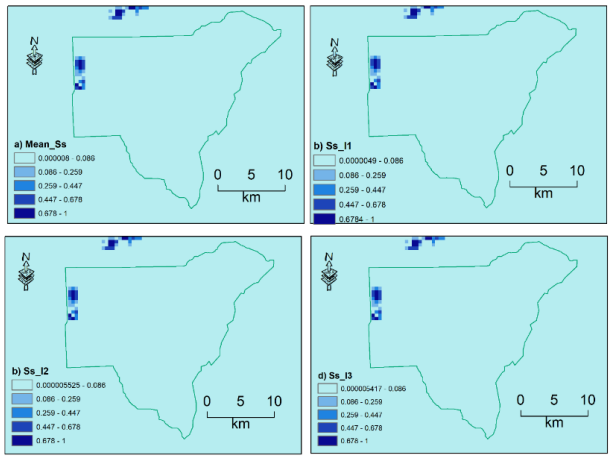

II. Well data

Groundwater level observation data was collected from the observation wells located as indicated in the table below.

FID	Well	Basin Name	x_utm	u_utm	layer
0	G-3559	C-1	550444.3167	2847685.455	2
1	G-1487	C-1	550519.9896	2841210.932	1
2	G-3575	C-1	550546.5751	2842791.586	1
3	G-3557	C-1	550577.9825	2841133.632	2
4	G-3551	C-1	550617.0479	2842582.673	2
5	G-855	C-1	553542.2976	2840111.66	1
6	G-3561	C-1	555888.6254	2839647.598	1
7	G-3899	C-1	562560.8404	2828425.116	1
8	S-182A	C-1	563929.9344	2831218.059	1
9	G-3897	C-100	558313.0165	2838524.13	2
10	G-551	C-100	560601.7506	2841677.074	2
11	G-553	C-100	566413.3732	2837210.462	2
12	G-860	C-100	567982.9416	2833985.237	1
13	G-580A	C-100	569994.4163	2839002.026	1
14	G-3558	C-2	552220.9629	2845562.369	2
15	G-3552	C-2	552308.5809	2841930.931	2
16	G-3898	C-2	552795.2485	2842345.688	2
17	G-3553	C-2	552908.902	2842360.907	2
18	G-3556	C-2	553073.6141	2842989.114	2
19	G-3560	C-2	553179.3858	2840937.701	2
20	G-3554	C-2	553940.0956	2842371.215	2
21	G-3555	C-2	554516.6955	2841096.941	2
22	G-3473	C-2	555833.5523	2844139.742	1
23	G-3439	C-2	556805.1815	2846939.101	1
24	G-3565	C-2	559672.4419	2843167.918	1
25	G-3572	C-2	560085.6941	2847295.057	2
26	G-3074	C-2	564149.5679	2842516.667	3
27	G-3563	C-2	565846.7281	2845756.636	1
28	G-1074B	C-2	566559.1025	2843176.106	3
29	G-3570	C-3	571219.1119	2849377.615	1
30	F-319	C-3	571445.2264	2843260.999	1
31	F-179	C-3	575581.5654	2847732.288	1

III. Model results evaluation

The table below indicates the steady mean water level and steady state calibrated water level values. Mean observed groundwater level (m, NAVD88), and computed groundwater level (m, NAVD88) before and after calibration.

Observation Well Name	Observed GWL (m)	Computed GWL (m), before calibration	Computed GWL (m) after calibration
G-3559	1.32	1.36	1.52
G-3557	1.23	1.19	1.28
G-3551	1.27	1.21	1.29
G-855	0.94	0.98	1.05
G-3561	0.83	0.87	0.91
G-3899	0.24	0.37	0.39
S-182A	0.32	0.35	0.59
G-3897	0.62	0.76	0.77
G-551	-0.50	-0.52	-0.94
G-553	0.50	0.45	0.48
G-860	0.33	0.25	0.56
G-580A	0.31	0.30	0.39
G-3558	1.03	1.06	1.25
G-3552	1.06	1.05	1.18
G-3898	0.95	1.00	1.12
G-3553	1.00	0.99	1.10
G-3556	0.99	0.97	1.11
G-3560	0.99	0.99	1.08
G-3554	1.05	0.92	1.01
G-3555	0.87	0.90	0.97
G-3473	0.81	0.80	0.74
G-3439	0.78	0.75	0.82
G-3565	0.53	0.55	0.44
G-3572	0.61	0.63	0.63
G-3074	-0.09	-0.05	0.31
G-3563	0.45	0.13	-0.07
G-1074B	-1.41	-1.44	-2.82
G-3570	0.37	0.28	0.23
F-319	0.26	0.22	0.17
F-179	0.15	-0.01	-0.09

The charts below portray the comparison of the observed and simulated (base model) sequential time series groundwater table fluctuation record on the observation wells is

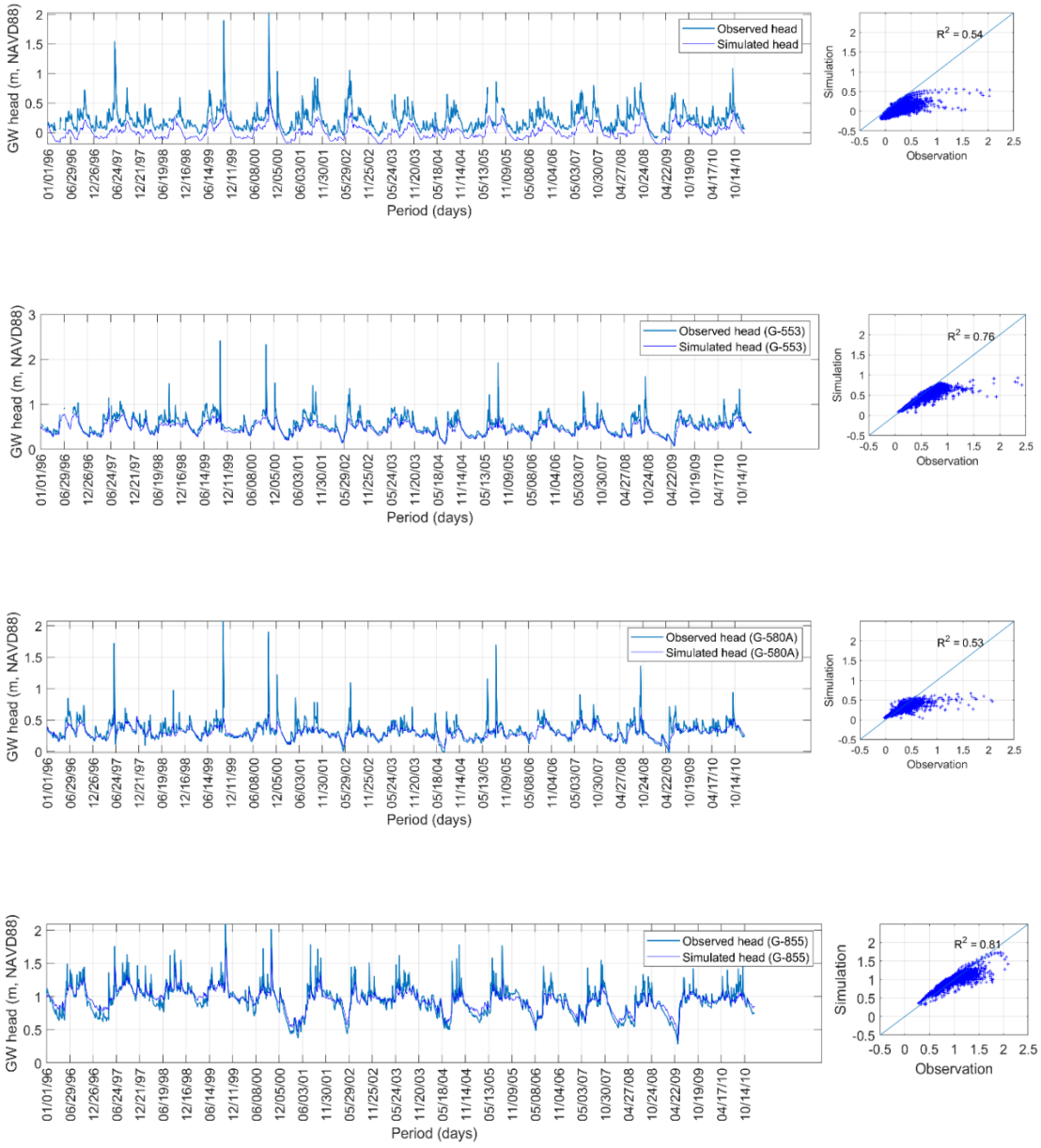

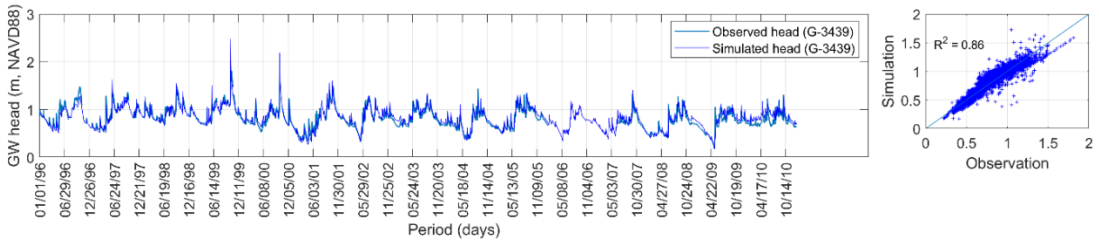
Observed head (G-3439)
Simulated head (G-3439)
GW head (m, NAVD88)
Period (days)
Simulation
Observation
R² = 0.86

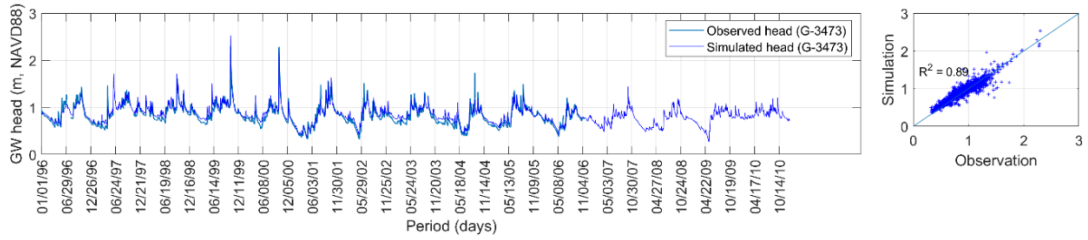
Observed head (G-3473)
Simulated head (G-3473)
GW head (m, NAVD88)
Period (days)
Simulation
Observation
R² = 0.89

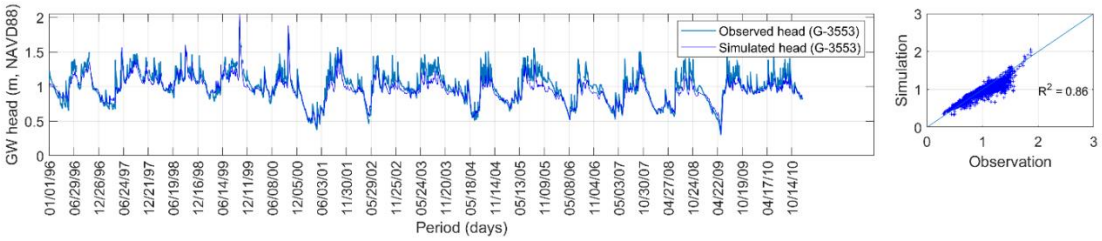
Observed head (G-3553)
Simulated head (G-3553)
GW head (m, NAVD88)
Period (days)
Simulation
Observation
R² = 0.86

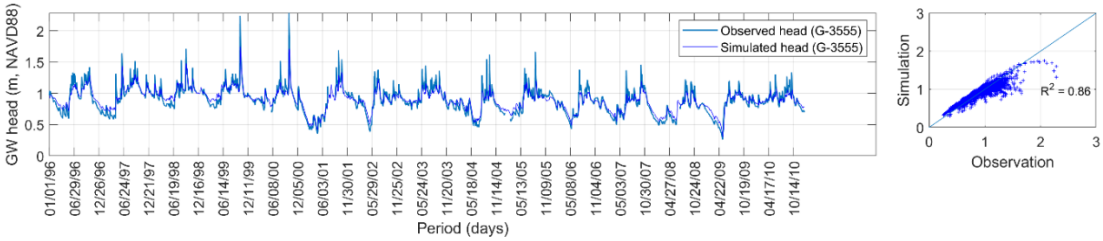
Observed head (G-3555)
Simulated head (G-3555)
GW head (m, NAVD88)
Period (days)
Simulation
Observation
R² = 0.86

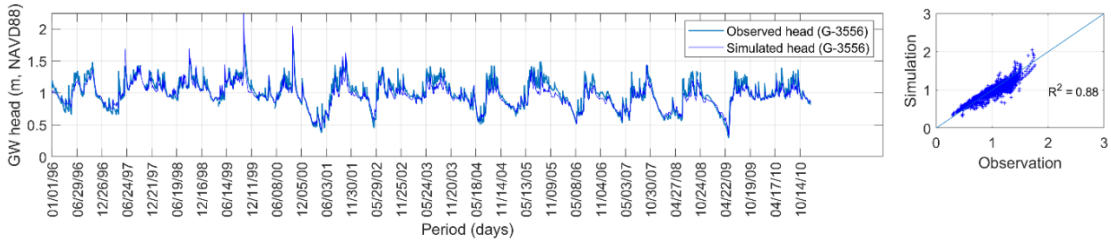
Observed head (G-3556)
Simulated head (G-3556)
GW head (m, NAVD88)
Period (days)
Simulation
Observation
R² = 0.88

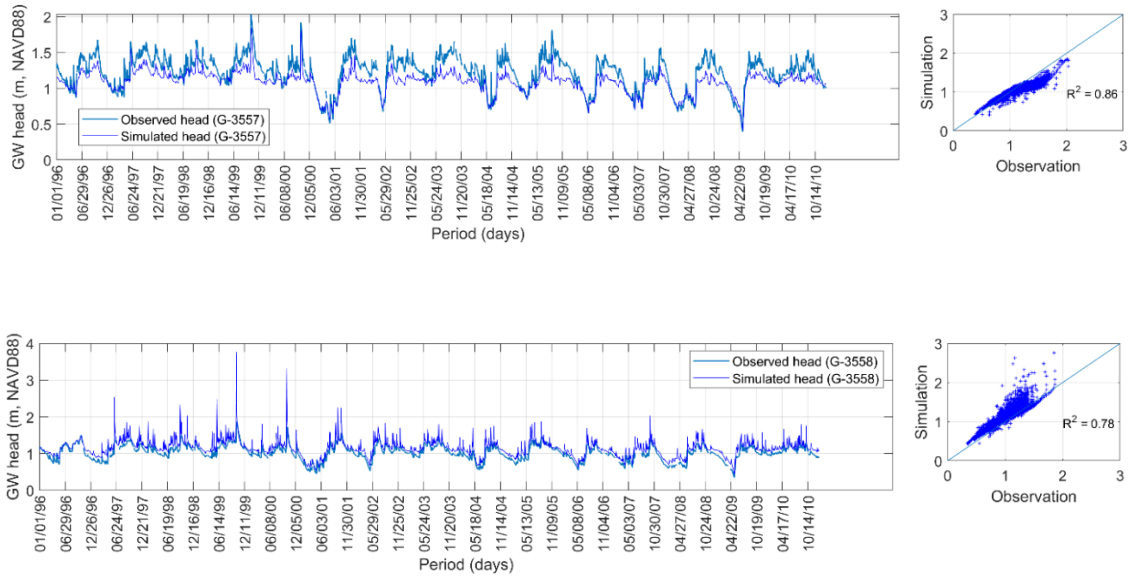

IV. Calibration parameter values

Steady state calibration was conductive by using K, aquifer leakage and recharge values. Uniformly distributed training points were for the application of the initial hydraulic conductivity, shown below.

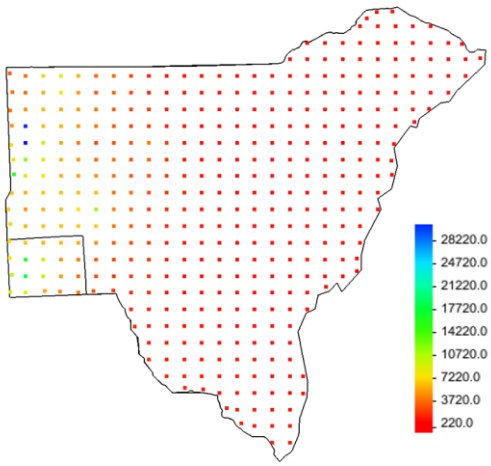

Calibration of the rive leakage helps to control the volume of groundwater recharge from canals and vise velars. Leakage calibration can be conducted along with other parameters. Initial vales of the river's leakage values were estimated bases on the reported river leakage data given is the USGS model. The reported values in the figure contains the rives leakance coefficient, and the conductance is the product of the leakance and the model grid size.

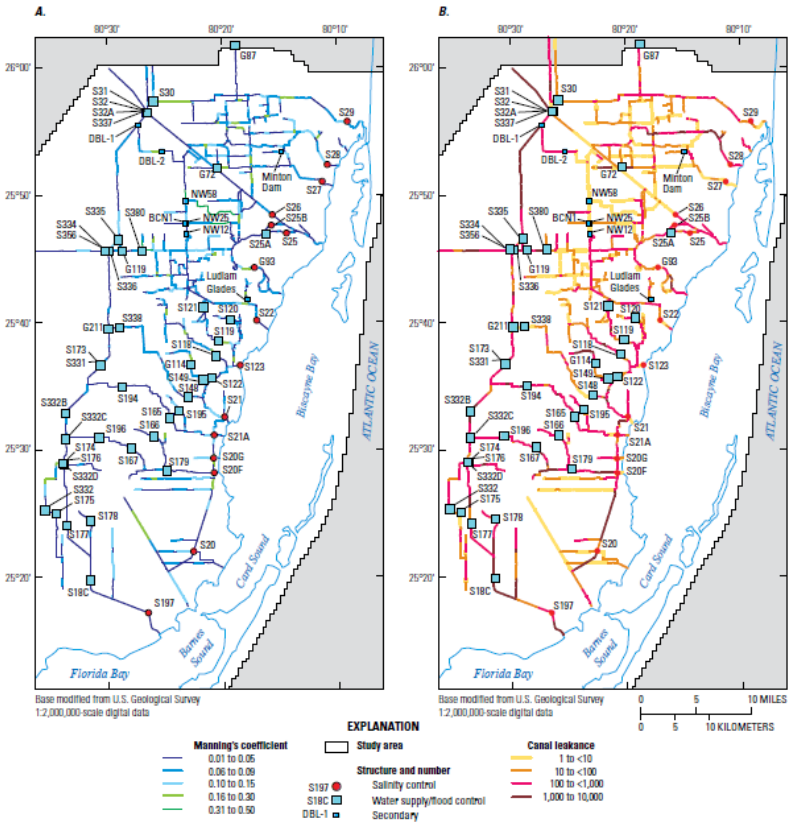

Channel hydraulic coefficients calibrated using a half km by half km grid size model. (pp 74, "Figure 39. Calibrated, A, canal roughness and B, bed leakance coefficients."). Because a digitized copy of the leakance coefficients was not found, in this study, the value of the corresponding canals was manually assigned to the

corresponding canal location as indicated in figure –b. While doing so, the canals in the study area were divided into 11 segments based on continuity of a given path. The initial, steady, and transient state model calibrated leakance values of the segments are indicted in the figure below.

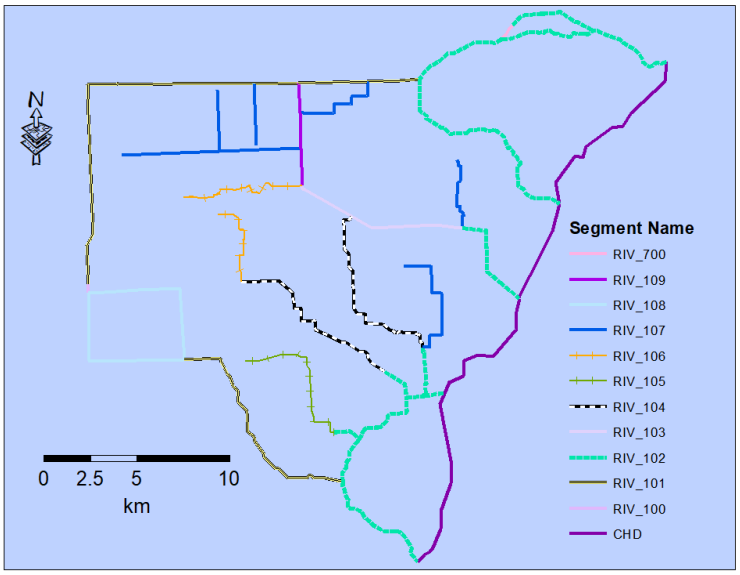

Spatial distribution of river leakance coefficient of defined segments.

Segments are defined based on continuity of the polygon. The initial value, calibration range and fitted values are given in the table below. Calibration information of river conductance, the input and output estimation (per day) is based on leakance. The river module in MODFLOW solves for conductance. All initial values are estimates that were estimated using the information in the figure above. The calibration results are given in the table below.

Segment Name	Initial value (dy-1)	Fitted Value (dy-1)	Minimum value (dy-1)	Maximum Value (dy-1)
RIV_101	2000	1917.1	100	5000
RIV_103	300	44.1	5	30000
RIV_104	300	25.6	0.001	1000
RIV_102	300	10.1	1	100
RIV_108	300	10.5	0.001	1500
RIV_107	5	15	1	100
RIV_700	2000	29948.8	1000	50000
RIV_105	10	20.8	0.001	100
RIV_109	300	1000.0	100	1000
RIV_106	300	2346.7	10	25000

Overall the steady state model calibration has improved the model performance (based on the observed and simulated groundwater level) as indicted in the table 1 above. The water balance components of the model were changed after the calibration, as indicted in the table below.

Diffused recharge

The diffused recharge estimation was based on the Thyssen polygons developed during the initial model simulation. Diffused recharge of 38 cm/year was estimated by model calibration (Langevin, 2003). In Miami-Dade County, the mean annual rainfall is 150 cm/year. Accordingly, the estimated effective recharge of 38 cm/year (Langevin, 2003) accounts for around 25% of the total annual rainfall in the locality. Therefore, in this study, the initial model was simulated using 25% of the areal precipitation in each recharge zone. In the table below the initial recharge value, the fitted value, and estimation rages are given.

Station	Recharge (m)	fitted (m)	Maximum (m)	Minimum (m)
S26_R	0.00038	0.00077	0.00034	0.00103
MIAMI.FS_R	0.00051	0.00120	0.00040	0.00120
S123	0.00048	0.00034	0.00034	0.00101
S21_R	0.00044	0.00034	0.00034	0.00101
S336_R	0.00031	0.00032	0.00027	0.00081
S338_R	0.00028	0.00082	0.00027	0.00082

Transient model calibration

Calibration stage: at the transient groundwater flow calibration, hydraulic conductivity, leakance, specific yield and specific storage values were used. The initial hydraulic conductivity was delineated in to five zones as indicated below.

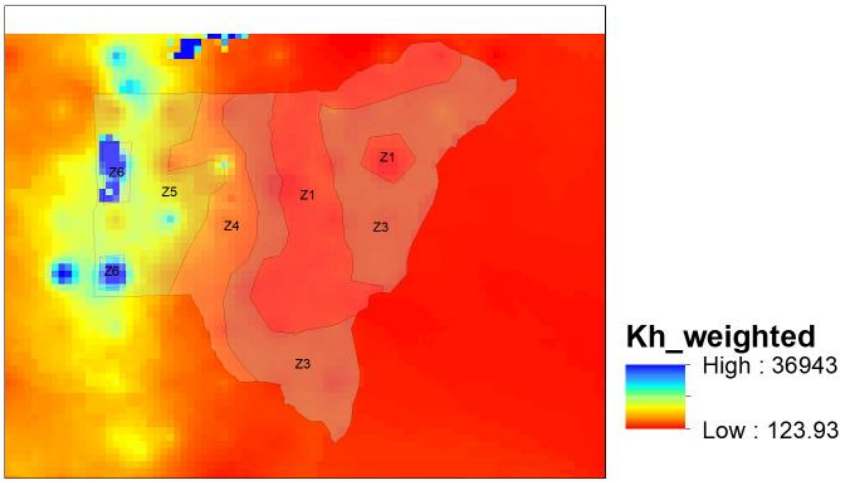

In addition to the initial hydraulic conductivity, the spatial distribution of calibrated zonal hydraulic conductivity value is given in the figure below.

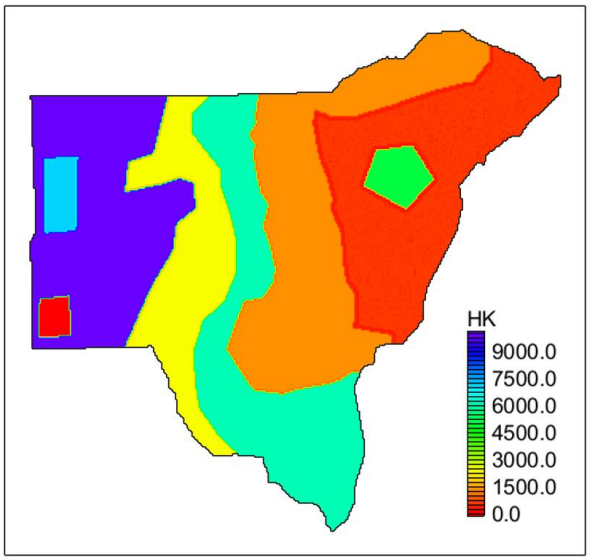

Hydraulic conductivity and recharge were used manually adjusted until an acceptable model performance was achieved.

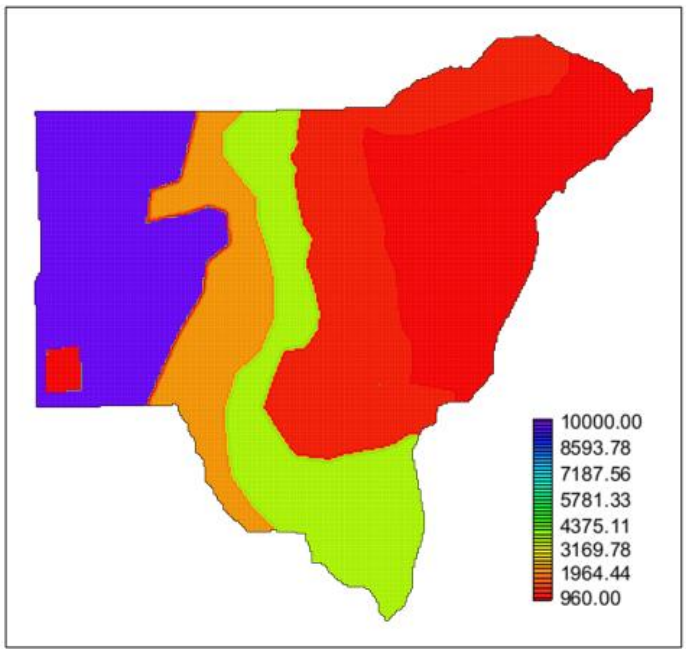

The hydraulic conductivity data was manually manipulated to fit with the expected realistic hydraulic conductivity information of the area.

The estimated leakance value of the river segments water used in initialize the transient model. The fitted value, and range of calibration values are given in the table below.

Segment Name	Initial value (dy^{-1})	Fitted Value (dy^{-1})	Minimum value (dy^{-1})	Maximum Value (dy^{-1})
RIV_101	1917.1	2631.2	100	5000
RIV_103	44.1	13.6	5	30000
RIV_104	25.6	25.6	0.001	1000
RIV_102	10.1	36.0	1	100
RIV_108	10.5	10.2	0.001	1500
RIV_107	15	12.0	1	100
RIV_700	29948.8	7896.3	1000	50000
RIV_105	20.8	44	0.001	100
RIV_109	1000.0	1450.0	100	1000
RIV_106	2346.7	3264.8	10	25000

Note that the initial leakance values used in the transient simulation are the fitted leakance are the fitted during the steady state calibration. The fitted value, however, is the result of the calibration followed by manual manipulation of the results. So tis value refer both the calibration and validation stage. Only a one zone of specific storage and specific yield was defined for the model calibration. The initial values of the Ss and Sy are given as rater files as shown in chapter four

Parameter	Fitted value	Minimum	Maximum
Specific storage	0.0001	0.00001	0.002
Specific yield	0.031	0.005	0.05

Diffused recharge was used calibrated in the validation stage of the transient groundwater flow model. Initially, the assumption that diffused recharge accounts for the 25% of the areal precipitation in each recharge zone was held valid. This is because of

the act that previous studies have estimated effective recharge of 38 cm/year (Langevin, 2003). In Miami-Dade County, the mean annual rainfall is 150 cm/year— and 38 cm/year accounts for around 25% of the total annual rainfall in the locality. Following this the recharge was changes (as trial and error) until a better fit was found. The final recharge used during transit model validation from the Miami iteration airport station is given as a sample, below. Measured total monthly rainfall (mm) in Miami international airport, table below, is given in mm per month.

Month	Jan	Feb	Mar	Apr	May	Jun	Jul	Aug	Sep	Oct	Nov	Dec	Total
1996	53.1	15.2	49.8	76.7	294.6	228.6	160.8	194.8	125.7	288.3	20.6	56.9	1565.1
1997	51.6	53.6	105.7	167.9	134.9	411.0	194.1	181.9	376.7	70.6	53.6	168.7	1970.0
1998	54.4	144.8	152.1	46.7	88.4	153.2	253.7	299.7	345.4	177.5	213.1	38.9	1968.0
1999	84.1	7.9	5.3	40.6	161.8	398.8	163.6	316.0	306.3	444.2	31.8	58.4	2018.8
2000	10.4	40.1	22.4	89.2	41.7	204.7	188.2	224.3	126.5	468.4	27.7	90.7	1534.2
2001	9.7	3.8	147.1	29.5	154.2	149.4	193.3	218.9	401.8	331.2	32.8	80.0	1751.6
2002	23.4	118.4	17.3	15.2	361.7	245.6	354.3	123.7	111.3	42.9	87.1	87.4	1588.3
2003	16.3	18.8	118.1	43.4	294.4	248.9	129.0	222.5	317.0	45.7	135.9	37.1	1627.1
2004	50.3	104.4	14.5	88.4	45.7	160.8	167.1	278.4	312.9	111.3	8.9	17.5	1360.2
2005	48.5	9.1	112.0	68.6	115.8	547.4	185.9	169.2	189.5	181.1	35.6	32.0	1694.7
2006	5.6	86.9	32.8	8.6	310.1	215.9	200.4	214.1	284.5	57.4	52.1	72.4	1540.8
2007	101.1	52.1	44.7	115.6	139.4	352.6	197.9	112.5	204.2	331.0	60.5	37.8	1749.3
2008	36.3	157.2	145.5	81.3	61.0	175.0	196.9	240.5	172.0	179.3	13.5	38.4	1496.8
2009	6.4	7.4	34.8	45.5	228.1	277.1	192.0	219.2	246.9	59.9	102.4	102.4	1522.0
2010	30.7	100.8	75.7	185.4	57.9	245.6	232.2	302.5	346.5	14.2	67.1	26.2	1684.8

The monthly estimated recharge from the MIA, the table below is given in in meters per month. The estimated monthly diffused recharge account 23% of the total monthly rainfall.

Month	Jan	Feb	Mar	Apr	May	Jun	Jul	Aug	Sep	Oct	Nov	Dec	Total
1996	0.012	0.004	0.011	0.018	0.068	0.053	0.037	0.045	0.029	0.066	0.005	0.013	0.360
1997	0.012	0.012	0.024	0.039	0.031	0.095	0.045	0.042	0.087	0.016	0.012	0.039	0.453
1998	0.013	0.033	0.035	0.011	0.020	0.035	0.058	0.069	0.079	0.041	0.049	0.009	0.453
1999	0.019	0.002	0.001	0.009	0.037	0.092	0.038	0.073	0.070	0.102	0.007	0.013	0.464
2000	0.002	0.009	0.005	0.021	0.010	0.047	0.043	0.052	0.029	0.108	0.006	0.021	0.353
2001	0.002	0.001	0.034	0.007	0.035	0.034	0.044	0.050	0.092	0.076	0.008	0.018	0.403
2002	0.005	0.027	0.004	0.004	0.083	0.056	0.081	0.028	0.026	0.010	0.020	0.020	0.365
2003	0.004	0.004	0.027	0.010	0.068	0.057	0.030	0.051	0.073	0.011	0.031	0.009	0.374
2004	0.012	0.024	0.003	0.020	0.011	0.037	0.038	0.064	0.072	0.026	0.002	0.004	0.313
2005	0.011	0.002	0.026	0.016	0.027	0.126	0.043	0.039	0.044	0.042	0.008	0.007	0.390
2006	0.001	0.020	0.008	0.002	0.071	0.050	0.046	0.049	0.065	0.013	0.012	0.017	0.354
2007	0.023	0.012	0.010	0.027	0.032	0.081	0.046	0.026	0.047	0.076	0.014	0.009	0.402
2008	0.008	0.036	0.033	0.019	0.014	0.040	0.045	0.055	0.040	0.041	0.003	0.009	0.344
2009	0.001	0.002	0.008	0.010	0.052	0.064	0.044	0.050	0.057	0.014	0.024	0.024	0.350
2010	0.007	0.023	0.017	0.043	0.013	0.056	0.053	0.070	0.080	0.003	0.015	0.006	0.387

VITA

ANTENEH ZEWDIE ABIY
aabiy001@fiu.edu

1998-2003	B.S., Applied Geology Mekelle University Mekelle, Ethiopia.
2007-2009	MS., Integrated Watershed Management and Hydrology (concentration Environmental Engineering) Cornell University Ithaca, NY.
2014-2020	Teaching Assistant Florida International University Miami, FL MS., Geosciences Florida International University Miami, FL. Doctoral Candidate Florida International University Miami, FL.
2017	Everglades Foundation Fellowship Fellow Everglades Foundation and FIU for Everglades Miami, FL.
2018	Dissertation Evidence Acquisition scholarship, Florida International University Miami, FL.
2019-2020	Dissertation Year Fellowship Florida International University Miami, FL.
2019	CERC Graduate Student of the year 2019. Florida International University Miami, FL

PUBLICATIONS AND PRESENTATIONS

- Gessesse, A.A., Melesse, A.M. and Abiy, A.Z., 2019. Land use dynamics and base and peak flow responses in the Choke mountain range, Upper Blue Nile Basin, Ethiopia. *International Journal of River Basin Management*, pp.1-13.
- Gessesse, A.A., Melesse, A.M., Abera, F.F. and Abiy, A.Z., 2019. Modeling Hydrological Responses to Land Use Dynamics, Choke, Ethiopia. *Water Conservation Science and Engineering*, pp.1-12.
- Abiy, A.Z., Melesse, A.M. and Abtew, W., 2019. Teleconnection of Regional Drought to ENSO, PDO, and AMO: Southern Florida and the Everglades. *Atmosphere*, *10*(6), p.295.

- Abiy, A.Z., Melesse, A.M., Seyoum, W.M. and Abtew, W., 2019. Drought and climate teleconnection and drought monitoring. In *Extreme Hydrology and Climate Variability* (pp. 275-295). Elsevier.
- Abiy, A.Z., Melesse, A.M., Abtew, W. and Whitman, D., 2019. Rainfall trend and variability in Southeast Florida: Implications for freshwater availability in the Everglades. *PloS one*, *14*(2).
- Abiy, A.Z. and Melesse, A.M., 2017. Evaluation of watershed scale changes in groundwater and soil moisture storage with the application of GRACE satellite imagery data. *Catena*, *153*, pp.50-60.
- Wagena, M.B., Sommerlot, A., Abiy, A.Z., Collick, A.S., Langan, S., Fuka, D.R. and Easton, Z.M., 2016. Climate change in the Blue Nile Basin Ethiopia: implications for water resources and sediment transport. *Climatic change*, *139*(2), pp.229-243.
- Abiy, A.Z., Demissie, S.S., MacAlister, C., Dessu, S.B. and Melesse, A.M., 2016. Groundwater Recharge and Contribution to the Tana Sub-basin, Upper Blue Nile Basin, Ethiopia. In *Landscape Dynamics, Soils and Hydrological Processes in Varied Climates* (pp. 463-481). Springer, Cham.
- Tebebu TY., Abiy AZ, et al. 2010. Surface and subsurface flow effects on permanent gully formation and upland erosion near Lake Tana in the northern Highlands of Ethiopia. Hydrology and Earth Systems Science, Vol. 14, pp. 2207-2217.
- Abiy, A.Z., Melesse, et al., 2016. Groundwater Vulnerability Analysis of the Tana Sub-basin: An Application of DRASTIC Index Method. In Landscape Dynamics, Soils and Hydrological Processes in Varied Climates (pp. 435-461). Springer International Publishing.
- Dessu, S.B., Seid, A.H., Abiy, A.Z. and Melesse, A.M., 2016. Flood forecasting and streamflow simulation of the upper Awash River basin, Ethiopia using geospatial stream flow model (GeoSFM). In Landscape Dynamics, Soils and Hydrological Processes in Varied Climates (pp. 367-384). Springer International Publishing.
- Anteneh Z. Abiy, Assefa M. Melesse. 2018. Historical drought variability in Southeast Florida and teleconnections to ENSO, PDO, and AMO. EGU General Assembly 2018. Vienna. 8–13 April.
- Anteneh Abiy, Assefa M. Melesse, Wossenu Abitew. 2017 Evaluation of regional hydroclimate variability and links to the hydrology and saltwater intrusion in South Florida.
- Anteneh Z. Abiy, Assefa M. Melesse. 2017. Drought Phases and Variabilities in Miami, the implication to freshwater availability in the Everglades. FCE-LTER